Leopold-Franzens-Universität Innsbruck
Fakultät für Mathematik, Informatik und Physik

Quantum simulation of nonlinear atom-photon dynamics in optical resonators

Dissertation
zur Erlangung des akademischen Grades
Doctor of Philosophy

vorgelegt von
Dipl. Phys. Raimar Marcel Sandner

Betreuer: Univ.-Prof. Dr. Helmut Ritsch, Institut für Theoretische Physik

Innsbruck, April 2016

In memoriam Wolfgang Sandner.

Zusammenfassung

Bei der Wechselwirkung zwischen Licht und Materie wird der Impuls, den Photonen führen, an Atome übertragen und umgekehrt. Die resultierenden mechanischen Kräfte können genutzt werden, um Atomwolken oder sogar einzelne Atome auf eine Temperatur nahe am absoluten Nullpunkt zu kühlen und auf kleinstem Raum gefangen zu halten, Bedingungen also bei denen die Quanteneigenschaften der Materie zu Tage treten.

Im freien Raum ist die Wechselwirkung zwischen einem einzelnen Photon und einem Atom jedoch schwach. Das optische Potential eines Lasers wird daher gewöhnlich von einer enormen Anzahl von Photonen generiert und spielt die Rolle eines klassischen Potentials. Ein optischer Resonator dagegen, also zwei sphärische Spiegel die einen Hohlraum bilden, kann einzelne Photonen einschließen und viele Male reflektieren bevor sie verloren gehen. Im Parameterbereich starker Kopplung der Hohlraum-Quantenelektrodynamik (Cavity QED) kann ein Photon von einem Atom wiederholt absorbiert und abgestrahlt werden, und selbst die Kräfte die von einem einzelnen Photon erzeugt werden können ausreichen, um ein Atom zu fangen. Umgekehrt hat die Bewegung eines Atoms einen großen Einfluss auf das Feld innerhalb des Hohlraums, da ein Atom die Resonanzfrequenz in Abhähngigkeit seiner Position relativ zur Mode verschiebt. Das optische Potential wird dadurch zu einer aktiven Komponente mit einer vielfältigen nicht-linearen Dynamik zwischen Atomen und Photonen. Photonen die aus dem Resonator entweichen transportieren Informationen über das System und dienen zusätzlich als Dissipationskanal, ein zentraler Bestandteil von auf Hohlraumresonatoren basierenden Kühlmethoden. Cavity QED bietet einige einzigartige Möglichkeiten zur Handhabung individueller Quanten-Objekte. Oft ist die Motivation in diesem Bereich Grundlagenforschung, zum Beispiel die direkte Beobachtung von Dekohärenz oder von nicht-klassischen Zuständen des Lichts und der Materie. Zusätzlich haben die entwickelten Techniken potentielle Anwendungen in der Quanten-Informationsverarbeitung und für Quantencomputer.

Diese Doktorarbeit fasst meine Forschung zur Theorie der Cavity QED zusammen. Fortschrittliche Computer ermöglichen heute die Simulation einiger Teilchen in Wechselwirkung mit einer oder mehreren Hohlraummoden, wobei die kompletten Quanteneigenschaften aller Bestandteile mit einbezogen werden können. Wir demonstrieren wie ein Ringresonator zur Entstehung von nicht-klassischen Impulskorrelationen und Verschränkung beiträgt. Numerische Simulationen zu einer resonatorgestützten Kühlmethode werden präsentiert, die verglichen mit konventioneller Laserkühlung für eine größere Klasse von Teilchen anwendbar ist und zu niedrigeren Temperaturen sehr nahe am Nullpunkt zu führen verspricht. Der letzte Teil dieser Arbeit beschäftigt sich mit dem Phänomen der Selbstorganisation, ein Phasenübergang

hin zu einer kristallinen Struktur, die durch Interferenz zwischen der Hohlraummode und seitlich eingestrahltem Laserlicht begünstigt wird. Wir untersuchen den Einfluss der Quantenstatistik auf den Ordnungsübergang und bestätigen eine stark herabgesetzte Schwelle für das Eintreten des Phasenübergangs bei einem degenerierten Fermigas, falls die Fermienergie eine bestimmte Resonanzbedingung erfüllt.

Abstract

When light and matter interacts, the momentum carried by photons is transferred to atoms and vice versa. The resulting mechanical forces can be tailored to cool atomic clouds or even single atoms to temperatures close to absolute zero and to trap them in a small region of space, a regime where the quantum nature of particles becomes significant.

In free space, however, the interaction of a single photon with an atom is weak. The optical potential of lasers therefore usually is generated by an enormous number of photons and plays the role of a classical potential. In contrast, an optical resonator composed of two spherical mirrors forming a cavity can confine single photons and reflect them many times before they are lost. In the strong coupling regime of *cavity quantum electrodynamics* (cavity QED), a photon can be repeatedly absorbed and re-emitted by an atom, and even a single photon can produce sufficiently large forces to trap an atom. Conversely, as an atom shifts the resonator frequency depending on its position relative to the field mode, the atomic motion has a large impact on the intra-cavity field. The optical potential becomes an active component with rich non-linear atom-photon dynamics. Photons leaking out of the resonator convey information about the system and additionally act as a channel of dissipation, a vital ingredient for cavity-assisted cooling schemes. Cavity QED offers unique possibilities for the manipulation of individual quantum objects. Fundamental research is often the motivation in this field, for example direct observation of decoherence or non-classical states of light and matter. Additionally, the developed techniques find potential applications in quantum information processing and quantum computing.

This thesis summarises my research in cavity QED theory. Advances in computational power allow the simulation of several particles interacting with one or several cavity modes while taking the full quantum nature of all constituents into account. In this few-particle regime, we demonstrate the emergence of non-classical momentum correlations and entanglement mediated by the two modes of a ring cavity. We present numerical simulations of a cavity-assisted cooling scheme which is expected to work with a larger class of particles and provide lower final temperatures than conventional laser cooling methods. In the last part, we turn to the phenomenon of self-organisation, a phase transition to a crystalline structure induced by interference between the cavity mode and laser light shone on the particles from the side. We investigate the impact of quantum statistics and confirm a strong suppression of the threshold for the onset of the phase transition if a degenerate Fermi gas fulfills certain resonance conditions.

Danksagung

Es ist mir ein großes Anliegen, all jenen Personen meine tiefe Dankbarkeit auszudrücken, die mich bei der Anfertigung dieser Dissertation betreut, unterstützt und begleitet haben.

Ganz besonders möchte ich mich bei Prof. Helmut Ritsch bedanken. Nicht nur seine physikalische Weitsicht und Intuition sowie stets ein offenes Ohr und wertvolle Ratschläge bei auftretenden Problemen zeichnen seine Betreuung aus, sondern auch viel Geduld und Verständnis für die jeweilige persönliche Situation. Darüber hinaus sorgt Helmut mit diversen Tiroler Freizeitaktivitäten, viel Humor und stets aktuellem technischem Spielzeug für eine sehr angenehme und motivierende Atmosphäre.

Die direkte Zusammenarbeit mit Wolfgang Niedenzu, Francesco Piazza und András Vukics war für mich unschätzbar wertvoll, sowohl aufgrund ihres enormen Sachverstands und ihrer Erfahrung, als auch wegen ihrer kollegialen und freundschaftlichen Art. Darüber hinaus möchte ich mich bei allen aktuellen und ehemaligen Mitgliedern der Gruppe bedanken, die ich während meiner Zeit in Innsbruck kennenlernen durfte: Erez Boukobza, Claudiu Genes, Tobias Grießer, Torsten Hinkel, Daniela Holzmann, Sebastian Krämer, Thomas Maier, Laurin Ostermann, Stefan Ostermann, David Plankensteiner, Matthias Sonnleitner, Valentin Torggler, Dominik Winterauer und Hashem Zoubi. Lebhafte Diskussionen und unvergessliche Stunden werden als schöne Erinnerung bleiben, sei es im Seminar, beim mittaglichen Kaffee, auf Wanderungen oder beim Tischfußball. Dank gebührt auch András Vukics and Peter Domokos für die große Gastfreundschaft, die ich bei meinen Besuchen in Budapest erfahren habe.

Hans Embacher danke ich für die unermüdliche Pflege der Computersysteme, ebenso Nicole Jorda, Birgit Laimer, Elke Stenico und Elke Wölflmaier für die kompetente Hilfe in allen Verwaltungsangelegenheiten.

Unendlich dankbar bin ich meiner ganzen Familie für den Rückhalt, den ich erfahren habe. Zusammen mit Kathrin wurde Tirol zur zweiten Heimat, das allerschönste Andenken an Innsbruck heißt Nora Marie und kam im August 2014 zur Welt.

Contents

Chapter 1

General introduction

1.1 Manipulation of single quantum objects

It is fair to say that the photon, the elementary constituent of light, has been at the very heart of the quantum revolution shaping the previous century, and the photon continues to amaze and surprise physicists to the present day. Indeed it was the discovery of the quantised character of light, made by Max Planck in the context of black-body radiation [1.1] and generalised by Albert Einstein in his work on the photoelectric effect [1.2], that paved the way towards a completely new understanding of nature.

The photon beautifully reveals the most intriguing principles of quantum mechanics. For example, a single photon can be 'split' and sent through an interferometer on two distinctive paths. Depending on the difference in path lengths, the photon interferes with itself constructively or destructively upon recombination, clearly exhibiting wavelike character [1.3]. At the same time a photon can be regarded as an indivisible particle in a sense that every attempt to detect which of the two paths has been chosen will yield a definite single result and destroy the interference pattern. The same particle-wave duality [1.4] and quantum interference has been demonstrated for electrons [1.5], atoms [1.6] and even molecules on the nanometre scale [1.7], entities which do not behave like waves in the theory of classical mechanics.

Einstein was rewarded the Nobel Prize 1921 for his discovery of the photoelectric effect [1.2], and in the following years Heisenberg, Dirac, and Schrödinger amongst others made important contributions to continue the development of the arising quantum theory and its mathematical framework [1.8]. However, quantum mechanics was at that time regarded solely as a mathematical instrument. Well suited to explain phenomena otherwise incompatible with a classical understanding of physics, like the spectral density of black-body radiation [1.1] or the coefficients for spontaneous and stimulated emission of light [1.9], it was thought to be otherwise inaccessible to direct experimental verification. Least was it deemed possible to create, manipulate and investigate individual quantum objects like single photons or single atoms. Too fragile seemed a photon which is easily absorbed by any surrounding matter converting its tiny portion of energy to heat, too volatile a microscopic atom moving with several hundred metres per second at room temperature beyond hope of non-destructive observation. Instead, *gedankenexperimente* were invented in order to challenge the new concepts, for example Schrödinger's famous cat [1.10] kept inside a closed box

together with a mechanism which releases poison, triggered by an atomic decay. By the quantum laws the cat is suspended in a controversial state of superposition between life and death. The process which prevents us from seeing quantum phenomena in daily life, such as a cat being simultaneously dead and alive, is the loss of extremely delicate quantum phase relations through irreversible interaction with the infinite degrees of freedom of the surroundings, including the box, air molecules and ultimately the many photons our eyes rely upon to make observations. Controlling this *decoherence* [1.11, 1.12] by sufficiently shielding a system from its environment, even on the microscopic scale, is a tremendous experimental challenge.

Almost a century later, in 2012 the Nobel laureates Serge Haroche and David J Wineland were honored "for ground-breaking experimental methods that enable measuring and manipulation of individual quantum systems". While Wineland is active in the field of trapped ions [1.14], Haroche's domain of research at l'Ecole Normale Supérieure (ENS) is *cavity quantum electrodynamics* (cavity QED) [1.13]. In his experiments, a pair of highly polished super-conducting spherical mirrors form an open cavity which acts as resonator for photons with frequencies in the microwave regime [1.15]. Such a device reflects single photons back and forth many times, trapping them for over a hundred milliseconds. During this time, the photons travel over 40 000 km between the mirrors, before they are lost by the virtue of mirror absorptions and scattering off small imperfections. This resembles the gedankenexperiment of the Einstein-Bohr photon box [1.16], and also a version of Schrödinger's cat could be realised, although not in the literal sense but as quantum-mechanical superposition of distinctive classical states of light [1.17].

Additionally to impressive photon storage times, the full power of the ENS experiments stems from the controlled interaction of cavity photons with single atoms traveling through the resonator. Due to the large number of photon round trips and by making use of two highly excited internal atomic Rydberg states which act as a very sensitive dipole antenna, the 'holy grail of cavity QED' was reached [1.13]. In the regime of *strong coupling* the interaction strength between cavity and atom exceeds the dissipation like photon loss and spontaneous emission. This has the consequence that, with atom and cavity tuned on resonance, a single photon can be absorbed by an atom and then re-emitted into the cavity many times before it is lost. Off resonance, an atomic beam can be prepared in a way that it extracts information about the light field one atom at a time while leaving the photons intact. For the first time it was possible to count and even monitor single photons throughout their lifetime without destroying them [1.17, 1.18].

Research towards non-destructive manipulation of individual quantum objects, a field in which cavity QED is only one of many routes [1.19–1.21], opens up the possibility to put fundamental concepts like decoherence to a test [1.22]. Additionally, it is strongly motivated by envisioned applications and algorithms which rely on this degree of control, for example in the realm of quantum information processing and quantum computing [1.23, 1.24].

1.2 Cooling and trapping neutral atoms with light forces

So far we have only considered interaction of light with the internal atomic dynamics, i.e. with the electrons orbiting the nucleus. Photons, however, carry momentum proportional to their frequency which manifests as a recoil kick on the center-of-mass motion of an atom absorbing or emitting a photon. While in the microwave regime this recoil is negligible, mechanical effects of light on matter play an important role in the optical frequency range. Let us first briefly discuss the radiative forces experienced by an atom in free space and the implications for trapping and cooling atoms with light before coming back to cavity QED and the case where ultracold atoms move inside a resonator for optical frequencies.

The forces acting on an atom illuminated by a coherent light source such as a laser [1.25, 1.26] can be split into two parts, the dipole force and the radiation pressure [1.27]. On the one hand, the dipole force has a conservative nature and gives rise to an *optical potential*. In a photon picture, it can be related to stimulated absorption and emission. For example, two running waves with opposite direction create a standing wave intensity pattern, and the dipole force in such an *optical lattice* can be explained by the momentum exchange corresponding to coherent scattering of photons from one beam to the other. In a classical picture, the dipole force can be interpreted in terms of the electric dipole induced within the atom by the field. As the interaction energy between the field and the dipole depends on the light intensity, an intensity gradient directly corresponds to a potential gradient. This also explains the change from an attractive to a repulsive force with respect to regions of high light intensity, when the driving laser is tuned below or above the atomic resonance, respectively. Below resonance the induced dipole oscillates in phase with the field, whereas above resonance it is forced out of phase, resulting in a sign change of the interaction energy. On the other hand, the radiation pressure is related to absorption of a laser photon followed by spontaneous emission to free space. The momentum of each absorbed photon is transferred to the atom leading to a force aligned with the direction of a running wave, whereas the two opposing forces cancel each other out in a standing wave. The recoil kick associated with spontaneous emission has no directional preference and therefore does not result in a net force on average. It does, however, contribute to momentum diffusion.

Shining light on atoms from opposite directions with the frequency tuned below an atomic resonance, the radiation pressure gives rise to a velocity-dependent friction force. This *Doppler cooling* method [1.28, 1.29] is limited by the natural linewidth of the atomic transition. Sub-Doppler temperatures are achievable by exploiting polarisation gradients and spatially overlapping optical potentials for different internal atomic states. In a simplified picture of *Sisyphus cooling*, the atoms constantly lose kinetic energy by running 'uphill' towards the maximum of one optical potential where they are optically pumped to the minimum of a different one and the process starts over [1.30]. Here the temperature is limited by the momentum diffusion induced by the recoil of a single photon scattering event (recoil limit).

The overwhelming success of laser cooling and trapping techniques [1.31–1.34]

opens the realm to experiments with ultracold quantum gases. From this extremely rich field [1.35] let us only highlight a few examples. A Bose-Einstein condensate (BEC) is a state of matter with temperatures close to absolute zero, where particles cease to exist as individual entities and instead form a collective coherent matter wave. Predicted in 1925 [1.36, 1.37], today BECs are routinely created for many atomic species and even molecules [1.38–1.44], often used as basis for further experiments. Ultracold atoms in optical lattices, i.e. optical potentials generated by the dipole-force of strong far-detuned counter-propagating laser beams, provide an excellent setting to engineer otherwise inaccessible Hamiltonians of condensed matter physics in an extensively controllable way [1.45, 1.46].

1.3 Cold atoms in optical resonators

In conventional optical lattices the light forces are generated by a large number of photons, and the back-action of scattered photons on the light field is negligible. This situation changes dramatically when ultracold atoms are placed inside a high-quality resonator for photons with optical frequencies [1.47, 1.48]. Vast improvements in the fabrication of cavity mirrors in combination with very small mode volumes made it possible to reach the aforementioned strong coupling also in the optical regime [1.49]. In such a cavity, even a single photon can create a dipole force strong enough to trap an atom [1.50, 1.51]. Furthermore, cavity-generated optical potentials are subject to quantum fluctuations and significant back-action from atomic motion and photon scattering, therefore taking an active role in the coupled atom-cavity dynamics [1.47, 1.48].

Even with reflectivities close to unity, cavity photons eventually leak out through the mirrors with a rate connected to the linewidth of the resonator. On the one hand, this signal can convey information like atomic trajectories [1.50, 1.51], on the other hand it constitutes a dissipation channel which can extract energy from atomic motion. This cavity cooling mechanism [1.52] takes advantage of the intra-cavity field reacting to atomic positions with a finite response time. In a carefully chosen parameter regime, the optical potential is deepened while an atom climbs a potential well and flattened while it slides down, resulting in a friction force and a loss of kinetic energy on average. One of the potential advantages compared to conventional laser cooling mentioned above is the fact that cavity cooling persists in the regime of low atomic excitation [1.53].

In this *dispersive regime* with a cavity far detuned from all internal atomic resonances, which is adopted throughout the present thesis, spontaneous emission from atoms is strongly suppressed and the exact internal structure becomes irrelevant. Instead, the atoms can be described as linearly polarisable particles acting as a position-dependent refractive index for the cavity mode. As a consequence, cavity-assisted cooling schemes might be extended to a large class of particles for which laser cooling cannot easily be applied due to missing suitable closed level cycles, such as molecules [1.54]. Furthermore, the final temperature is limited by the cavity linewidth

which can be significantly narrower than most optical lines, making sub-Doppler and even sub-recoil cavity cooling possible [1.55].

In many ways the dispersive regime at optical frequencies constitutes an orthogonal approach to cavity QED, compared to the microwave experiments discussed above. While in the latter case the atom momentum is fixed and the internal atomic dynamics plays the crucial role, the former case focuses on the external, motional atomic aspects like cavity-mediated light forces, long-range interactions and self-organisation phenomena [1.47, 1.48]. It is worth noting that even if linear polarisability is assumed, the dynamical equations governing the quantised motion of ultracold particles coupled to a cavity mode are inherently non-linear [1.56].

1.4 Outline of the thesis

The findings presented in this thesis contribute to a deeper understanding of the microscopic dynamics of moving-particle cavity QED in the dispersive regime. By taking advantage of high-performance computing clusters, advances in computational power allow numerical simulations of the full quantum state of up to five particles moving inside a high-quality optical resonator, taking into account the quantised nature of the motional degrees of freedom and the intra-cavity-field on equal footings.

This thesis is organised in four parts, it contains three published articles in the field of cavity QED theory and one published release announcement for a programming framework intended to assist in the implementation of efficient quantum simulations. At the beginning of each publication, a note indicates the current author's contributions. Part I is an introduction to cavity QED and the notion of open quantum systems as well as the numerical methods used to simulate their dynamics. Part II describes the programming framework whose ongoing development, extension and improvement was a substantial part of this thesis. The parts III and IV contain all the research results and correspond to the two distinct geometries of a laser driving the optical resonator directly and a laser which pumps the particles from the side, respectively.

The article of chapter 7 presents an optomechanical approach to two particles moving inside a ring cavity. Through the cavity-mediated interactions between the particles, it reveals classically forbidden positive momentum correlations and entanglement, which is particularly strong directly after the detection of a photon lost from the cavity. Chapter 8 summarises our work on an improved cavity-assisted cooling scheme with the prospect to reach temperatures below the recoil limit and, ultimately, quantum degeneracy. The impact of quantum statistics on the cooling dynamics in a ring cavity and a standing-wave cavity geometry are numerically investigated, respectively. Chapter 10 is concerned with the phenomenon of self-organisation, a phase transition towards a cristalline state with long-range order that is observed with transversally pumped particles in a cavity. In particular, the dependence of this phase transition on quantum statistics is numerically examined for few particles in the fully quantised regime. We can confirm a recently predicted suppression of the

pump strength threshold for self-organisation of quantum-degenerate fermions, given that a resonance condition with respect to the Fermi momentum is fulfilled.

Part I

Introduction to cavity QED

Chapter 2

Open quantum systems

In quantum mechanics, the state of an isolated system is described by a normalised state vector $|\psi(t)\rangle$ in a Hilbert space $\mathcal{H}$ with the time evolution given by the Schrödinger equation

$$\mathrm{i}\hbar\frac{\mathrm{d}}{\mathrm{d}t}|\psi(t)\rangle = H(t)\,|\psi(t)\rangle\,. \tag{2.1}$$

While the Hamiltonian $H(t)$ can in principle be explicitly time dependent, this is not the case for the Hamiltonians appearing in this thesis, therefore we write $H(t) \equiv H$ in the Schrödinger picture. Equation (2.1) defines a unitary time evolution, in particular the norm of the state $|\psi(t)\rangle$ is preserved for all times and the evolution is fully reversible.

Such an isolated system represents a highly idealised situation, as in fact a real experiment always interacts with its environment. In the context of quantum optics, this environment is the continuum of radiative modes, usually represented by a thermal reservoir, with the special case of the vacuum state as a zero-temperature reservoir. In principle the environment could be included in the Hamiltonian H to obtain once again an isolated system with a unitary time evolution. However, this approach can lead to an overcomplicated model which is hard or impossible to solve, and even if we could solve it, the microscopic details of how photons are carried away from the system are of little interest in most cases. Instead, we strive to retain the physical effect of the reservoir on the system, in particular adding quantum noise, dissipation and radiative shifts, while assuming that the effect the system has on the environment can be neglected. A classical analogon is, for example, the Brownian motion of a heavy particle submerged in a liquid or gas: instead of tracking the countless collisions with the environment, we describe the net effect of damping and diffusion these collisions have.

Dissipation is a key ingredient in all quantum optics experiments. On the one hand it has to be controlled or minimised because it destroys coherence, which is often sought-after as a characteristic quantum property. On the other hand, dissipation is essential in all cooling schemes as it is the only way how a system can lose energy and entropy [2.1, 2.2]. In the framework of decoherence and open quantum systems, the state vector $|\psi(t)\rangle$ is replaced by a density operator $\rho(t)$, which additionally to pure states can describe statistical mixtures as more general quantum states. The

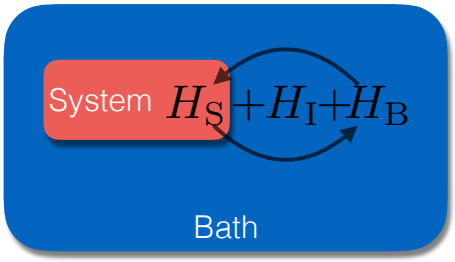

Figure 2.1: A small system with Hamiltonian H_S is coupled by the interaction Hamiltonian H_I to the environment, described by the Hamiltonian H_B and acting as a heat bath.

unitary time evolution of eq. (2.1) is replaced by the von Neumann equation

$$\frac{\mathrm{d}}{\mathrm{d}t}\rho(t) = -\frac{\mathrm{i}}{\hbar}\left[H, \rho(t)\right] \tag{2.2}$$

in this formalism. In the following section we will introduce a general closed equation of motion for the density operator of an open system, the *master equation*. This equation belongs to the important class of quantum Markov processes with weak coupling to a reservoir [2.3, 2.4]. In section 3.4 we will introduce the specific master equation describing particles moving in an optical resonator.

2.1 Master equation

We consider the situation of a small system weakly coupled to a large environment as sketched in fig. 2.1. The total Hamiltonian can be written as

$$H = H_S + H_I + H_B, \tag{2.3}$$

where H_S, H_B and H_I are the Hamiltonians of the system, the bath and the interaction, respectively. The interaction Hamiltonian in an interaction picture with respect to $H_S + H_B$ is

$$H_I(t) = \mathrm{e}^{-\frac{\mathrm{i}}{\hbar}(H_S+H_B)t} H_I \mathrm{e}^{\frac{\mathrm{i}}{\hbar}(H_S+H_B)t}. \tag{2.4}$$

Starting from the von Neumann equation for the total density operator $\rho(t)$ in the interaction picture

$$\frac{\mathrm{d}}{\mathrm{d}t}\rho(t) = -\frac{\mathrm{i}}{\hbar}\left[H_I(t), \rho(t)\right], \tag{2.5}$$

one can derive an equation local in time for the reduced density matrix describing the system alone, i.e. $\rho_S := \mathrm{tr}_B\, \rho(t)$, where tr_B denotes the trace over the reservoir degrees of freedom [2.4]

$$\frac{\mathrm{d}}{\mathrm{d}t}\rho_S(t) = -\int_0^\infty \mathrm{d}s\ \mathrm{tr}_B\left[H_I(t), \left[H_I(t-s), \rho_S(t)\otimes\rho_B\right]\right]. \tag{2.6}$$

Two important approximations have been made to arrive at eq. (2.6). The *Born approximation* is essentially a weak-coupling assumptions which states that $\rho(t) \approx \rho_{\mathrm{S}}(t) \otimes \rho_{\mathrm{B}}$ factorises at all times and allows us to neglect terms of higher than second order in H_{I}. Here, ρ_{B} is the stationary state of the bath, which we assume is not affected by the system. The *Markov approximation*, which states that the reservoir auto-correlation timescale τ_{B} is much smaller than the timescale τ_{S} on which the system changes appreciably, allows us to make the right hand side of eq. (2.6) depend on the current value of $\rho_{\mathrm{S}}(t)$ alone instead of the history of the system, and to extend the integration limit to infinity. It is important to keep in mind that the master equation is a coarse-grained equation of motion, in the sense that it cannot resolve the dynamics of very short times on the order of τ_{B}.

For a finite-dimensional system with D states, eq. (2.6) can be brought into the so-called *standard-* or *Lindblad form* [2.4], here transformed back to the Schrödinger picture density operator (also denoted $\rho_{\mathrm{S}}(t)$ for brevity)

$$\frac{\mathrm{d}}{\mathrm{d}t}\rho_{\mathrm{S}}(t) = -\frac{\mathrm{i}}{\hbar}\left[\tilde{H}_{\mathrm{S}}, \rho_{\mathrm{S}}(t)\right] + \sum_{k=1}^{D^2-1} \frac{\gamma_k}{2}\left(2J_k\rho_{\mathrm{S}}(t)J_k^\dagger - J_k^\dagger J_k\rho_{\mathrm{S}}(t) - \rho_{\mathrm{S}}(t)J_k^\dagger J_k\right), \quad (2.7)$$

where the *jump operators* J_k belong to the specific dissipation channel with rate $\gamma_k \geq 0$. The first term involving $\tilde{H}_{\mathrm{S}}$ is the coherent part of the dynamics and generates unitary evolution similar to the von Neumann equation (2.2). In general $H_{\mathrm{S}} \neq \tilde{H}_{\mathrm{S}}$, the interaction with the bath can introduce additional coherent dynamics, for example Lamb- and Stark shifts or dipole-dipole interaction.

The specific form of $\tilde{H}_{\mathrm{S}}$, J_k and γ_k depends on the details of the interaction Hamiltonian H_{I} at hand. In general, to obtain these quantities, one has to evaluate one-sided Fourier transforms of reservoir correlation functions such as

$$\int_0^\infty \mathrm{d}s\, \mathrm{e}^{\mathrm{i}\omega s}\left\langle B_\alpha^\dagger(t)B_\beta(t-s)\right\rangle \equiv \int_0^\infty \mathrm{d}s\, \mathrm{e}^{\mathrm{i}\omega s}\,\mathrm{tr}_{\mathrm{B}}\left\{B_\alpha^\dagger(t)B_\beta(t-s)\rho_{\mathrm{B}}\right\}, \quad (2.8)$$

where B_α and B_β are interaction-picture operators acting on the bath and ω is a transition frequency of H_{S}. For a steady-state reservoir, the correlations are independent of t. The imaginary parts of the correlations eq. (2.8) contribute to the Hamiltonian $\tilde{H}_{\mathrm{S}}$, whereas the real parts lead to dissipation described by J_k and γ_k.

In numerical simulations we are always dealing with finite-dimensional systems, and the assumptions which justify the Born-Markov approximation are often very well fulfilled in quantum optics, which explains the importance of eq. (2.7) for this thesis. In the next section we will discuss two specific numerical methods for solving the master equation.

2.2 Numerical methods

2.2.1 The master equation as ordinary differential equation

The right-hand side of the master equation (2.7) is often abbreviated by a *Liouvillian* operator $\mathcal{L}$, a linear super-operator acting not on a state but on a density matrix ρ,

where we now drop the subscript and understand ρ as the reduced density matrix of the system:

$$\frac{\mathrm{d}}{\mathrm{d}t}\rho = \mathcal{L}\rho. \tag{2.9}$$

For a finite-dimensional system with dimension D, the master equation is a first-order differential equation in a D^2-dimensional vector space, by writing the density matrix ρ as a vector with D^2 complex entries and the super-operator $\mathcal{L}$ as a $D^2 \times D^2$ matrix acting on this vector. The time evolution of an initial state $\rho(0)$ can then be obtained by an *ordinary differential equation* (ODE) solver with standard numerical methods*. Implementations include `C++QED` [2.6–2.9], which is discussed in detail in part II of this thesis, or `QuTiP` [2.10], a Python implementation of the popular but discontinued Matlab Quantum Optics Toolbox [2.11].

This method is only suited for systems typically up to a few thousand states. Because of the scaling with D^2, for larger systems it soon becomes impossible to store the density matrix in memory, or the calculation of a time step takes impractically long.

2.2.2 Monte Carlo wave function method

For systems of intermediate complexity, before entering the realm of true many-body physics, the Monte Carlo wave-function method (MCWF) has proven to be well suited [2.12–2.14]. It provides a numerical method for calculating the time dependence of any expectation value or even the full density matrix ρ. Instead of operating on the density matrix with a size of D^2 c-numbers†, the MCWF method integrates several realisations of state vectors, each consisting of only D c-number entries. A copy of the initial state vector is evolved coherently with an effective non-hermitian Hamiltonian H_{nH} and subjected to quantum jumps at random times, thus building up a quantum trajectory of the system. While the dissipation channel m and the times of quantum jumps are chosen randomly (hence the name Monte Carlo), the method assures the correct dissipation rates by its selection rules described below.

Starting with the master equation eq. (2.7) written in the equivalent form

$$\frac{\mathrm{d}}{\mathrm{d}t}\rho(t) = \frac{\mathrm{i}}{\hbar}\left(H_{\mathrm{nH}}\rho(t) - \rho(t)H_{\mathrm{nH}}^\dagger\right) + \sum_m J_m\rho(t)J_m^\dagger \equiv \mathcal{L}\rho(t) \tag{2.10}$$

$$H_{\mathrm{nH}} = H - \frac{\mathrm{i}\hbar}{2}\sum_m J_m^\dagger J_m, \tag{2.11}$$

the method consists of repeating the following two steps to evolve $|\psi(t)\rangle$, nicely summarised in [2.7]

*for example the fourth-order adaptive stepsize Runge-Kutta Cash-Karp method [2.5]

†Here we are only interested in the scaling with N, using hermitiancy and unit trace the density matrix has $D(D+1)/2 - 1$ independent entries

(1) Evolve the normalised state vector $|\psi(t)\rangle$ for a short time δt with the non-hermitian Hamiltonian H_{nH} according to the differential equation

$$\mathrm{i}\hbar\frac{\mathrm{d}}{\mathrm{d}t}|\psi(t)\rangle = H_{\mathrm{nH}}|\psi(t)\rangle\,, \tag{2.12}$$

to obtain to first order in δt

$$|\psi_{\mathrm{nH}}(t+\delta t)\rangle = \mathrm{e}^{-\frac{\mathrm{i}}{\hbar}H_{\mathrm{nH}}\delta t}|\psi(t)\rangle = \left(1-\frac{\mathrm{i}t}{\hbar}H_{\mathrm{nH}}\delta t\right)|\psi(t)\rangle + \mathcal{O}(\delta t^2). \tag{2.13}$$

Because H_{nH} is non-hermitian, the norm of the state is not preserved, in fact it decreases according to

$$\begin{aligned}\||\psi_{\mathrm{nH}}(t+\delta t)\rangle\|^2 &= \langle\psi(t)|(1+\mathrm{i}H_{\mathrm{nH}}^\dagger\delta t/\hbar)(1-\mathrm{i}H_{\mathrm{nH}}\delta t/\hbar)|\psi(t)\rangle + \mathcal{O}(\delta t^2)\\ &= 1-\delta t\sum_m\langle\psi(t)|J_m^\dagger J_m|\psi(t)\rangle + \mathcal{O}(\delta t^2) \le 1.\end{aligned} \tag{2.14}$$

We define δp to be the total loss of the squared norm and δp_m the loss to a particular dissipation channel, i.e.

$$\delta p_m = \delta t\,\langle\psi(t)|J_m^\dagger J_m|\psi(t)\rangle \qquad\qquad \delta p = \sum_m \delta p_m, \tag{2.15}$$

and we require δt to be sufficiently small so that $\delta p \ll 1$.

(2) A quantum jump occurs with probability δp. We choose a random number $0 \le \varepsilon < 1$, and if $\delta p \le \varepsilon$ (which is the case most of the times because $\delta p \ll 1$) then no jump occurs and the new state is obtained by normalising $|\psi_{\mathrm{nH}}(t+\delta t)\rangle$:

$$|\psi(t+\delta t)\rangle = \frac{1}{\sqrt{1-\delta p}}|\psi_{\mathrm{nH}}(t+\delta t)\rangle\,. \tag{2.16}$$

However, if the random number indicates that a quantum jump occurred, i.e. $\varepsilon < \delta p$, the decay channel is chosen randomly among the J_m according to the probability distribution $\Pi_m = \delta p_m/\delta p$. In practice, this can be done with the already drawn ε by choosing the m for which $\sum_{j=1}^{m-1}\delta p_j \le \varepsilon < \sum_{j=1}^{m}\delta p_j$. The new state is obtained by applying the jump operator and normalising the state:

$$|\psi(t+\delta t)\rangle = \sqrt{\frac{\delta t}{\delta p_m}}J_m|\psi(t)\rangle\,. \tag{2.17}$$

We will refer to the deterministic step (1) and the stochastic step (2) as the *Hamiltonian* and the *Liouvillian* part of the method, respectively. Of course in real applications of the MCWF method the first-order time evolution as obtained from eq. (2.13) would lead to stability problems. Instead, this integration step has to be performed with a stable method as the integration in sec. 2.2.1.

Let us now consider N trajectories labeled $|\psi_n(t)\rangle$, obtained with different seeds for the random number generator, all starting with the same initial condition $|\psi_n(0)\rangle = |\psi\rangle$. We define the ensemble average

$$\overline{\sigma}_N(t) := \frac{1}{N}\sum_{n=1}^{N} |\psi_n(t)\rangle \langle\psi_n(t)| . \tag{2.18}$$

In the limit $N \to \infty$, the averaged density operator $\overline{\sigma}(t) := \lim_{N\to\infty} \overline{\sigma}_N$ can be shown to be a solution of the original master equation [2.14]

$$\frac{\mathrm{d}}{\mathrm{d}t}\overline{\sigma}(t) = \mathcal{L}\overline{\sigma}(t). \tag{2.19}$$

If $\rho(0) = |\psi\rangle\langle\psi|$ is a pure state, then $\rho(t) \equiv \overline{\sigma}(t)$ for all t. Truncation to finite N leads to an approximate solution $\rho(t) \approx \overline{\sigma}_N(t)$. In the general case of a mixed initial state $\rho(0) = \sum_i p_i |\psi^{(i)}\rangle\langle\psi^{(i)}|$ with $p_i > 0$ and $\sum_i p_i = 1$, the MCWF method can be carried out for each of the pure states $|\psi^{(i)}\rangle$ to obtain the trajectories $|\psi_n^{(i)}(t)\rangle$ and ensemble averages

$$\overline{\sigma}_N^{(i)}(t) = \frac{1}{N}\sum_{n=1}^{N} |\psi_n^{(i)}(t)\rangle \langle\psi_n^{(i)}(t)| . \tag{2.20}$$

The approximate solution of the master equation in this case is

$$\rho(t) \approx \sum_i p_i \overline{\sigma}_N^{(i)}(t). \tag{2.21}$$

In many cases it is not possible to reconstruct the density matrices $\overline{\sigma}_N^{(i)}(t)$ because of their size. Still one can use the MCWF method to obtain approximations to expectation values of system operators. If A is such a system operator and $\langle A\rangle(t) = \mathrm{tr}\{A\rho(t)\}$ is the trajectory of its expectation value, then

$$\langle A\rangle(t) \approx \frac{1}{N}\sum_{n=1}^{N}\sum_i p_i \langle\psi_n^{(i)}(t)|A|\psi_n^{(i)}(t)\rangle . \tag{2.22}$$

The prize to pay for the more favorable scaling with D instead of D^2 is that we have to average over a whole ensemble of quantum trajectories in order to obtain expectation values, and finite ensemble sizes always introduce statistical noise. It arises the question of convergence and if one gains from the MCWF method compared to integrating the master equation directly. An answer is given in [2.15], where it is shown that for a prescribed statistical error the scaling of the CPU time with D is in favour of the stochastic method for sufficiently large systems. Furthermore, in situations where the density matrix cannot be held in computer memory due to its size and integration of (2.9) becomes impossible, the MCWF method might still be able to provide valuable insight into the system dynamics, and single trajectories reflect microscopic processes [2.16]. Finally, while parallelising ODE solvers seems difficult and connected with considerable overhead, the MCWF method is intrinsically parallel and can easily take advantage of a high-performance computing cluster environment.

Chapter 3

Ultracold particles in optical resonators

3.1 Optical resonators

Many objects in everyday live show iridescent behaviour, an apparent change of colour depending on the angle of view at which they are observed. Examples can be found in nature where the inside surface of certain sea shells or the wings of butterflies shimmer in all colours, but also in man made objects like compact discs and soap bubbles. These effects are caused by multiple beam interference when visible light is reflected many times on the two surfaces of a thin semi-transparent layer. Depending on the angle of observation, this interference is constructive for some wavelengths and destructive for others [3.1]. A Fabry-Pérot interferometer has the same underlying principle: two high-quality parallel mirrors reflect incident light many times, filtering out most wavelengths due to destructive interference, while certain narrow bandwidths of light can pass the device almost unmitigated [3.2]. The term optical resonator comes from a slightly different point of view: the space between the mirrors contains several modes of the electromagnetic field, which are capable of self-oscillations. The oscillator can be driven by shining light with a resonant frequency onto the mirrors, and at this frequency also the most energy is irradiated from the resonator by dissipation.

The Fabry-Pérot interferometer has become an invaluable tool both in classical optics and quantum optics. To name just a few examples, it is used for spectral analysis of light with very good resolution, as filter device in fiber optics networks of telecommunication and as resonator for many types of lasers. Optical resonators have improved to a degree where they can be used as 'containers' for light, storing photons for times on the order of several microseconds in the optical regime [3.3] and over a hundred milliseconds in the microwave regime [3.4]. This allows to explore non-classical states of the electromagnetic field, for example Fock states with a well-defined number of photons. Furthermore, compared to free space, a photon which is reflected many times can interact much more strongly with matter like ions, atoms or molecules inside the resonator. In the context of quantum optics the mirrors are usually curved instead of plain (cf. fig. 3.1a and section 3.2.1) and their distance is small, which increases the stability of the resonator mode. The term 'optical cavity', which we use as synonym for an optical resonator, is motivated by such a setup.

Even though we are interested in the optical cavity as a quantum device, it is instructive to review the classical theory of the Fabry-Pérot interferometer [3.5], as it

explains terms like the finesse, quality factor and linewidth of a resonator and their relations to each other, which can be directly applied to the quantum case.

Transmittance of a Fabry-Pérot interferometer

Figure 3.1b shows the idealised version of a Fabry-Pérot interferometer consisting of two transparent parallel plates at a distance d apart from each other, each with a non-reflective and a highly reflective surface. The electric field amplitude is attenuated by the factor r (the factor t) upon reflection (transmission) at the border from the optical thicker to the optical thinner region of the mirrored plate surface. The quantities r' and t' stand for reflection and transmission at the border from the optical thinner to the optical thicker region, respectively. The angle of incidence is $\theta \ll 1$ and we ignore any dependence of r and t on θ. A wave reflected inside the plate acquires a relative phase shift of π compared to a wave reflected at the outside, which is expressed by the relation $r = -r'$, and energy conservation requires $tt' = 1 - r^2$ [3.5]. As we are only interested in relative phase differences of the partial waves, we can describe the incident wave by its scalar complex amplitude E_0. Each round trip inside the interferometer results in a phase shift

$$\delta = \frac{4\pi d}{\lambda}\cos\theta = \frac{2\omega d}{c}\cos\theta, \tag{3.1}$$

where λ is the wavelength of the light, $\omega = 2\pi c/\lambda$ its angular frequency and c is the speed of light. The complex amplitude of the reflected light (cf. fig. 3.1b) can be written as

$$E_r = E_0 r + E_0 t r' t' e^{-\mathrm{i}\delta} + E_0 t r'^3 t' e^{-\mathrm{i}2\delta} + \dots \tag{3.2a}$$

$$= E_0\left[r + r' t t' e^{-\mathrm{i}\delta}\left(1 + (r'^2 e^{-\mathrm{i}\delta}) + (r'^2 e^{-\mathrm{i}\delta})^2 + \dots\right)\right] \tag{3.2b}$$

$$= E_0\left[r + \frac{r' t t' e^{-\mathrm{i}\delta}}{1 - r'^2 e^{-\mathrm{i}\delta}}\right] = E_0\left[\frac{r(1 - e^{-\mathrm{i}\delta})}{1 - r^2 e^{-\mathrm{i}\delta}}\right]. \tag{3.2c}$$

Similarly, the transmitted amplitude is

$$E_t = E_0 t t'\left[1 + r'^2 e^{-\mathrm{i}\delta} + (r'^2 e^{-\mathrm{i}\delta})^2 + \dots\right] = E_0\left[\frac{1 - r^2}{1 - r^2 e^{-\mathrm{i}\delta}}\right]. \tag{3.3}$$

The intensity of a light field with amplitude E is proportional to $|E|^2/2$. With eqs. (3.2) and (3.3) we can calculate the reflected Intensity $I_r \sim |E_r|^2/2$ and the transmitted Intensity $I_t \sim |E_t|^2/2$ in terms of the incident intensity $I_0 \sim |E_0|^2/2$:

$$\frac{I_r}{I_0} = \frac{F\sin^2(\delta/2)}{1 + F\sin^2(\delta/2)} \qquad \frac{I_t}{I_0} = \frac{1}{1 + F\sin^2(\delta/2)}, \tag{3.4}$$

where we have introduced the coefficient of finesse $F = \left(\frac{2r}{1-r^2}\right)^2$.

From now on let us consider orthogonal incident light, i.e. $\cos\theta = 1$. The transmitted intensity is maximal when $\delta = 2\pi n$ for integer n. For a fixed distance d, using eq. (3.1)

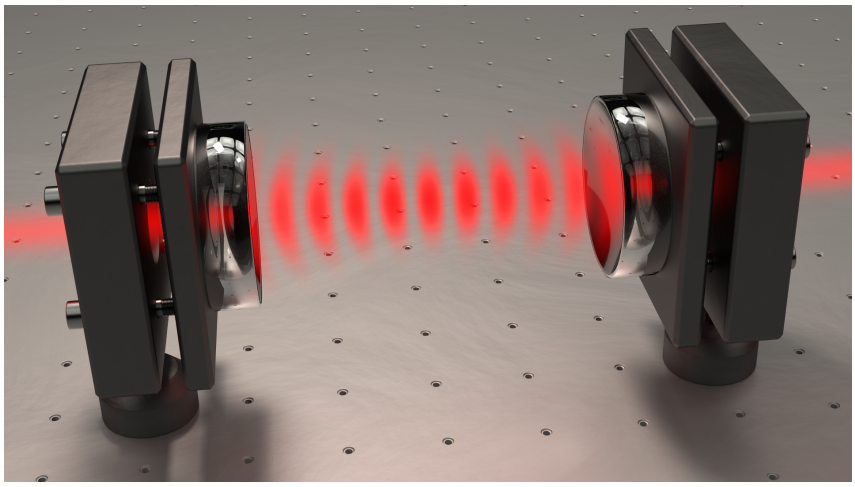

(a) Artist's view of a microwave resonator with spherical mirrors. The standing wave intensity pattern is visualised by a red glow. In the optical regime, the cavity length and mode waist is on the order of µm.

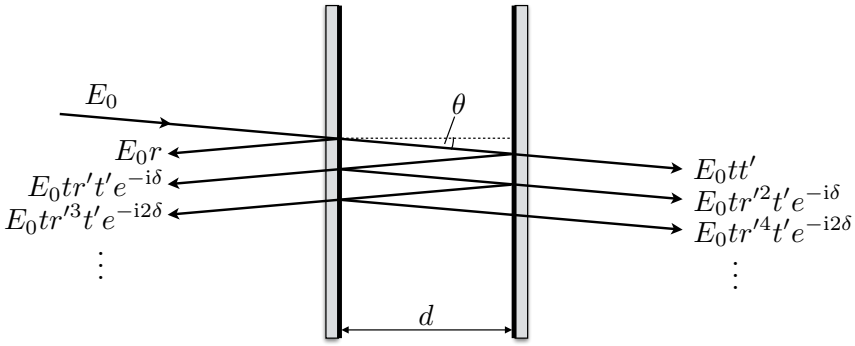

(b) An idealized Fabry-Pérot interferometer. The incident light wave arriving from the left is partly reflected and partly transmitted through the device. The partial waves with different numbers of round trips inside the resonator acquire different relative phases and attenuations and can interfere constructively or destructively.

Figure 3.1: Optical resonator and schematic view.

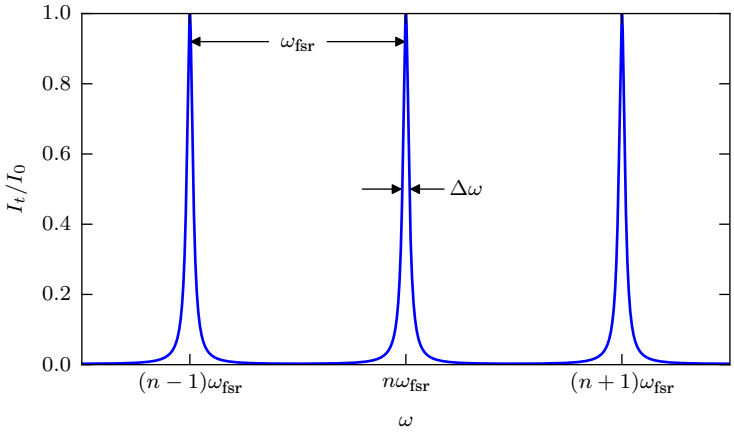

Figure 3.2: The transmittance of a Fabry-Pérot interferometer with highly reflecting mirrors ($r = 0.95$ in this case) has sharp maxima at frequencies separated by the free spectral range ω_{fsr}. The linewidth $\Delta\omega$ is equal to the intensity damping rate of the resonator.

this condition in terms of the frequency of the light is $\omega = n\pi c/d$. Two frequencies of maximal transmittance are separated by the free spectral range $\omega_{\mathrm{fsr}} = \pi c/d$. The transmittance function, which is also called Airy function, is plotted in fig. 3.2.

Linewidth, finesse and decay rate

The linewidth $\Delta\omega$ of an optical resonator is defined as the full width at half maximum of the transmittance function in frequency space (cf. fig. 3.2). From its definition it is apparent that the Airy function reaches $1/2$ whenever its argument is $\delta_{\max} \pm \delta_{1/2}$, where $\delta_{\max}$ is the position of a maximum and

$$\delta_{1/2} = 2 \arcsin\left(\frac{1}{\sqrt{F}}\right) \approx \frac{2}{\sqrt{F}}. \tag{3.5}$$

The approximation holds for large reflectivities, i.e. $1/\sqrt{F} \ll 1$. By solving eq. (3.1) for ω and inserting $\delta_{1/2}$, we find

$$\omega_{1/2} = \frac{c}{d\sqrt{F}} = \frac{\omega_{\mathrm{fsr}}}{\pi\sqrt{F}}, \tag{3.6}$$

and the linewidth is $\Delta\omega = 2\omega_{\mathrm{fsr}}/(\pi\sqrt{F})$. The ratio of the free spectral range to the linewidth is called finesse $\mathcal{F}$, it only depends on the reflectivity of the mirrors:

$$\mathcal{F} \equiv \frac{\omega_{\mathrm{fsr}}}{\Delta\omega} = \frac{\pi\sqrt{F}}{2} = \frac{\pi|r|}{1-r^2}. \tag{3.7}$$

The decay rate γ of the intra-cavity intensity in the absence of external driving can be estimated by the following consideration: the light is reflected once each half

round trip inside the resonator, which is completed in a time d/c. Therefore the fractional intensity loss during this time is $1 - r^2$, and we can calculate the rate γ as

$$\gamma = \frac{1 - r^2}{d/c} = \frac{(1 - r^2)\omega_{\mathrm{fsr}}}{\pi} = \frac{|r|\omega_{\mathrm{fsr}}}{\mathcal{F}} \approx \Delta\omega. \tag{3.8}$$

This clearly demonstrates the connection between linewidth and intensity decay rate (or equivalently photon decay rate) of an optical resonator. It is worth noting that the correspondence eq. (3.8) holds for the angular frequency of the light, measured in radians per seconds. In terms of the ordinary frequency ν measured in hertz it reads $\gamma = 2\pi\Delta\nu$. Usually, in the literature of experimental physics one finds $\gamma/(2\pi)$ quoted in hertz.

Instead of the decay rate for the intensity we use the decay rate of the field amplitude $\kappa = \gamma/2$ throughout the remainder of this thesis. In addition to the finesse, a commonly used quantity to describe the behaviour of a resonant system is the quality factor $Q = \omega_0/\Delta\omega$, the ratio between the resonance frequency and the linewidth. A 'high-Q optical resonator' is one where the light is stored for a long time compared to its optical period. The following relations connect the decay rate, the finesse and the quality factor:

$$\kappa = \frac{\omega_{\mathrm{fsr}}}{2\mathcal{F}} = \frac{\omega_0}{2Q}. \tag{3.9}$$

3.2 Quantisation of the electromagnetic field

Maxwell's equations exhibit a distinctive wavelike character of radiation and explain beautifully phenomena like interference and diffraction of light. They also give rise to independent orthogonal modes of the free electromagnetic field, each of which has a fixed spatial form and harmonic time dependence, whereas the only remaining free parameter is a complex amplitude. Therefore each mode resembles a harmonic oscillator, and in the classical theory the energy of such an oscillator is a continuous quantity which can have any value.

At the beginning of the 20th century, in contrast to believes prevalent at that time, Max Planck postulated that the exchange of energy between radiation of frequency ν and the oscillators in the walls of a black body (one which only absorbs and emits but does not reflect or transmit radiation) is only possible in discrete portions of $h\nu$ [3.6]. This idea, even though reluctantly embraced by Planck himself, enabled him to correctly reproduce the experimentally observed spectral energy density of the black-body radiation. The new fundamental constant h, which today is named after Planck, lies at the heart of modern quantum physics. Albert Einstein went one step further by realising that the discrete energy exchange is not some strange property of the black-body's oscillators, rather it is the electromagnetic field itself which is quantized [3.7]. He developed a theory where light travels in discrete wave packets with energy $h\nu$, now known as photons [3.7]. A prominent experimental manifestation of the photon is the photoelectric effect which Einstein was able to explain in his

work: light shined on metal can dissociate electrons, but only if a threshold frequency is reached, regardless of the intensity of the light. Below this threshold, each photon does not carry enough energy to overcome the electrons' binding energy. For the same reason, above threshold, the energy of the emitted electrons only depends on the frequency and not on the intensity of the light.

Because every field mode behaves like a harmonic oscillator, the mathematical description is completely analogous to that of a mechanical oscillator*[3.1, 3.9]. For each mode l with frequency ω_l and mode function $\boldsymbol{f}_l(\boldsymbol{r})$ there are operators $\hat{a}_l$ and $\hat{a}_l^\dagger$, which destroy and create a photon in this mode, respectively. They follow the bosonic commutation relation $[\hat{a}_l, \hat{a}_{l'}^\dagger] = \delta_{ll'}$. The Hamilton operator of the electromagnetic field in a resonator with subtracted zero point energy can be written as

$$H_\mathrm{F} = \sum_l \hbar\omega_l \hat{a}_l^\dagger \hat{a}_l. \tag{3.10}$$

The mode functions constitute an orthogonal system which is expressed by the relation $\int \boldsymbol{f}_l^*(\boldsymbol{r}) \cdot \boldsymbol{f}_{l'}(\boldsymbol{r}) \mathrm{d}^3\boldsymbol{r} = \delta_{ll'} V_l$, where V_l is the mode volume. They are solutions of the Helmholtz equation

$$\Delta \boldsymbol{f}_l(\boldsymbol{r}) + \frac{\omega_l^2}{c^2} \boldsymbol{f}_l(\boldsymbol{r}) = 0. \tag{3.11}$$

Boundary conditions such as a vanishing tangential electric field at the cavity mirrors determine the possible values of ω_l. The electric field operator of a single mode in the Schrödinger picture can be expressed as a linear combination of $\hat{a}_l$ and $\hat{a}_l^\dagger$:

$$\hat{\boldsymbol{E}}_l(\boldsymbol{r}) = \mathrm{i}\sqrt{\frac{\hbar\omega_l}{2\varepsilon_0 V_l}} \left(\boldsymbol{f}_l(\boldsymbol{r}) \hat{a}_l - \boldsymbol{f}_l^*(\boldsymbol{r}) \hat{a}_l^\dagger \right), \tag{3.12}$$

where ε_0 is the vacuum permittivity.

We will now discuss two configurations with relevance to this thesis in more detail: the field inside a standing-wave cavity with spherical mirrors and plain waves in free space.

3.2.1 Standing-wave cavity

A cavity with spherical mirrors (cf. fig. 3.1a) supports an infinite number of fundamental TEM_{00} Gaussian modes, for each fixed number of anti-nodes n there are two degenerate modes with orthogonal polarisation. The two mode functions in paraxial approximation can be written as [3.9]

$$\boldsymbol{f}_{1,2}(r,x) = \boldsymbol{\epsilon}_{1,2} \frac{w0}{w(x)} \exp\left(-\frac{r^2}{w(x)^2}\right) \cos\left(kx - \arctan\frac{2x}{kw_0^2} + \frac{kr^2}{2R(x)} + \frac{(n-1)\pi}{2}\right), \tag{3.13a}$$

*In the framework of non-relativistic quantum electrodynamics, the equations of motion of the electromagnetic field coupled to charges moving slowly compared to the speed of light can be derived from a standard Lagrangian. Quantisation is then performed in a canonical way by assigning operators and appropriate commutation relations to the truly independent variables and associated conjugate momenta [3.8]. Here we only present the results relevant to this thesis.

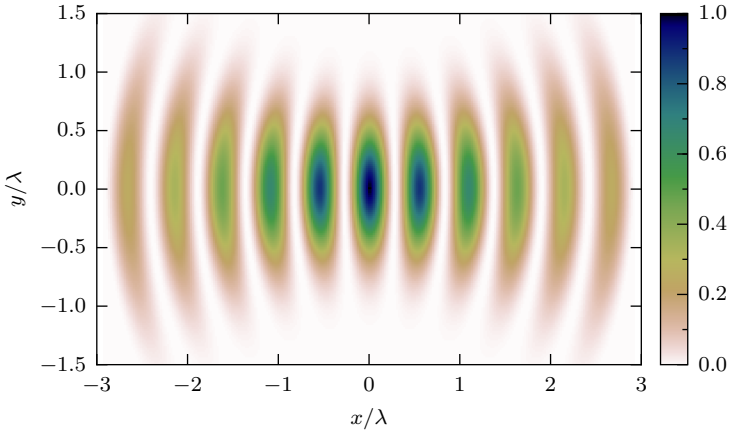

Figure 3.3: Cut through the mode function $|\boldsymbol{f}_{1,2}(r,x)|^2$ inside a standing-wave cavity with spherical mirrors as given by eq. (3.13). Near the cavity center the wave fronts are approximately plain.

with

$$w(x) = w_0\sqrt{1+\left(\frac{2x}{kw_0^2}\right)^2} \qquad R(x) = x\left(1+\left(\frac{kw_0^2}{2x}\right)^2\right). \tag{3.13b}$$

The cavity is aligned along the x-axis with the origin at the cavity center between the two mirrors, $r = \sqrt{y^2+z^2}$ is the radial distance from the center line, w_0 is the minimum width of the mode at $x = 0$, $\boldsymbol{\epsilon}_{1,2}$ are two orthogonal polarisation unit vectors (possibly complex) and $R(x)$ is the radius of the wave-front at position x. The cavity length is $L \approx n\lambda/2$ where $\lambda = 2\pi/k$ is the wave length associated to the mode. Near the cavity center the curvature becomes zero and the wave fronts are plain as shown in fig. 3.3. At the position of the mirrors, the wave-front radius coincides with that of the mirrors, $R(\pm L/2) \equiv R$. The mode waist w_0 is determined by R through eq. (3.13b) and the mode volume is given by

$$V = \frac{\pi}{4}w_0^2 L. \tag{3.14}$$

We assume that all particles interacting with the cavity are located near the cavity center where the true mode function is well approximated by

$$\boldsymbol{f}_{1,2}(r,x) = \boldsymbol{\epsilon}_{1,2}\exp\left(-\frac{r^2}{w_0^2}\right)\begin{cases}\cos(kx) & \text{for } n \text{ odd}\\ \sin(kx) & \text{for } n \text{ even.}\end{cases} \tag{3.15}$$

Additionally, in all our models the particles are confined to one dimension along the x-axis by an appropriate trap and the polarisation is fixed by the particle's dipole

moment orientation. We are left with an effectively one dimensional mode function $\boldsymbol{f}(x) = \boldsymbol{\epsilon}\cos(kx)$ (or $\sin(kx)$), the free cavity Hamiltonian

$$H_{\mathrm{F}} = \hbar\omega_{\mathrm{c}}\hat{a}^{\dagger}\hat{a} \tag{3.16}$$

and the electric field operator

$$\hat{\boldsymbol{E}}(x) = \mathrm{i}\sqrt{\frac{\hbar\omega_{\mathrm{c}}}{2\varepsilon_0 V}}\cos(kx)\left(\boldsymbol{\epsilon}\hat{a} - \boldsymbol{\epsilon}^{*}\hat{a}^{\dagger}\right), \tag{3.17}$$

where $\omega_{\mathrm{c}} = ck$ and V is given by eq. (3.14).

3.2.2 Plain waves

The free electromagnetic field is conveniently quantised by introducing a cubic volume with edge length L and by imposing periodic boundary conditions. The volume has to be large compared to the relevant experimental scales so that all expectation values are independent of L. Taking the limit $L \to \infty$ in the end yields the free space case. This approach leads to plain wave mode functions of the form

$$\boldsymbol{f}_{\boldsymbol{k}\sigma}(\boldsymbol{r}) = \boldsymbol{\epsilon}_{\boldsymbol{k}\sigma}\mathrm{e}^{\mathrm{i}\boldsymbol{k}\cdot\boldsymbol{r}} \tag{3.18}$$

which are indexed by the wave vector $\boldsymbol{k}$ and the polarisation $\sigma \in \{1, 2\}$. The two polarisation vectors $\boldsymbol{\epsilon}_{1,2}$ are orthogonal to each other and to $\boldsymbol{k}$. For linear polarisation, the vectors can be chosen real, whereas complex vectors describe elliptically or circularly polarised light.

The periodic boundary conditions define the discrete values of the wave vector

$$\boldsymbol{k} = \frac{2\pi}{L}(n_x, n_y, n_z) \qquad n_x, n_y, n_z \in \mathbb{N}, \tag{3.19}$$

and the mode frequencies $\omega_{\boldsymbol{k}}$ through the dispersion relation $\omega_{\boldsymbol{k}} = c|\boldsymbol{k}|$. The operator of the electric field is the sum over all single-mode operators eq. (3.12):

$$\hat{\boldsymbol{E}}(\boldsymbol{r}) = \mathrm{i}\sum_{\boldsymbol{k},\sigma}\sqrt{\frac{\hbar\omega_{\boldsymbol{k}}}{2\varepsilon_0 L^3}}\left(\boldsymbol{\epsilon}_{\boldsymbol{k}\sigma}\mathrm{e}^{\mathrm{i}\boldsymbol{k}\cdot\boldsymbol{r}}\hat{a}_{\boldsymbol{k}\sigma} - \boldsymbol{\epsilon}^{*}_{\boldsymbol{k}\sigma}\mathrm{e}^{-\mathrm{i}\boldsymbol{k}\cdot\boldsymbol{r}}\hat{a}^{\dagger}_{\boldsymbol{k}\sigma}\right). \tag{3.20}$$

3.3 Jaynes-Cummings model

The simplest possible non-trivial model for coupling matter to radiation consists of a single two-level atom, fixed in space, interacting with a single cavity mode. This so-called Jaynes-Cummings model [3.10] is analytically solvable and still contains enough physics to be relevant for real experiments.

Strictly speaking there are no two-level atoms. In fact, an atom with electrons moving in the electrostatic potential of the core (neglecting coupling to the transverse electromagnetic field for the moment) has an infinite number of discrete bound

eigenstates. However, under the condition that we can single out two atomic states, a ground state $|g\rangle$ and an excited state $|e\rangle$ separated by an energy $\hbar\omega_\mathrm{a}$, as well as a single cavity mode (cf. fig. 3.2) with frequency ω_c near ω_a, the James-Cummings model can provide satisfactory results. We assume that ω_a is far detuned from all other cavity resonance frequencies, and that all other atomic transition frequencies are far detuned from any cavity mode[†]. The neglected states and cavity modes can be treated in perturbation theory and lead to small energy shifts, which we assume to be integrated into ω_a and ω_c. Finally we assume that the atom is tightly trapped or very heavy, so that we can neglect its center-of-mass motion on experimental timescales. The full Hamiltonian of the model

$$H = H_0 + H_\mathrm{int} \tag{3.21}$$

is the sum of the free Hamiltonian describing the uncoupled subsystems

$$H_0 = \hbar\omega_\mathrm{c}\hat{a}^\dagger\hat{a} + \omega_\mathrm{a}\hat{\sigma}^\dagger\hat{\sigma} \tag{3.22}$$

and their interaction Hamiltonian H_int, which we will discuss below. Here, the operators $\hat{\sigma} = |g\rangle\langle e|$ and $\hat{\sigma}^\dagger = |e\rangle\langle g|$ correspond to de-excitation and excitation of the atom, respectively.

As previously discussed, an electric field mode is a harmonic oscillator like a mass on a spring. Likewise, the mathematical description of a two-level atom is analogue to a spin-½: The state of a two-level atom can be mapped to a point (Bloch vector) on the unit sphere (Bloch sphere). With the north and south pole being mapped to $|e\rangle$ and $|g\rangle$, respectively, free evolution of the atom corresponds to a rotation of the Bloch vector around the z-axis, whereas coherent driving of the atom corresponds to a rotation around an axis in the x-y-plane. In this sense the Jaynes-Cummings model is the theory of coupling a spring to a spin (spin boson model) [3.9]. The coupling Hamiltonian in dipole- and long-wavelength approximation reads

$$H_\mathrm{int} = -\hat{\boldsymbol{d}} \cdot \hat{\boldsymbol{E}}(X), \tag{3.23}$$

where X is the position of the atom and $\hat{\boldsymbol{d}}$ is the atomic dipole operator. The hydrogen atom for example has $\hat{\boldsymbol{d}} = q\hat{\boldsymbol{r}}$, where $\hat{\boldsymbol{r}}$ is the position operator of the electron relative to the core and q is the charge of the electron. Equation 3.23 is the first term of a multipole expansion of the electromagnetic field [3.8]. It is justified to keep only the dipole term in this expansion if the dipole moment of our two states does not vanish and if the wavelength of the mode is large compared to the size of the atom, which is usually the case in cavity QED.

For symmetry reasons a neutral atom has no permanent dipole, i.e. $\langle g|\hat{\boldsymbol{d}}|g\rangle = \langle e|\hat{\boldsymbol{d}}|e\rangle = 0$, and we can write the dipole operator in the atomic basis as

$$\hat{\boldsymbol{d}} = \boldsymbol{d}\hat{\sigma} + \boldsymbol{d}^*\hat{\sigma}^\dagger, \tag{3.24}$$

[†]Far detuned in this context means with respect to the characteristic frequencies like the linewidth of the states in question and the coupling strength between cavity and atom

where $\boldsymbol{d} = \langle g|\hat{\boldsymbol{d}}|e\rangle$. We can make $\boldsymbol{d}\cdot\boldsymbol{\epsilon}$ purely imaginary by choosing the phase of $|g\rangle$ and $|e\rangle$, then by using eq. (3.17) the interaction Hamiltonian becomes

$$H_{\mathrm{int}} = \mathrm{i}\sqrt{\frac{\hbar\omega_{\mathrm{c}}}{2\varepsilon_0 V}}\cos(kX)(\boldsymbol{d}\hat{\sigma} + \boldsymbol{d}^*\hat{\sigma}^\dagger)\cdot(\boldsymbol{\epsilon}\hat{a} - \boldsymbol{\epsilon}^*\hat{a}^\dagger). \tag{3.25}$$

In the Hamiltonian (3.25), the terms proportional to $\hat{\sigma}\hat{a}^\dagger$ and $\hat{\sigma}^\dagger\hat{a}$ correspond to energy conserving processes where an excitation is exchanged between the atom and the mode, whereas $\hat{\sigma}\hat{a}$ and $\hat{\sigma}^\dagger\hat{a}^\dagger$ correspond to energy non-conserving processes with the simultaneous (de-)excitation of the atom and the mode. In an interaction picture with respect to H_0 one finds the former terms oscillating with the *difference* of the frequencies ω_{c} and ω_{a}, whereas the latter oscillate with the *sum* of these frequencies. Arguing that the rapidly oscillating terms average out quickly during the evolution of the system, these terms are ignored in the rotating wave approximation (RWA) [3.11]. We can make $\boldsymbol{d}\cdot\boldsymbol{\epsilon}^*$ purely imaginary by choosing the phase of $|g\rangle$ and $|e\rangle$ so that eq. (3.21) becomes the Jaynes-Cummings Hamiltonian

$$H = \hbar\omega_{\mathrm{c}}\hat{a}^\dagger\hat{a} + \hbar\omega_{\mathrm{a}}\hat{\sigma}^\dagger\hat{\sigma} + \hbar g(X)(\hat{\sigma}\hat{a}^\dagger + \hat{\sigma}^\dagger\hat{a}) \tag{3.26}$$

with the coupling constant

$$g(X) = -\mathrm{i}\boldsymbol{d}\cdot\boldsymbol{\epsilon}^*\sqrt{\frac{\omega_{\mathrm{c}}}{2\hbar\varepsilon_0 V}}\cos(kX). \tag{3.27}$$

The eigenstates of the system without coupling is given by the tensor products $|g,n\rangle$ and $|e,n\rangle$ where $|n\rangle$ is a Fock state of the field mode. The Hamiltonian commutes with the operator for the total number of excitations

$$M = \hat{a}^\dagger\hat{a} + \hat{\sigma}^\dagger\hat{\sigma}, \tag{3.28}$$

which consequently is a constant of motion. The Hilbert space can be decomposed into invariant subspaces

$$\mathcal{H} = \bigoplus_{n\in\mathbb{N}} \mathcal{H}_n, \tag{3.29}$$

where $\mathcal{H}_0$ is spanned by $|g,0\rangle$ and $\mathcal{H}_n$, $n>0$, is spanned by the doublets $|g,n\rangle$ and $|e,n-1\rangle$. In this basis, the matrix representation of H on the manifold $\mathcal{H}_n$ $(n>0)$ is

$$H_n = \hbar\begin{pmatrix} n\omega_{\mathrm{c}} & \Omega_n/2 \\ \Omega_n/2 & n\omega_{\mathrm{c}} - \Delta \end{pmatrix}, \tag{3.30}$$

where $\Omega_n = 2g(X)\sqrt{n}$ is called *n-photon Rabi frequency* and $\Delta = \omega_{\mathrm{c}} - \omega_{\mathrm{a}}$ is the detuning between cavity and atom. As a consequence of the RWA, the problem of diagonalising H is reduced to diagonalising 2×2 matrices of the form eq. (3.30). It is worth noting that this Hamiltonian is formally equivalent to that of a spin-½ placed in a magnetic field with a component proportional to Δ along the quantisation axis z and a component proportional to Ω_n along the x-axis. With the definition

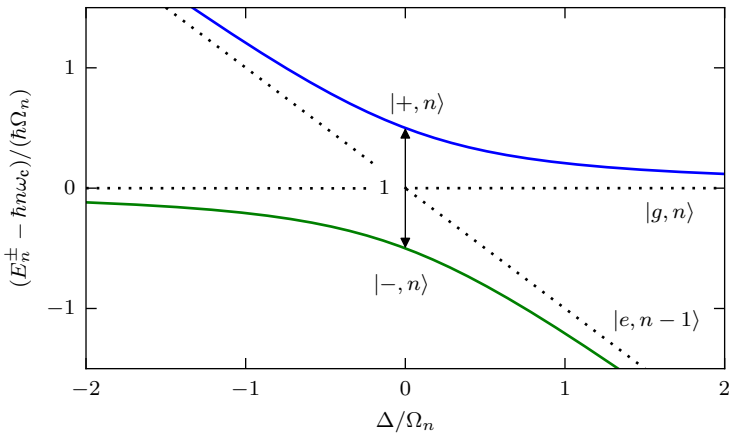

Figure 3.4: Energy of the dressed states (solid) and the uncoupled states (dotted) as a function of the cavity-atom detuning Δ. The coupling turns the level crossing into an avoided crossing with energy splitting $\hbar\Omega_n = 2\hbar g\sqrt{n}$ at resonance, which increases with the total number of excitations n.

$\tilde{\Omega}_n := \sqrt{\Delta^2 + \Omega_n^2}$, the eigenvalues $E_n^{\pm}$ and corresponding normalised eigenstates $|\pm, n\rangle$ of H_n are [3.12]

$$E_n^{\pm} = \hbar n\omega_c - \hbar\frac{\Delta}{2} \pm \hbar\frac{\tilde{\Omega}_n}{2} \tag{3.31a}$$

$$\begin{aligned} |+,n\rangle &= \cos(\theta_n/2)\,|g,n\rangle + \sin(\theta_n/2)\,|e,n-1\rangle \\ |-,n\rangle &= -\sin(\theta_n/2)\,|g,n\rangle + \cos(\theta_n/2)\,|e,n-1\rangle\,, \end{aligned} \tag{3.31b}$$

where the mixing angle θ_n is the angle of the fictitious magnetic field with the z-axis, i.e. $\tan\theta_n = \Omega_n/\Delta$. Using basic trigonometric identities, the components of the eigenstates can be expressed in terms of the physical parameters:

$$\cos\frac{\theta_n}{2} = \sqrt{\frac{\tilde{\Omega}_n + \Delta}{2\tilde{\Omega}_n}} \qquad \sin\frac{\theta_n}{2} = \sqrt{\frac{\tilde{\Omega}_n - \Delta}{2\tilde{\Omega}_n}}. \tag{3.32}$$

The eigenstates eq. (3.31b) describe combined excitations of the bare atom 'dressed' with the cavity field, hence their name *dressed states*. Figure 3.4 shows their energies as a function of the detuning Δ. At resonance ($\Delta = 0$) where the energies of the uncoupled states cross, the coupling results in an avoided crossing with minimal energy splitting $\hbar\Omega_n$ (*normal mode splitting*). In this regime, a ground state atom placed in the cavity with a Fock state of n photons undergoes Rabi oscillations: the probability of finding the atom in the excited state oscillates with frequency Ω_n in time between 0 and 1. In the *strong coupling regime* where the coupling g is much larger than the decay rate of both the cavity and the atom, Rabi oscillations and normal mode splitting are visible even on the single-photon level [3.13].

In the opposite far detuned regime $|\Delta| \gg \Omega_n$, the dressed states approach the uncoupled states as can be seen in fig. 3.4 and from eq. (3.31b). To lowest order in $\Omega_n/|\Delta|$, the energies $E_{g,n}$ and $E_{e,n}$ of the uncoupled states are shifted as a result of the coupling according to

$$\delta E_{g,n} = \hbar \frac{g(X)^2}{\Delta} n \tag{3.33a}$$

$$\delta E_{e,n} = -\hbar \frac{g(X)^2}{\Delta} (n+1). \tag{3.33b}$$

From the point of view of the cavity, the atom acts as a dielectric which has an index of refraction and shifts the mode frequency by

$$\delta\omega_\mathrm{c} = \pm \frac{g(X)^2}{\Delta}, \tag{3.34}$$

where the positive (negative) sign holds for an atom in its ground (excited) state. From the point of view of the atom which is brought into a cavity with n photons, the shifts can be interpreted as light shifts of the atomic states and the transition frequency:

$$\delta\omega_\mathrm{a} = -\frac{g(X)^2}{\Delta} (2n+1). \tag{3.35}$$

This shift has a contribution proportional to the photon number and a constant Lamb shift contribution induced by the interaction of the excited atomic state with the cavity vacuum fluctuations. Note that $g(X)$ has a periodic spatial dependency, the gradients of the light shifts eqs. (3.33a) and (3.33b) are proportional to the dipole force a cavity exerts on an atom in its ground state or excited state, respectively. For ground state atoms, positive detuning results in a force towards the nodes of the mode (low-field-seeker), whereas for negative detuning the force is directed towards the anti-nodes (high-field-seeker). This aspect is further discussed in sec. 3.4.1.

3.4 Master equation for moving particles in a cavity

Let us extend the simple Jaynes-Cummings model to N atoms and take into account several important aspects: center-of-mass motion of the two-level atoms along the cavity axis, coherent driving of the cavity or the atom with a laser of frequency ω_L, and dissipation via spontaneous emission from the atoms or loss of photons through the cavity mirrors. In the regime of ultracold particles, quantum fluctuations of the atomic motion become relevant, and the motion has to be described by the momentum operator $\hat{P}$ and position operator $\hat{X}$ with the canonical commutation relation $[\hat{X}, \hat{P}] = \mathrm{i}\hbar$. Dissipation is introduced through coupling to the environment, which is formed by the continuum of electromagnetic field modes in our case. Consequently, instead of Schrödinger's equation for a state vector the system has to be described by a master equation acting on a density matrix (cf. sec. 2.1). In this section we discuss

the structure of the master equation and some approximations with relevance to this thesis [3.14].

In the master equation

$$\dot{\rho} = -\frac{\mathrm{i}}{\hbar}\,[H,\rho] + \mathcal{L}\rho \tag{3.36}$$

the Hamiltonian H describes coherent evolution and the super-operator $\mathcal{L}$ is responsible for dissipation. H can be written as

$$H = -\hbar\Delta_\mathrm{c}\hat{a}^\dagger\hat{a} + \sum_{j=1}^{N}\left[\frac{\hat{P}_j^2}{2M} - \hbar\Delta_\mathrm{a}\hat{\sigma}_j^\dagger\hat{\sigma}_j + \hbar g\cos(k\hat{X}_j)(\hat{\sigma}_j^\dagger\hat{a} + \hat{\sigma}_j\hat{a}^\dagger)\right] + H_\mathrm{L}, \tag{3.37}$$

where we introduced the constant of maximal atom-field coupling $g \equiv g(0)$, and the laser pump is described by

$$H_\mathrm{L} = \begin{cases} \sum_{j=1}^{N}\hbar\Omega(\hat{\sigma}_j + \hat{\sigma}_j^\dagger) & \text{transversal pump of the atoms} \\ \hbar\eta(\hat{a} + \hat{a}^\dagger) & \text{longitudinal pump through the mirror.} \end{cases} \tag{3.38}$$

The first case applies to a laser pumping the atoms from the side with a coupling strength Ω, whereas the second case corresponds to a laser pumping the cavity directly through one of the semi-transparent mirrors with a coupling strength η. We assume Ω and η to be real for the sake of a slightly simpler notation. The contribution of each particle is labeled with the index j. Equation (3.37) is reported in a reference frame rotating with the laser frequency, therefore eq. (3.38) is time-independent and the free evolution of the cavity and the internal dynamics of the atom are proportional to the detunings $\Delta_\mathrm{c} = \omega_\mathrm{L} - \omega_\mathrm{c}$ and $\Delta_\mathrm{a} = \omega_\mathrm{L} - \omega_\mathrm{a}$, respectively. In the kinetic energy term of the atoms, $\hat{P}_j$ is the center-of-mass momentum operator and M is the total mass of the particle. Coupling between the cavity and the particles in RWA and long-wavelength approximation is similar to the Jaynes-Cummings case (3.26), with the difference that this time the center-of-mass position operator $\hat{X}_j$ in the argument of the cavity field mode function makes the coupling position-dependent and describes the mechanical recoil connected to the emission or absorption of a cavity photon by an atom.

The Liouvillian $\mathcal{L}$ of the master equation (3.36) is

$$\begin{aligned}\mathcal{L}\rho = {}& \kappa\left(2\hat{a}\rho\hat{a}^\dagger - \hat{a}^\dagger\hat{a}\rho - \rho\hat{a}^\dagger\hat{a}\right) \\ & + \gamma\left(-\hat{\sigma}^\dagger\hat{\sigma}\rho - \rho\hat{\sigma}^\dagger\hat{\sigma} + 2\int_{-1}^{1}\mathrm{d}u\,N(u)\hat{\sigma}\mathrm{e}^{-\mathrm{i}ku\hat{X}}\rho\hat{\sigma}^\dagger\mathrm{e}^{\mathrm{i}ku\hat{X}}\right).\end{aligned} \tag{3.39}$$

The first summand proportional to the cavity field decay rate κ takes into account loss of photons through the cavity mirrors, whereas the second summand proportional to the atomic coherence decay rate γ accounts for the effect of photons spontaneously emitted from excited atoms into free space. In this process, the anisotropy of dipole radiation is reflected by the normalised distribution

$$N(u) = \frac{3}{8}\left(1 + u^2\left(1 - 3\tilde{u}^2\right) + \tilde{u}^2\right). \tag{3.40}$$

Here, u and $\tilde{u}$ are the normalised projections of the photon emission direction and of the atomic dipole vector $\boldsymbol{d}$ onto the cavity axis, respectively. $N(u)$ is obtained by making use of the symmetry with respect to rotation around the cavity axis and integrating the full angular distribution of dipole radiation [3.15] over the azimuth angle. The momentum recoil associated with the spontaneous emission of photons is represented by the momentum kick operators $\mathrm{e}^{\pm \mathrm{i}ku\hat{X}}$.

Let us add a few additional remarks concerning the validity of the master equation eq. (3.36). We neglect collisional scattering between the particles, which is justified for low densities or spin-polarised fermions without s-wave scattering. In the microwave regime, thermal photons usually play an important role and lead to additional jump operators in the Liouvillian eq. (3.39). At optical frequencies, however, thermal photons can be safely ignored even at room temperature. For the coupling of the atoms to the environment we assumed that each particle interacts with its individual bath, ignoring effects like free-space dipole-dipole interaction. This is justified if the particles are far apart from each other compared to the optical wavelength or if the atomic dipole is small, e.g. in the low-excitation regime discussed below. Finally, adding more cavity modes to the model is straight forward, for example to describe a ring cavity, just by adding the corresponding free Hamiltonians, interaction terms and Liouvillians to the master equation.

3.4.1 Important approximations

The dispersive regime

We are interested in the regime where the atomic detuning Δ_a is the largest frequency, i.e. $|\Delta_\mathrm{a}| \gg |\omega_\mathrm{sys}|$. Here, ω_sys stands for any of the 'system frequencies' $\kappa, \Delta_\mathrm{c}, \Omega, g$. Such a separation of timescales has the physical consequence that the fast internal atomic dynamics follow the much slower external dynamics of the laser and the cavity adiabatically, and the internal degrees of freedom can be eliminated from the picture. The effect of the internal degrees of freedom on the cavity and external motion can be described entirely by two-time correlation functions of $\hat{\sigma}^\dagger$ and $\hat{\sigma}$, corresponding to second order atomic excitation processes. The result is a master equation for the cavity and the center-of-mass atomic motion alone, where we have traced over the internal degrees of freedom. Note that we don't necessarily assume $|\Delta_\mathrm{a}| \gg \gamma$ at this point, so for now we will keep terms of order $\gamma/|\Delta_\mathrm{a}|$. As a consequence we find that the cavity introduces a new channel of dissipation where a cavity photon is lost by exciting the atom followed by spontaneous emission. Below we will discuss under which conditions spontaneous emission can be neglected.

The technical details of the adiabatic elimination are described in sec. 3.5, here we present the resulting effective master equation

$$\dot{\rho} = -\frac{\mathrm{i}}{\hbar}\left[H_\mathrm{eff}, \rho\right] + \mathcal{L}_\mathrm{eff}\rho, \tag{3.41a}$$

where

$$H_{\text{eff}} = -\hbar\left[\Delta_{\text{c}} - \sum_{j=1}^{N} U_0 \cos^2(k\hat{X}_j)\right]\hat{a}^\dagger\hat{a} + \sum_{j=1}^{N}\frac{\hat{P}_j^2}{2M} + H_{\text{L,eff}} \tag{3.41b}$$

$$\begin{aligned}\mathcal{L}_{\text{eff}}\rho = {}& \kappa(2\hat{a}\rho\hat{a}^\dagger - \hat{a}^\dagger\hat{a}\rho - \rho\hat{a}^\dagger\hat{a}) \\ & + \gamma_{\text{eff}}\sum_{j=1}^{N}\left[-\hat{b}_j^\dagger\hat{b}_j\rho - \rho\hat{b}_j^\dagger\hat{b}_j + 2\int_{-1}^{1}\mathrm{d}u\, N(u)\hat{b}_j\rho\hat{b}_j^\dagger\right]\end{aligned} \tag{3.41c}$$

$$\hat{b}_j = \left(\cos(k\hat{X}_j)\hat{a} + \frac{\Omega}{g}\right)e^{-\mathrm{i}ku\hat{X}_j} \tag{3.41d}$$

$$H_{\text{L,eff}} = \begin{cases}\sum_{j=1}^{N}\hbar\eta_{\text{eff}}\cos(k\hat{X}_j)(\hat{a}+\hat{a}^\dagger) & \text{transversal pump} \\ \hbar\eta(\hat{a}+\hat{a}^\dagger) & \text{longitudinal pump.}\end{cases} \tag{3.41e}$$

In the case of a longitudinally driven cavity the pump term is unchanged. If the particles are illuminated transversally, this term acts as an effective pump for the cavity mode with a strength and phase depending on the particle's position. The effective parameters of eq. (3.41) are

$$U_0 = \frac{\Delta_{\text{a}}g^2}{\Delta_{\text{a}}^2+\gamma^2} \qquad \eta_{\text{eff}} = \frac{\Delta_{\text{a}}g\Omega}{\Delta_{\text{a}}^2+\gamma^2} \qquad \gamma_{\text{eff}} = \frac{\gamma g^2}{\Delta_{\text{a}}^2+\gamma^2}. \tag{3.42}$$

In eq. (3.41b), the term $\hbar U_0\cos^2(k\hat{X}_j)\hat{a}^\dagger\hat{a}$ can be interpreted as a cavity frequency shift resulting from a position-dependent and fluctuating refractive index, or as a periodic optical potential for the particle depending on the fluctuating photon number. The sign of Δ_{a} also determines the sign of the cavity-particle detuning, as $\omega_{\text{c}} - \omega_{\text{a}} = \Delta_{\text{a}} - \Delta_{\text{c}} \approx \Delta_{\text{a}}$. From eq. (3.42) it is clear that in a cavity which is red-detuned from the particles (i.e. $\Delta_{\text{a}} < 0$ and $U_0 < 0$) particles are high-field-seekers, whereas for blue detuning (i.e. $\Delta_{\text{a}} > 0$ and $U_0 > 0$) particles are low-field-seekers.

Spontaneous emission

For the remainder of this thesis we will assume that the effective spontaneous emission γ_{eff} can be ignored. Let us specify in more detail under which experimental conditions this is achievable and justified.

In the regime $\gamma \ll |\Delta_{\text{a}}|$ we can approximate the effective parameters U_0, η_{eff} and γ_{eff} eq. (3.61) to lowest order in $\gamma/|\Delta_{\text{a}}|$:

$$U_0 \approx \frac{g^2}{\Delta_{\text{a}}} \qquad \eta_{\text{eff}} \approx \frac{g\Omega}{\Delta_{\text{a}}} \qquad \gamma_{\text{eff}} \approx \frac{\gamma g^2}{\Delta_{\text{a}}^2}. \tag{3.43}$$

For the case $\gamma \ll |\omega_{\text{sys}}|$ or $\gamma \sim |\omega_{\text{sys}}|$ spontaneous emission can be neglected as γ_{eff} is of the same order of magnitude as terms which have already been discarded in the derivation of eq. (3.41).

In the regime $\gamma \gg |\omega_{\text{sys}}|$ one might choose to increase the experimentally easily accessible parameters Δ_{a} and Ω while keeping $|\Omega|/|\Delta_{\text{a}}| \ll 1$ constant, until the

regime $\gamma \ll |\Delta_a|$ is reached. As a consequence γ_{eff} is again small compared to both U_0 and η_{eff} and spontaneous emission can be ignored. The effective pump strength η_{eff} is not affected by this scaling, however U_0 might become very small. For example, if the atoms are pumped from the side to study the effect of self-organisation (cf. part IV), then η_{eff} compared to a critical pump strength is the important parameter and U_0 might even tend toward zero. If, however, the cavity and not the atom is pumped, i.e. for $\Omega = \eta_{\text{eff}} = 0$, then U_0 is the only remaining parameter in which the effective coupling of the atom to the cavity becomes manifest. In this case it depends on the specific system at hand, whether for a given detuning, which should be large enough to suppress spontaneous emission, the cavity-atom coupling U_0 can be made sufficiently large to retain interesting physics. This might be achieved, for example, by reducing the cavity mode volume to increase g.

Strongly driven cavity limit

For the case that the cavity mode is strongly driven by the laser, a coherent steady state $|\alpha\rangle$ with

$$\alpha = \frac{\eta}{\kappa - \mathrm{i}\Delta_c} \tag{3.44}$$

establishes. If $|\alpha| \gg 1$ quantum fluctuations and also the back-action of the particles onto the cavity field are negligible. To describe such a situation with a classical coherent field we formally replace $\hat{a}$ with α and $\hat{a}^\dagger$ with α^* in the master equation [3.14].

3.5 Additional material: adiabatic elimination of the excited atomic state

In this section we discuss the details of the adiabatic elimination to derive the effective master equation (3.41) from the more general equation (3.36). To keep the notation simple we restrict ourselves to one particle, the extension to N particles is straight forward if we neglect dipole-dipole interaction.

In the dispersive limit where Δ_a is the largest frequency (cf. sec. 3.4.1), conceptually the adiabatic elimination is performed by a projection of the total density matrix ρ_tot onto the subspace of interest, where the internal degrees of freedom have been traced over. A formal solution for the projected master equation can be iteratively inserted back into itself, which yields an integrodifferential equation and an expansion in the small parameter $\varepsilon \sim |\omega_\mathrm{sys}|/|\Delta_\mathrm{a}|$, where ω_sys is any of the small frequencies Ω, g, κ and Δ_c. A master equation for the projected density matrix can be obtained by truncating this expansion after the quadratic term and justifying the Markov approximation, i.e. the future evolution depends only on the current state and not its past.

Let us now undertake these steps in more detail, following closely the derivations given in [3.16–3.18]. To demonstrate the technique we will start with a model without external motion in sec. 3.5.1 and then turn to the slightly more involved case in sec. 3.5.2 where the center-of-mass motion of the atom is retained.

3.5.1 Model without center-of-mass motion

First we write the master equation (3.36) with fixed position of the atom in the form

$$\dot{\rho}_\mathrm{tot}(t) = \mathcal{L}_\mathrm{a}\rho_\mathrm{tot}(t) + \varepsilon(\mathcal{L}_\mathrm{c} + \mathcal{L}_\mathrm{I})\rho_\mathrm{tot}(t) \tag{3.45a}$$

$$\mathcal{L}_\mathrm{a}\rho = \mathrm{i}\left[\Delta_\mathrm{a}\hat{\sigma}^\dagger\hat{\sigma}, \rho\right] + \gamma\mathcal{D}[\hat{\sigma}](\rho) \tag{3.45b}$$

$$\varepsilon\mathcal{L}_\mathrm{c}\rho = \mathrm{i}\left[\Delta_\mathrm{c}\hat{a}^\dagger\hat{a}, \rho\right] + \kappa\mathcal{D}[\hat{a}](\rho) \tag{3.45c}$$

$$\varepsilon\mathcal{L}_\mathrm{I}\rho = -\mathrm{i}g\left[\hat{\sigma}^\dagger\hat{a} + \hat{\sigma}\hat{a}^\dagger, \rho\right] - \mathrm{i}\Omega\left[\hat{\sigma}^\dagger + \hat{\sigma}, \rho\right], \tag{3.45d}$$

where we have made the separation of timescales explicit by inserting the small parameter $\varepsilon \ll 1$ to keep track of the order in the expansion. Then we define the projections

$$P\rho_\mathrm{tot} := \mathrm{tr}_\mathrm{a}\left\{\rho_\mathrm{tot}\right\} \otimes \lim_{t\to\infty} \exp(\mathcal{L}_\mathrm{a}t)\rho_0^\mathrm{a} \equiv \rho_\mathrm{c} \otimes \rho_\mathrm{ss}^\mathrm{a} \tag{3.46a}$$

$$Q\rho_\mathrm{tot} := (1 - P)\rho_\mathrm{tot} \tag{3.46b}$$

where ρ_0^a is the atomic initial state, $\rho_\mathrm{ss}^\mathrm{a} = |g\rangle\langle g|$ is the atomic steady state under the evolution induced by $\mathcal{L}_\mathrm{a}$ and $\rho_\mathrm{c} = \mathrm{tr}_\mathrm{a}\left\{\rho_\mathrm{tot}\right\}$ is the trace over the internal degrees of

freedom. We have $P^2 = P$, $Q^2 = Q$ and easily verify the following relations:

$$P\mathcal{L}_\mathrm{c} = \mathcal{L}_\mathrm{c}P \qquad Q\mathcal{L}_\mathrm{c} = \mathcal{L}_\mathrm{c}Q \tag{3.47a}$$

$$P\mathcal{L}_\mathrm{a} = \mathcal{L}_\mathrm{a}P = 0 \qquad Q\mathcal{L}_\mathrm{a} = \mathcal{L}_\mathrm{a} = \mathcal{L}_\mathrm{a}Q \tag{3.47b}$$

$$P\mathcal{L}_\mathrm{I}P = 0 \tag{3.47c}$$

We denote $v(t) := P\rho_\mathrm{tot}(t)$ and $w(t) := Q\rho_\mathrm{tot}(t)$ and can write the projected master equation as

$$\dot{v}(t) = \varepsilon\mathcal{L}_\mathrm{c}v(t) + \varepsilon P\mathcal{L}_\mathrm{I}w(t) \tag{3.48a}$$

$$\dot{w}(t) = (\mathcal{L}_\mathrm{a} + \varepsilon\mathcal{L}_\mathrm{c} + \varepsilon Q\mathcal{L}_\mathrm{I})w(t) + \varepsilon Q\mathcal{L}_\mathrm{I}v(t). \tag{3.48b}$$

The iterative expansion in ε could be performed in the time domain, but is most conveniently seen by taking the Laplace transform $f(t) \to \tilde{f}(s) := \int_0^\infty \exp(-st)f(t)$ of eq. (3.48). This turns the set of differential equations into an algebraic set of equations

$$s\tilde{v}(s) - v(0) = \varepsilon\mathcal{L}_\mathrm{c}\tilde{v}(s) + \varepsilon P\mathcal{L}_\mathrm{I}\tilde{w}(s) \tag{3.49a}$$

$$s\tilde{w}(s) - w(0) = (\mathcal{L}_\mathrm{a} + \varepsilon\mathcal{L}_\mathrm{c} + \varepsilon Q\mathcal{L}_\mathrm{I})\,\tilde{w}(s) + \varepsilon Q\mathcal{L}_\mathrm{I}\tilde{v}(s). \tag{3.49b}$$

Solving for $\tilde{w}(s)$ yields

$$\tilde{w}(s) = \left[s - (\mathcal{L}_\mathrm{a} + \varepsilon\mathcal{L}_\mathrm{c} + \varepsilon Q\mathcal{L}_\mathrm{I})\right]^{-1}(\varepsilon Q\mathcal{L}_\mathrm{I}\tilde{v}(s) + w(0))\,, \tag{3.50}$$

which can be inserted back into eq. (3.49a):

$$s\tilde{v}(s) - \Big(v(0) + \varepsilon P\mathcal{L}_\mathrm{I}\left[s - (\mathcal{L}_\mathrm{a} + \varepsilon\mathcal{L}_\mathrm{c} + \varepsilon Q\mathcal{L}_\mathrm{I})\right]^{-1} w(0)\Big) = \varepsilon\mathcal{L}_\mathrm{c}\tilde{v}(s) + \varepsilon^2 P\mathcal{L}_\mathrm{I}\left[s - (\mathcal{L}_\mathrm{a} + \varepsilon\mathcal{L}_\mathrm{c} + \varepsilon Q\mathcal{L}_\mathrm{I})\right]^{-1} Q\mathcal{L}_\mathrm{I}\tilde{v}(s). \tag{3.51}$$

We will ignore the term proportional to ε in the left hand side of eq. (3.51) because it leads only to a small correction of the initial conditions $v(0)$ which will not accumulate over time. Then we drop terms of third and higher order in ε on the right hand side to arrive at

$$s\tilde{v}(s) - v(0) = \Big\{\varepsilon\mathcal{L}_\mathrm{c} + \varepsilon^2 P\mathcal{L}_\mathrm{I}\left[s - \mathcal{L}_\mathrm{a}\right]^{-1} Q\mathcal{L}_\mathrm{I}\Big\}\,\tilde{v}(s). \tag{3.52}$$

By inverting the Laplace transform we find an integrodifferential equation for $v(t)$, which is correct to second order in ε:

$$\dot{v}(t) = \varepsilon\mathcal{L}_\mathrm{c}v(t) + \varepsilon^2 P\mathcal{L}_\mathrm{I}\int_0^t \mathrm{d}\tau \exp(\mathcal{L}_\mathrm{a}\tau)Q\mathcal{L}_\mathrm{I}v(t-\tau). \tag{3.53}$$

The physical interpretation of this equation is quite clear: the change of the reduced system v at time t has two contributions, the first term on the right hand side describes the 'free' evolution of the cavity decoupled from the atom, the second term is the effect of the coupling to second order in $\mathcal{L}_\mathrm{I}$. By reading this term from right to left we can identify the absorption of a cavity or a laser photon ($\mathcal{L}_\mathrm{I}v(t-\tau)$) at time

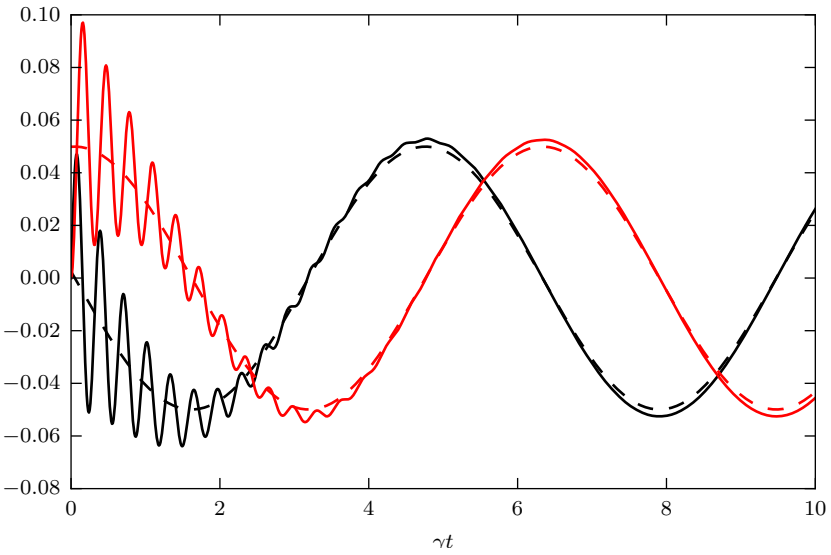

Figure 3.5: Demonstration of validity of the Markov approximation. The real part (black) and the imaginary part (red) of the function $\int_0^t \mathrm{d}\tau e^{(-\gamma+\mathrm{i}\Delta_\mathrm{a})\tau} f(t-\tau)$ (solid) is compared to its Markov approximation $\int_0^\infty \mathrm{d}\tau e^{(-\gamma+\mathrm{i}\Delta_\mathrm{a})\tau} f(t) = f(t)/(\gamma - \mathrm{i}\Delta_\mathrm{a})$ (dashed). After the initial oscillations have damped out ($t \gg \gamma^{-1}$), the Markov approximation follows the original function closely. The parameters are $f(t) = e^{\mathrm{i}\omega t}, \Delta_\mathrm{a} = 20, \gamma = 1, \omega = 1$.

$t - \tau$ to create an atomic dipole moment $|e\rangle\langle g|$, followed by the 'free' evolution of the atom for a time τ where the dipole is oscillating and decaying ($\exp(\mathcal{L}_\mathrm{a}\tau)$) and a second interaction with the cavity or laser at time t to re-absorb the excitation ($P\mathcal{L}_\mathrm{I}$). All the possible times τ back in the history of the system, at which the atomic excitation could have been created, are now summed up to form the integral over τ.

A crucial step to turn eq. (3.53) into a master equation for $v(t)$ is to apply the Markov approximation which makes the right hand side dependent on $v(t)$ instead of $v(t-\tau)$. We note again that $v(t-\tau) = \rho_\mathrm{c}(t-\tau) \otimes \rho_\mathrm{ss}^\mathrm{a}$, and $\exp(\mathcal{L}_\mathrm{a}\tau)$ only acts on the internal atomic degrees of freedom of $\mathcal{L}_\mathrm{I} v(t-\tau)$, letting the induced dipole oscillate with the frequency Δ_a and decay with the rate γ, while the typical rate of change for ρ_c is on the order of ω_sys. For the case that $\gamma \gg |\omega_\mathrm{sys}|$, the Markov approximation is easily justified, because the integrand decays on a time which is short compared to the rate of change in $\rho_\mathrm{c}(t-\tau)$. But even if γ is small compared to ω_sys we have a highly oscillating part and a slowly varying part $\rho_\mathrm{c}(t-\tau)$. Loosely speaking, in such a situation only the times near $\tau = 0$ (on the order of Δ_a^{-1}) contribute to the integral because everything else averages out.

To make this argument a little bit more rigorous, let us define $\tilde{\rho}_\mathrm{c}(\omega)$ as the Fourier transform of $\rho_\mathrm{c}(t)$, which is non-zero only for frequencies $\omega \ll \Delta_\mathrm{a}$ due to our assumptions, i.e. for frequencies with $|\omega|/|\Delta_\mathrm{a}| \sim \varepsilon$. One exemplary integral which

appears in eq. (3.53), with a highly oscillating and a slowly varying part, will look like

$$\int_0^t \mathrm{d}\tau\, \mathrm{e}^{(-\gamma+\mathrm{i}\Delta_\mathrm{a})\tau}\rho_\mathrm{c}(t-\tau) = \frac{1}{\sqrt{2\pi}}\int_{-\infty}^{\infty}\mathrm{d}\omega\int_0^t \mathrm{d}\tau e^{(-\gamma+\mathrm{i}\Delta_\mathrm{a})\tau}\tilde{\rho}_\mathrm{c}(\omega)e^{\mathrm{i}\omega(t-\tau)} \tag{3.54a}$$

$$= \frac{1}{\sqrt{2\pi}}\int_{-\infty}^{\infty}\mathrm{d}\omega\,\frac{\tilde{\rho}_\mathrm{c}(\omega)e^{\mathrm{i}\omega t}}{\gamma-\mathrm{i}\Delta_\mathrm{a}+\mathrm{i}\omega}\left(1-e^{(-\gamma+\mathrm{i}\Delta_\mathrm{a}-\mathrm{i}\omega)t}\right) \tag{3.54b}$$

$$\overset{t\gg\gamma^{-1}}{=} \frac{1}{\sqrt{2\pi}}\int_{-\infty}^{\infty}\mathrm{d}\omega\,\frac{\tilde{\rho}_\mathrm{c}(\omega)e^{\mathrm{i}\omega t}}{\gamma-\mathrm{i}\Delta_\mathrm{a}}+\mathcal{O}(\varepsilon) = \frac{\rho_\mathrm{c}(t)}{\gamma-\mathrm{i}\Delta_\mathrm{a}}+\mathcal{O}(\varepsilon) \tag{3.54c}$$

$$= \int_0^\infty \mathrm{d}\tau e^{(-\gamma+\mathrm{i}\Delta_\mathrm{a})\tau}\rho_\mathrm{c}(t)+\mathcal{O}(\varepsilon), \tag{3.54d}$$

where we have assumed $t \gg \gamma^{-1}$ in eq. (3.54c) so that any transient from the initial condition has damped out[‡]. The functions of eq. (3.54) are illustrated in fig. 3.5. This shows that we can apply the Markov approximation to eq. (3.53) and also extend the integration to infinity, with corrections of order ε^3 which can be neglected:

$$\dot{v}(t) = \varepsilon\mathcal{L}_\mathrm{c}v(t)+\varepsilon^2 P\mathcal{L}_\mathrm{I}\int_0^\infty \mathrm{d}\tau\exp(\mathcal{L}_\mathrm{a}\tau)Q\mathcal{L}_\mathrm{I}v(t) \equiv \varepsilon\mathcal{L}_\mathrm{c}v(t)+\varepsilon^2 B(t). \tag{3.55}$$

It is not at all obvious that eq. (3.55) is a master equation of Lindblad form. To find the effective Liouvillian for $v(t)$, let us now expand the compact notation and evaluate the integral.

$$\varepsilon^2 B(t) = -\int_0^\infty \mathrm{d}\tau\,\mathrm{tr}_\mathrm{a}\Big\{\Big[(g\hat{a}+\Omega)\hat{\sigma}^\dagger+(g\hat{a}^\dagger+\Omega)\hat{\sigma},\, \exp(\mathcal{L}_\mathrm{a}\tau)\left[(g\hat{a}+\Omega)\hat{\sigma}^\dagger+(g\hat{a}^\dagger+\Omega)\hat{\sigma},\rho_\mathrm{c}(t)\otimes\rho_\mathrm{ss}^\mathrm{a}\right]\Big]\Big\}\otimes\rho_\mathrm{ss}^\mathrm{a} \tag{3.56}$$

We will use $\hat{\sigma}\rho_\mathrm{ss}^\mathrm{a} = \rho_\mathrm{ss}^\mathrm{a}\hat{\sigma}^\dagger = 0$ and abbreviate

$$\int_0^\infty \mathrm{d}\tau\,\mathrm{tr}_\mathrm{a}\left\{\hat{\sigma}\exp(\mathcal{L}_\mathrm{a})\hat{\sigma}^\dagger\rho_\mathrm{ss}^\mathrm{a}\right\} = \int_0^\infty \mathrm{d}\tau\left\langle\hat{\sigma}(\tau)\hat{\sigma}^\dagger\right\rangle_{\rho_\mathrm{ss}^\mathrm{a}} =: S \tag{3.57a}$$

$$\int_0^\infty \mathrm{d}\tau\,\mathrm{tr}_\mathrm{a}\left\{\hat{\sigma}^\dagger\exp(\mathcal{L}_\mathrm{a})\rho_\mathrm{ss}^\mathrm{a}\hat{\sigma}\right\} = \int_0^\infty \mathrm{d}\tau\left\langle\hat{\sigma}^\dagger\hat{\sigma}(\tau)\right\rangle_{\rho_\mathrm{ss}^\mathrm{a}} = S^*, \tag{3.57b}$$

which leads to

$$\begin{aligned}\varepsilon^2 B(t) = &-g^2\left(S\hat{a}^\dagger\hat{a}v(t)-(S+S^*)av(t)\hat{a}^\dagger+S^*v(t)\hat{a}^\dagger\hat{a}\right)\\ &-g\Omega\left(S\hat{a}^\dagger v(t)-S^*\hat{a}v(t)-Sv(t)\hat{a}^\dagger+S^*v(t)\hat{a}\right)\end{aligned} \tag{3.58a}$$

$$\begin{aligned}= &\,g^2\,\mathrm{Re}(S)D[\hat{a}+\Omega/g]\,(v(t))\\ &-\mathrm{i}g^2\,\mathrm{Im}(S)\left[\hat{a}^\dagger\hat{a},v(t)\right]-\mathrm{i}g\Omega\,\mathrm{Im}(S)\left[\hat{a}+\hat{a}^\dagger,v(t)\right].\end{aligned} \tag{3.58b}$$

[‡]For $t\sim\gamma^{-1}$ or if γ is strictly zero here, this highly oscillating term can be neglected nevertheless with a rotating-wave-type argument.

To evaluate S we use $\langle\hat{\sigma}(\tau)\rangle = (-\gamma + \mathrm{i}\Delta_\mathrm{a})\langle\hat{\sigma}(\tau)\rangle$ for any inital atomic density matrix under the evolution induced by $\mathcal{L}_\mathrm{a}$. The quantum regression theorem then tells us, that for the function $f(\tau) = \left\langle \hat{\sigma}(\tau)\hat{\sigma}^\dagger \right\rangle_{\rho_\mathrm{ss}^\mathrm{a}}$ with $f(0) = 1$ we have $f'(\tau) = (-\gamma + \mathrm{i}\Delta_\mathrm{a})f(\tau)$ and therefore $f(\tau) = \exp((-\gamma + \mathrm{i}\Delta_\mathrm{a})\tau)$. We readily derive

$$S = \int_0^\infty \mathrm{d}\tau f(\tau) = \frac{1}{\gamma - \mathrm{i}\Delta_\mathrm{a}} = \frac{\gamma + \mathrm{i}\Delta_\mathrm{a}}{\gamma^2 + \Delta_\mathrm{a}^2}. \tag{3.59}$$

The final form of the master equation for v is therefore

$$\dot{v} = -\frac{\mathrm{i}}{\hbar}\left[H_\mathrm{eff}, v\right] + \mathcal{L}_\mathrm{eff} v \tag{3.60a}$$

$$H_\mathrm{eff} = -\hbar(\Delta_\mathrm{a} - U_0)\hat{a}^\dagger\hat{a} + \eta_\mathrm{eff}(\hat{a} + \hat{a}^\dagger) \tag{3.60b}$$

$$\mathcal{L}_\mathrm{eff} v = \kappa D[\hat{a}](v) + \gamma_\mathrm{eff} D[\hat{a} + \Omega/g](v) \tag{3.60c}$$

where we have defined

$$U_0 = \frac{\Delta_\mathrm{a} g^2}{\Delta_\mathrm{a}^2 + \gamma^2} \qquad \eta_\mathrm{eff} = \frac{\Delta_\mathrm{a} g\Omega}{\Delta_\mathrm{a}^2 + \gamma^2} \qquad \gamma_\mathrm{eff} = \frac{\gamma g^2}{\Delta_\mathrm{a}^2 + \gamma^2}. \tag{3.61}$$

We can identify the frequencies of eq. (3.61) with a dispersive shift of the cavity resonance frequency, an effective pump via coherent scattering of laser photons into the cavity and an effective loss of cavity photons via spontaneous emission from the atom, respectively.

3.5.2 Model with center-of-mass motion

Let us now include the center-of-mass motion of the two-level atom, moving in one dimension along the cavity axis. In this case external and internal dynamics of the atom are coupled, as every absorption (or emission) of a plain wave photon with wave number k is associated with a momentum kick $\hbar k u$ described by the phase factor $\exp(\overset{+}{(-)}\mathrm{i}kuX)$, where u is the projection of the normalised photon wave vector onto the cavity axis. Spontaneous emission is not isotropic, therefore it is convenient to define the normalised angular distribution of dipole radiation $N(u)$ given in eq. (3.40).

The full master equation is now

$$\dot{\rho}_\mathrm{tot} = \left[\mathcal{L}_\mathrm{a}^\mathrm{int} + \mathcal{R} + \varepsilon(\mathcal{L}_\mathrm{a}^\mathrm{ext} + \mathcal{L}_\mathrm{c} + Q\mathcal{L}_\mathrm{I})\right]\rho_\mathrm{tot} \tag{3.62a}$$

with

$$\mathcal{L}_\mathrm{a}^\mathrm{int}\rho = \mathrm{i}\left[\Delta_\mathrm{a}\hat{\sigma}^\dagger\hat{\sigma}, \rho\right] + \gamma D[\hat{\sigma}](\rho) \tag{3.62b}$$

$$\mathcal{R}\rho = 2\gamma\int_{-1}^{1}\mathrm{d}u\, N(u)\hat{\sigma}e^{-\mathrm{i}ku\hat{X}}\rho\hat{\sigma}^\dagger e^{\mathrm{i}ku\hat{X}} - 2\gamma\hat{\sigma}\rho\hat{\sigma}^\dagger \tag{3.62c}$$

$$\varepsilon\mathcal{L}_\mathrm{c}\rho = \mathrm{i}\left[\Delta_\mathrm{c}\hat{a}^\dagger\hat{a}, \rho\right] + \kappa D[\hat{a}](\rho) \tag{3.62d}$$

$$\varepsilon\mathcal{L}_\mathrm{a}^\mathrm{ext} = -\frac{\mathrm{i}}{\hbar}\left[\frac{\hat{P}^2}{2M}, \rho\right] \tag{3.62e}$$

$$\varepsilon\mathcal{L}_\mathrm{I}\rho = -\mathrm{i}\left[\left(g(\hat{X})a + \Omega\right)\hat{\sigma}^\dagger + \mathrm{h.c.}, \rho\right]. \tag{3.62f}$$

Here $g(x) = g\cos(kx)$ combines the coupling constant g and the cavity mode function, k is the photon wave number of a cavity photon, M is the atomic mass and $\hat{X}$ ($\hat{P}$) is the center-of-mass position (momentum) operator with $[\hat{X}, \hat{P}] = \mathrm{i}\hbar$. We assume that the frequencies associated with the center-of-mass motion of the atom are small compared to the internal dynamics, i.e. the recoil frequency $\omega_\mathrm{R} = \hbar k^2/2M \ll |\Delta_\mathrm{a}|$ and the atom is precooled so that $k\overline{p}/M \ll |\Delta_\mathrm{a}|$ with $\overline{p} = (\langle \hat{P}^2 \rangle)^{1/2}$. Extra care has to be taken because the superoperator $\mathcal{R}$ couples external and internal dynamics of the atom. The action of $\mathcal{R}$ has been factored out of $\mathcal{L}_\mathrm{a}^\mathrm{int}$ so that the latter acts on the internal degrees of freedom alone and $P\mathcal{L}_\mathrm{a}^\mathrm{int} = \mathcal{L}_\mathrm{a}^\mathrm{int} P = 0$ still holds. For $\mathcal{R}$ we find $\mathcal{R}P = 0$ and $P\mathcal{R} = P\mathcal{R}Q$.

The projected master equations are

$$\dot{v}(t) = \varepsilon(\mathcal{L}_\mathrm{c} + \mathcal{L}_\mathrm{a}^\mathrm{ext})v(t) + (P\mathcal{R} + \varepsilon P\mathcal{L}_\mathrm{I})w(t) \tag{3.63a}$$

$$\dot{w}(t) = \left(\mathcal{L}_\mathrm{a}^\mathrm{int} + Q\mathcal{R} + \varepsilon\left(\mathcal{L}_\mathrm{c} + \mathcal{L}_\mathrm{a}^\mathrm{ext} + Q\mathcal{L}_\mathrm{I}\right)\right) w(t) + \varepsilon Q\mathcal{L}_\mathrm{I} v(t). \tag{3.63b}$$

Again we use the Laplace transform and neglect the small corrections to the initial condition $v(0)$ to find

$$\begin{aligned} s\tilde{v}(s) - v(0) = \varepsilon &\left(\mathcal{L}_\mathrm{c} + \mathcal{L}_\mathrm{a}^\mathrm{ext}\right) \\ &+ \varepsilon^2 P\mathcal{L}_\mathrm{I}\left[s - \left(\mathcal{L}_\mathrm{a}^\mathrm{int} + Q\mathcal{R} + \varepsilon(\mathcal{L}_\mathrm{c} + \mathcal{L}_\mathrm{a}^\mathrm{ext} + Q\mathcal{L}_\mathrm{I})\right)\right]^{-1} Q\mathcal{L}_\mathrm{I}\tilde{v}(s) \\ &+ \varepsilon P\mathcal{R}\left[s - \left(\mathcal{L}_\mathrm{a}^\mathrm{int} + Q\mathcal{R} + \varepsilon\left(\mathcal{L}_\mathrm{c} + \mathcal{L}_\mathrm{a}^\mathrm{ext} + Q\mathcal{L}_\mathrm{I}\right)\right)\right]^{-1} Q\mathcal{L}_\mathrm{I}\tilde{v}(s). \end{aligned} \tag{3.64}$$

We now use the power series expansion $(A - B)^{-1} = A^{-1} + A^{-1}BA^{-1} + \ldots$ and keep only terms up to order ε^2, further we use the fact that $\mathcal{R}BP \neq 0$ only if B is at least quadratic in $\mathcal{L}_\mathrm{I}$:

$$\begin{aligned} s\tilde{v}(s) - v(0) \approx \varepsilon\left(\mathcal{L}_\mathrm{c} + \mathcal{L}_\mathrm{a}^\mathrm{ext}\right)\tilde{v}(s) &+ \varepsilon^2 P\mathcal{L}_\mathrm{I}\left[s - \mathcal{L}_\mathrm{a}^\mathrm{int}\right]^{-1} Q\mathcal{L}_\mathrm{I}\tilde{v}(s) \\ &+ \varepsilon^2 PR\left[s - \mathcal{L}_\mathrm{a}^\mathrm{int}\right]^{-1} Q\mathcal{L}_\mathrm{I}\left[s - \mathcal{L}_\mathrm{a}^\mathrm{int}\right]^{-1} Q\mathcal{L}_\mathrm{I}\tilde{v}(s) \end{aligned} \tag{3.65}$$

Let us transform this equation back to the time domain:

$$\begin{aligned} \dot{v}(t) = \varepsilon(\mathcal{L}_\mathrm{c} + \mathcal{L}_\mathrm{a}^\mathrm{ext})v(t) &+ \varepsilon^2 P\mathcal{L}_\mathrm{I}\int_0^t \mathrm{d}\tau\, \exp(\mathcal{L}_\mathrm{a}^\mathrm{int}\tau) Q\mathcal{L}_\mathrm{I} v(t-\tau) \\ &+ \varepsilon^2 P\mathcal{R}\int_0^t \mathrm{d}\tau\, \exp(\mathcal{L}_\mathrm{a}^\mathrm{int}\tau) Q\mathcal{L}_\mathrm{I}\int_0^{t-\tau} \mathrm{d}\tau'\, \exp(\mathcal{L}_\mathrm{a}^\mathrm{int}\tau') Q\mathcal{L}_\mathrm{I} v(t-\tau-\tau') \end{aligned} \tag{3.66}$$

The interpretation of the first and second term in the right hand side is the same as in eq. (3.53). The third term is a momentum diffusion term caused by spontaneous emission from the atom. It corresponds to the creation of an atomic dipole $|e\rangle\langle g|$ at

time $t-\tau-\tau'$, free evolution of the dipole for the time τ', excitation to the upper state $|e\rangle\langle e|$ at time $t-\tau$, free evolution of the excited state population for the time τ and a spontaneous emission event with associated atomic recoil ($P\mathcal{R}$) at time t. The two integrations over τ and τ' take into account all the possible combinations of times when the first and second interaction events with $\mathcal{L}_\mathrm{I}$ occur. The Markov approximation $v(t-\tau)\to v(t)$ in the second term and $v(t-\tau-\tau')\to v(t)$ in the third term can be justified in the same way as before. We have now arrived at an equation analog to eq. (3.55).

$$\begin{aligned}\dot{v}(t) &= \varepsilon(\mathcal{L}_\mathrm{c}+\mathcal{L}_\mathrm{a}^\mathrm{ext})v(t)+\varepsilon^2 P\mathcal{L}_\mathrm{I}\int_0^\infty \mathrm{d}\tau\,\exp(\mathcal{L}_\mathrm{a}^\mathrm{int}\tau)QL_I v(t)\\ &\qquad+\varepsilon^2 P\mathcal{R}\int_0^t \mathrm{d}\tau\,\exp(\mathcal{L}_\mathrm{a}^\mathrm{int}\tau)Q\mathcal{L}_\mathrm{I}\int_0^{t-\tau}\mathrm{d}\tau'\,\exp(\mathcal{L}_\mathrm{a}^\mathrm{int}\tau')Q\mathcal{L}_\mathrm{I}v(t) \qquad (3.67)\\ &\equiv \varepsilon(\mathcal{L}_\mathrm{c}+\mathcal{L}_\mathrm{a}^\mathrm{ext})v(t)+\varepsilon^2 B(t)+\varepsilon^2 M(t) \qquad (3.68)\end{aligned}$$

The term labeled $B(t)$ gives the same expression as eq. (3.58b) where g is now replaced by $g(\hat{X})=g\cos(k\hat{X})$. The momentum diffusion term $M(t)$ is evaluated to

$$\begin{aligned}M(t) = 2\gamma\Bigg(&\int_{-1}^1 \mathrm{d}u\Big[N(u)(g(\hat{X})\hat{a}+\Omega)e^{-\mathrm{i}ku\hat{X}}\rho_\mathrm{c}(t)(g(\hat{X})\hat{a}^\dagger+\Omega)e^{\mathrm{i}ku\hat{X}}\Big]\\ &-\big[g(\hat{X})\hat{a}+\Omega\big]\rho_\mathrm{c}(t)\big[g(\hat{X})\hat{a}^\dagger+\Omega\big]\Bigg)\\ \times\int_0^t \mathrm{d}\tau\int_0^{t-\tau}\mathrm{d}\tau'\Bigg[&\mathrm{tr}_\mathrm{a}\left\{\hat{\sigma}\left(\exp(\mathcal{L}_\mathrm{a}^\mathrm{int}\tau)\hat{\sigma}^\dagger\exp(\mathcal{L}_\mathrm{a}^\mathrm{int}\tau')\rho_\mathrm{ss}^\mathrm{a}\hat{\sigma}\right)\hat{\sigma}^\dagger\right\}\\ &+\mathrm{tr}_\mathrm{a}\left\{\hat{\sigma}\left(\exp(\mathcal{L}_\mathrm{a}^\mathrm{int}\tau)\left(\exp(\mathcal{L}_\mathrm{a}^\mathrm{int}\tau')\hat{\sigma}^\dagger\rho_\mathrm{ss}^\mathrm{a}\right)\hat{\sigma}\right)\hat{\sigma}^\dagger\right\}\Bigg]\otimes\rho_\mathrm{ss}^\mathrm{a}.\end{aligned} \qquad (3.69)$$

The integrand of the integration over τ and τ' is

$$\begin{aligned}&\mathrm{tr}_\mathrm{a}\left\{\hat{\sigma}\left(\exp(\mathcal{L}_\mathrm{a}^\mathrm{int}\tau)\hat{\sigma}^\dagger\exp(\mathcal{L}_\mathrm{a}^\mathrm{int}\tau')\rho_\mathrm{ss}^\mathrm{a}\hat{\sigma}\right)\hat{\sigma}^\dagger\right\}\\ &\quad+\mathrm{tr}_\mathrm{a}\left\{\hat{\sigma}\left(\exp(\mathcal{L}_\mathrm{a}^\mathrm{int})\tau\left(\exp(\mathcal{L}_\mathrm{a}^\mathrm{int}\tau')\hat{\sigma}^\dagger\rho_\mathrm{ss}^\mathrm{a}\right)\hat{\sigma}\right)\hat{\sigma}^\dagger\right\} = 2e^{-2\gamma\tau}\,\mathrm{Re}\left\{e^{(-\gamma+\mathrm{i}\Delta_\mathrm{a})\tau'}\right\}\end{aligned} \qquad (3.70)$$

and thus

$$2\int_0^t \mathrm{d}\tau\,e^{-2\gamma\tau}\int_0^{t-\tau}\mathrm{d}\tau'\,\mathrm{Re}\left\{e^{(-\gamma+\mathrm{i}\Delta_\mathrm{a})\tau'}\right\} = \frac{1+e^{-2\gamma t}-2e^{-\gamma t}\cos(\Delta_\mathrm{a}t)}{\gamma^2+\Delta_\mathrm{a}^2}\overset{t\gg\gamma^{-1}}{\downarrow}=\frac{1}{\gamma^2+\Delta_\mathrm{a}^2}. \qquad (3.71)$$

The term proportional to $\left[g(\hat{X})\hat{a}+\Omega\right]\rho_{\mathrm{c}}(t)\left[g(\hat{X})\hat{a}^{\dagger}+\Omega\right]$ in eq. (3.69) cancels with the corresponding term appearing in $D[g(\hat{X})\hat{a}+\Omega](\rho_{\mathrm{c}}(t))$ from $B(t)$. Putting this all together we find the master equation

$$\dot{v}(t) = -\frac{\mathrm{i}}{\hbar}\left[H_{\mathrm{eff}}, v\right] + \mathcal{L}_{\mathrm{eff}} v \tag{3.72a}$$

where

$$H_{\mathrm{eff}} = -\mathrm{i}\hbar\left(\Delta_{\mathrm{c}} - U_0\cos^2(k\hat{X})\right)\hat{a}^{\dagger}\hat{a} + \frac{\hat{P}^2}{2M} + \hbar\eta_{\mathrm{eff}}\cos(k\hat{X})(\hat{a}+\hat{a}^{\dagger}) \tag{3.72b}$$

$$\mathcal{L}_{\mathrm{eff}} v = \kappa D[\hat{a}](v) + \gamma_{\mathrm{eff}}\left(-\hat{b}^{\dagger}\hat{b}v - v\hat{b}^{\dagger}\hat{b} + 2\int_{-1}^{1}\mathrm{d}u\, N(u)\hat{b}v\hat{b}^{\dagger}\right) \tag{3.72c}$$

$$\hat{b} = \left(\cos(k\hat{X})a + \frac{\Omega}{g}\right)e^{-\mathrm{i}kuX}. \tag{3.72d}$$

The effective parameters U_0, η_{eff} and γ_{eff} are defined in eq. (3.61). While for the sake of simplicity we have derived this result for a single atom moving in only one dimension, the derivation can be easily extended to N atoms moving in two or three dimensions [3.18, 3.19].

Part II

A C++/Python application-programming framework for simulating open quantum dynamics

Chapter 4

Background to the programming framework

As discussed in the sections 2.1 and 3.4, the quantum optical master equation can be used to describe a wide range of dissipative quantum systems encountered in quantum optics. However, solving master equations of the form (2.7) and (3.41) is numerically challenging. In a Hilbert space with N quantum states, to calculate the time evolution of the density matrix ρ directly, a system of N^2 coupled equations has to be solved. With conventional computing power this direct approach is typically possible for systems with up to a few thousand states. However already the Hilbert space of a few particles coupled to one or two resonator modes with typical spatial resolution for the quantized motion of the particles can easily have several ten thousands of states.

When pushing the limits regarding system sizes, an efficient use of computing resources is crucial for successful simulations. A lot of experience with the MCWF method was gathered in the Innsbruck quantum optics group of Helmut Ritsch. However, every new generation of PhD students dealing with moving-particle cavity QED ended up re-inventing the wheel by implementing their own version, mostly with a limited degree of modularity and re-usability. In 2006, this led to an effort by András Vukics to bundle the available expertise in a highly modular purely object-oriented programming framework utilizing the modern programming language C++, hence the birth and naming choice of `C++QED` version 1 [4.1]. Version 2 of the framework introduced a multi-array concept and advanced compile-time algorithms, tailored to the tensor product structure of composite quantum systems [4.2].

Other approaches exist for simulating the dynamics of open quantum systems, for example the Matlab Quantum Optics Toolbox (active development has stopped in 2002) [4.3] and `QuTiP`, an actively developed implementation written in Python [4.4]. Here the user interface for the definition of a system consists of quantum operators and state vectors as well as the operation of the former on the latter. In contrast, `C++QED` operates on a higher level of abstraction: it allows the user to build composite quantum systems out of predefined building blocks ('small' subsystems like modes, particles, qbits, multi-level atoms etc.) and establish interactions between the constituents (Jaynes-Cummings, mode coupling, photon scattering etc.). This allows to define complex open quantum systems in a few lines of code (cf. the example listing 4.1). The time evolution of a given initial state can be simulated with a number of available time-evolution drivers: full quantum dynamics (Schrödinger equation,

for closed quantum systems), full master equation, single Monte Carlo trajectory or ensemble of Monte Carlo trajectories. Albeit this high level of abstraction certainly comes at the cost of limited flexibility, C++QED proved to be particularly useful in the context of cavity QED [4.5–4.9], and furthermore facilitates the user in implementing customized building blocks and interactions.

The further development of C++QED is one of the main achievements of this thesis. The focus herein was on the improvement of usability and stability as well as the implementation of new features, which lead to a new milestone release [4.10] and are summarised in sec. 4.3. First, however, we will give a brief outline of the C++QED design characteristics and a simple use case example in sections 4.1 and 4.2, respectively.

4.1 Framework characteristics

The C++QED framework aims for maximal performance by taking advantage of optimisations both on the physics side and on the numerical side of the problem. Here we summarise some of these aspects, for a more detailed discussion we refer to the documentation [4.1, 4.2, 4.11].

Interaction picture Adaptive numerical methods usually struggle with very different timescales in the system. The time step has to be chosen small enough to resolve the fast dynamics, consequently an excessive amount of steps has to be taken to appreciably advance the slowly varying part. For example, the kinetic energy term in the master equation (3.37) proportional to $\hat{P}^2$ can have arbitrarily large matrix entries in a momentum state basis, depending on the desired spatial resolution of the simulation. Transforming to an interaction picture with respect to the exactly solvable parts of the Hamiltonian, whenever possible, helps to avoid this problem.

Instead of eq. (2.12) we solve

$$\mathrm{i}\hbar\frac{\mathrm{d}}{\mathrm{d}t}\left|\psi_{\mathrm{I}}\right\rangle = H_{\mathrm{nH,I}}\left|\psi_{\mathrm{I}}\right\rangle, \tag{4.1a}$$

where

$$\left|\psi\right\rangle = U\left|\psi_{\mathrm{I}}\right\rangle \tag{4.1b}$$

$$H_{\mathrm{nH,I}} = U^{-1}\left(H_{\mathrm{nH}}U - \mathrm{i}\frac{\mathrm{d}}{\mathrm{d}t}U\right) \tag{4.1c}$$

and U is the operator transforming between the two pictures. Note that in the context of dissipative state vector trajectories, U is generally non-unitary [4.1]. For example, a single moving particle interacting with a single lossy mode in the dispersive regime might have the transformation

$$U(t-t_0) = \exp\left(\left[-\frac{\mathrm{i}}{\hbar}\frac{\hat{P}^2}{2M} - \frac{\mathrm{i}}{\hbar}\left((U_0-\Delta_{\mathrm{c}}) - \mathrm{i}\kappa\right)\hat{a}^\dagger\hat{a}\right](t-t_0)\right). \tag{4.2}$$

In C++QED, the interaction picture is aligned to the Schrödinger picture after each step of the MCWF method by applying U. On the one hand it is more convenient in terms of code-reusability to calculate the quantum jumps and expectation values in the Schrödinger picture. On the other hand, because U is not unitary, its matrix elements can become very large or very small for $t \to \infty$, leading to numerical problems.

Adaptive-stepsize MCWF algorithm As discussed in sec. 2.2.2, the MCWF method consists of a deterministic *Hamiltonian* part and a stochastic *Liouvillian* part. The Runge-Kutta Cash-Karp method used for the Hamiltonian part has an intrinsic time step management, which chooses integration time steps δt as large as possible while assuring $H_{\mathrm{nH,I}}\delta t \ll 1$ in order to stay within a prescribed relative and absolute error margin. In an adaptive-stepsize version of the MCWF method, also the Liouvillian part has to be considered for finding the optimal time step. The additional requirement of a small total jump probability δp in each step will be violated not only if the jump rates increase too much, but also if the time step δt is chosen too large. In the C++QED implementation, the time step is decreased if either the Hamiltonian or the Liouvillian part requires this, and it is increased if both these parts agree.

To this end, two additional parameters controlling the time step are introduced: a limit $\delta p_{\mathrm{limit}}$ and a tolerance $\delta p'_{\mathrm{limit}} > \delta p_{\mathrm{limit}}$ against overshooting this limit. After the Hamiltonian part, if at time $t + \delta t$ the total jump probability is found to be larger than $\delta p_{\mathrm{limit}}$ but still within the tolerance, the method continues while decreasing the time step tried in the next cycle to counteract the increasing jump probability. If at time $t + \delta t$ the total jump probability is even larger than the tolerance $\delta p'_{\mathrm{limit}}$ allows, then the Hamiltonian step is discarded altogether and the method resumes from time t with a decreased time step δt.

Modular and object-oriented architecture C++ is an object-oriented programming language with modelling techniques like virtual inheritance, polymorphism and the notion of public and private interfaces [4.12]. Making heavy use of these features, C++QED consists of a large class hierarchy to avoid code duplication whenever possible and improve maintainability. For example, the simulation of a two-level atom shares large portions of code with the simulation of a cavity mode, as do the different kinds of time evolution methods. The framework's interface is organised in well-separated layers of abstraction: on the highest level, the user can combine existing free systems (referred to as *frees*) and *interactions* to build composite quantum systems (cf. sec. 4.2). On an intermediate level, the user might write customised interactions and frees. Finally, on the lowest innermost level, the very internals of the framework like the various simulation methods, data structures and input/output operations are defined.

Exploitation of momentum space Usually cavity QED is most naturally formulated in momentum space, tailored to the kinetic energy term of moving particles as well as to periodic mode functions and optical potentials. If all modes involved have the

same wavelength, the interaction matrices in this basis are of tri-diagonal form, for which C++QED offers specialised classes.

Compile-time algorithms C++ is a compiled programming language, which means that the computation of results starting from human-readable source code is done in two stages: in stage (1) the source code is transformed by a compiler to binary machine code forming an *executable* file, whereas in stage (2) this executable is processed together with the input data to generate the results. Through the technique of *template metaprogramming* (TMP) [4.12], it is possible to shift parts of the computation from stage (2) to stage (1). Specifically, the C++ language allows to parameterise types with other types and to perform calculation with these parameter types as operands, which ultimately makes TMP a Turing-complete programming language of its own [4.13], acting completely in stage (1). C++QED takes advantage of TMP in two ways [4.2]. First, TMP is used to perform several structural tests on the definition of the input model in order to recognise inconsistencies at a very early stage. Second, as much information about the model as possible is processed already at the compile time stage (1) to produce executable code which is highly optimised for the specific model and thus reduce the runtime. The advantage is obvious, as typically a C++QED program is compiled once and then executed many times to simulate different physical parameters or different MCWF trajectories. An example for typical compile-time information is the number and interaction graph of the involved subsystems, whereas typical runtime information includes the dimensionality of each subsystem and parameters like detuning, pump strength and decay rate.

Multi-platform and open source C++QED completely builds on free and open source libraries and is itself released under the Boost Software License, a license which was certified by the *Open Source Initiative* in 2008 and allows non-commercial and commercial use, modification and distribution of the software [4.14]. Supported platforms are the operating systems Linux and Mac OS X. Additionally, although untested, it should run on Windows with minor adjustments to the installation process.

4.2 Example

To demonstrate the usage of C++QED and the MCWF method introduced in sec. 2.2.2 we will investigate the simple model sketched in fig. 4.1: a cavity coupled to two stationary and transversally pumped two-level atoms. Note that for this low-dimensional system the full master equation is easily integrable, providing us with a reference solution to which we can compare the MCWF method. In order to further demonstrate the validity of the adiabatic elimination of the excited atomic state (cf. secs. 3.4.1 and 3.5), the dispersive regime is chosen, i.e. the detuning between atoms and cavity defines the largest frequency scale of the system. This model can be described by the following code:

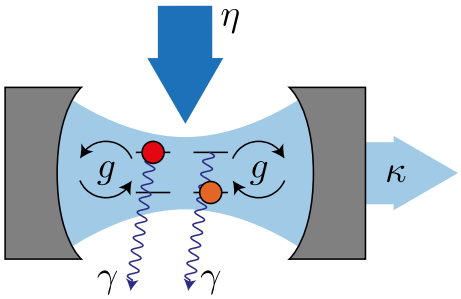

Figure 4.1: Two stationary two-level atoms coupled to a lossy cavity and pumped from the side.

```
1  #include "EvolutionComposite.h"
   #include "Mode.h"
3  #include "Qbit.h"
   #include "JaynesCummings.h"
5
   int main(int argc, char **argv)
7  {
     // Definition and handling of system parameters
9    ParameterTable p;
     evolution::Pars pe(p);
11   mode::ParsLossy plm(p);
     qbit::ParsPumpedLossy plq(p);
13   jaynescummings::Pars pjc(p);

15   QM_Picture& qmp=updateWithPicture(p,argc,argv,"--");

17   // Definition of free susbsystems and interactions
     qbit::Ptr myQbit=qbit::make(plq,qmp);
19   mode::Ptr myMode=mode::make(plm,qmp);
     jaynescummings::Ptr myJC=jaynescummings::make(myQbit,myMode,pjc);
21
     // Initial condition
23   quantumdata::StateVector<1> psi_a = qbit::init(plq);
     quantumdata::StateVector<3> psi = mode::init(plm)*psi_a*psi_a;
25
     // Definition of system layout, evolution of system
27   evolve(psi, composite::make(_<1,0>(myJC),_<2,0>(myJC)),pe);

29 }
```

Listing 4.1: Script simulating two qubits in a cavity mode.

Lines 9–13 introduce objects collecting all parameters like physical frequencies, dimensions and solver options. All these parameters have sensible default values which can be overwritten by command-line parameters. Note that we have chosen to only use one set of parameters for both qbits, which will therefore share all their parameters. Line 15 processes the command-line, thus finalising all parameters and assessing which physical picture to use, i.e. Schrödinger picture, unitary interaction picture or

interaction picture (the default). Lines 18–20 create the individual subsystems and interactions while assigning them the finalised parameters: a qbit, a cavity mode and the Jaynes-Cummings interaction. Again a single qbit object is sufficient to simulate both qbits, as they are indistinguishable. Lines 23–24 define the initial conditions and also the order of the subsystems. In our case the mode has the subsystem index 0 because its initial state is at the first position of the tensor product, whereas the two qbits have the subsystem indices 1 and 2. Finally, in line 27, the interaction graph is defined and the simulation is started. Here it is stated that subsystem 1 interacts with subsystem 0 via the Jaynes-Cummings interaction, as does subsystem 2 with subsystem 0.

Figure 4.2 shows the results of the MCWF simulations. In fig. 4.2a, two exemplary trajectories are plotted together with their individual random quantum jumps. Figure 4.2b illustrates the convergence with increasing number of trajectories N and also compares the result to a model with adiabatically eliminated excited atomic state.

4.3 Development achievements

This section summarises the main contributions of the current thesis' author to the `C++QED` framework.

Code base It is now possible to continue simulations from where they left off. This 'trajectory resume' makes it possible to reuse existing data if longer trajectories are needed, or to simulate sequences of piecewise constant parameters as in chapter 8. To this end a new binary input/output mechanism including compression for trajectory state files has been implemented, which eliminates rounding errors when a trajectory is continued.

The existing ring cavity interaction between a moving particle and two modes has been fixed to include the interference term, i.e. scattering from one mode to the other via the particle. This implementation additionally optimises the regularly encountered case where the two modes have the same wavelength, such that the interaction remains tri-diagonal.

Momentum and position correlations can now be calculated within the framework with a high time resolution.

Several bugs were fixed to improve the overall code quality.

A Python interface to the `C++QED` framework Python is a cross-platfrom dynamical programming language popular in the scientific community. Amongst other things it provides a scientific toolbox (SciPy) including numerical routines (NumPy) [4.15] and bindings to many third-party C/C++ libraries for convenient use. Such an interface has been implemented for the `C++QED` library. Although it is not feature complete yet, it demonstrates how simulations can be started and controlled within Python, relieving the user from the syntactically and conceptually stricter C++ syntax. An example Python script is shown in the publication chapter 5.

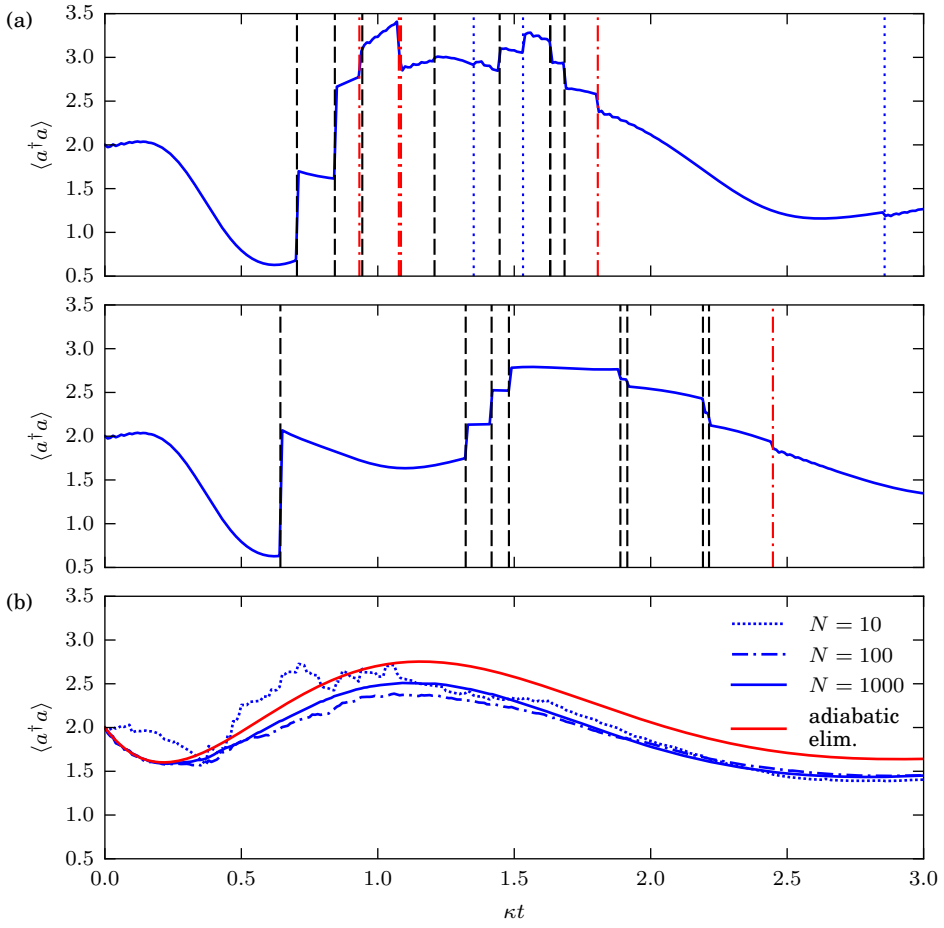

Figure 4.2: (a) Two typical quantum trajectories of the photon number expectation value. The times at which jumps occured due to a photon lost from the cavity (dashed) or spontaneously emitted by the first atom (dotted) and the second atom (dash-dotted) are indicated by vertical lines. (b) Ensemble average of the photon expectation value for different numbers N of trajectories. For $N = 1000$, the trajectory is indistinguishable from the full master equation integration. The red line was obtained by a model where the excited atomic states are adiabatically eliminated, which leaves a cavity driven with the effective pump strength η_{eff} and the additional decay rate γ_{eff} given in eq. (3.42). The parameters are $(\Delta_{\text{a}}, \gamma, \Omega, \Delta_{\text{c}}, g) = (-400, 10, 30, -4, 20)\kappa$

.

Note that Python is an interpreted language and as such is missing the compilation stage in which `C++QED` performs important computations as discussed in sec. 4.1. Instead, in the context of Python this is handled by on-demand compilation and loading of modules as soon as the simulation script is executed. Resulting compiled modules are cached for later use. The actual simulations are computed purely within the `C++QED` library, thus there is no performance penalty usually associated with an interpreted language.

Infrastructure A new cross-platform build system has been integrated which makes it easier for end users to compile the framework and which improves MacOS support. Installation packages for the popular Linux distributions Ubuntu and Arch have been prepared. The project has been migrated to the git version control system, integration of the git revision number into compiled programs and ultimately the generated output files guarantees reproducibility of simulations.

High-performance computing cluster integration Typically `C++QED` is used in a high-performance computing cluster (HPC) environment to simulate many trajectories in parallel. Submitting jobs to the cluster's scheduler is a non-trivial task. A Python tool has been developed which makes it easier to use `C++QED` in such an environment [4.16]. Its features include submitting several job arrays to the cluster corresponding to predefined sets of physical parameters, post-processing of the results and tools to recover in case of failures.

Physical and structural test suite To reduce the probability of introducing new bugs during development, an extensive test suite has been implemented, testing both physical correctness of simulations as well as various structural aspects of the framework. In the former category of tests, mainly well known limiting cases are simulated and compared either to analytic results or numerical simulations of corresponding approximations. Furthermore it is assured that results acquired with the various time evolution methods agree. In the latter category, tests assure correct functionality of the Python interface including on-demand compilation and of template meta programming techniques. It is possible to run the complete test suite, only individual tests or tests belonging to certain fine grained categories, thus making it easy during development to test only the aspects which are of interest.

Chapter 5

Publication

Computer Physics Communications **185**, 2380 (2014)

C++QEDv2 Milestone 10: a C++/Python application-programming framework for simulating open quantum dynamics[†]

Raimar Sandner[1] and András Vukics[2]

[1]*Institute for Theoretical Physics, University of Innsbruck, Technikerstraße 25, 6020 Innsbruck, Austria*
[2]*Institute for Solid State Physics and Optics, Wigner Research Centre of the Hungarian Academy of Sciences, P.O. Box 49, H-1525 Budapest, Hungary*

The v2 Milestone 10 release of C++QED is primarily a feature release, which also corrects some problems of the previous release, especially as regards the build system. The adoption of C++11 features has led to many simplifications in the codebase. A full doxygen-based API manual is now provided together with updated user guides. A largely automated, versatile new testsuite directed both towards computational and physics features allows for quickly spotting arising errors. The states of trajectories are now saveable and recoverable with full binary precision, allowing for trajectory continuation regardless of evolution method (single/ensemble Monte Carlo wave-function or Master equation trajectory). As the main new feature, the framework now presents Python bindings to the highest-level programming interface, so that actual simulations for given composite quantum systems can now be performed from Python.

URL: http://www.sciencedirect.com/science/article/pii/S0010465514001349
DOI: 10.1016/j.cpc.2014.04.011

[†]The author of the present thesis wrote the Python frontend, the build system and testsuite of the C++QED framework. In addition, he contributed significantly in the design and implementation of the C++ codebase, such as the trajectory-state input/output feature.

New version program summary

*Program Title:*C++QED

Catalogue identifier: AELU_v2_0

Program summary URL: `http://cpc.cs.qub.ac.uk/summaries/AELU_v2_0.html`

Program obtainable from:
CPC Program Library, Queen's University, Belfast, N. Ireland

Programming language: C++/Python

Computer: i386–i686, x86_64

Operating system: in principle cross-platform, as yet tested only on UNIX-like systems (including Mac OS X)

RAM: The framework itself takes about 60MB, which is fully shared. The additional memory taken by the program which defines the actual physical system (script) is typically less than 1MB. The memory storing the actual data scales with the system dimension for state-vector manipulations, and the square of the dimension for density-operator manipulations. This might easily be GBs, and often the memory of the machine limits the size of the simulated system.

Classification: 4.3 Differential Equations, 4.13 Statistical Methods, 6.2 Languages

External routines: Boost C++ libraries, GNU Scientific Library, Blitz++, FLENS, NumPy, SciPy

Catalogue identifier of previous version: AELU_v1_0

Journal reference of previous version: Comput. Phys. Comm. 183 (2012) 1381

Does the new version supersede the previous version?: Yes

Nature of problem:
Definition of (open) composite quantum systems out of elementary building blocks [5.1, 5.2]. Manipulation of such systems, with emphasis on dynamical simulations such as Master-equation evolution [5.3] and Monte Carlo wave-function simulation [5.4].

Solution method:
Master equation, Monte Carlo wave-function method

Reasons for new version:
The new version is mainly a feature release, but it does correct some problems of the previous version, especially as regards the build system.

Summary of revisions:
We give an example for a typical Python script implementing the ring-cavity system presented in Sec. 3.3 of Ref. [5.1]:

	C++11 code	Python code

invoking the framework	`#include "EvolutionComposite.h"`
	`#include "ParticleTwoModes.h"`
	
	`int main(int argc, char* argv[])`
	`{`
		`import sys`
		`from cpypyqed import *`

command-line parameters	`ParameterTable p;`
	
	`evolution::Pars pe(p);`
	
	`particle::Pars pp(p);`
	`mode::ParsLossy pmP(p,"P");`
	`mode::ParsPumpedLossy pmM(p,"M");`
	`particlecavity::ParsAlong pcP(p,"P");`
	`particlecavity::ParsAlong pcM(p,"M");`
	
	`pcP.modeCav=MFT_PLUS;`
	`pcM.modeCav=MFT_MINUS;`
	
	`auto qmp=updateWithPicture(p,`
	`argc,argv,"--");`
		`p=parameters.ParameterTable()`
		
		`pe=evolution.Pars(p)`
		
		`pp=particle.Pars(p)`
		`pmP=mode.ParsLossy(p,"P")`
		`pmM=mode.ParsLossy(p,"M")`
		`pcP=particlecavity.ParsAlong(p,"P")`
		`pcM=particlecavity.ParsAlong(p,"M")`
		
		`pcP.modeCav=ModeFunctionType.PLUS`
		`pcM.modeCav=ModeFunctionType.MINUS`
		
		`qmp=updateWithPicture(p,`
		`sys.argv,"--")`

defining free elements	`particle::Ptr part (make(pp ,qmp));`
	`mode ::Ptr plus (make(pmP,qmp));`
	`mode ::Ptr minus(make(pmM,qmp));`
		`part=particle.make(pp ,qmp)`
		`plus = mode.make(pmP,qmp)`
		`minus= mode.make(pmM,qmp)`

initial condition	`auto psi(wavePacket(pp)*` `init(pmP)*init(pmM));`	`psi=particle.wavePacket(pp)**` `mode.init(pmP)**mode.init(pmM)`

defining interactions & composite on the fly, and evolving the system	`evolve<0>(`
	`psi,`
	`composite::make(`
	`_<1,0>(ParticleAlongCavity(plus,`
	`part,pcP)),`
	`_<2,0>(ParticleAlongCavity(minus,`
	`part,pcM)),`
	`_<1,2,0>(ParticleTwoModes(plus,`
	`minus,part,pcP,pcM))),`
	`pe);}`
		`evolve(`
		`psi,`
		`makeComposite({`
		`(1,0):ParticleAlongCavity(plus,`
		`part,pcP),`
		`(2,0):ParticleAlongCavity(minus,`
		`part,pcM),`
		`(1,2,0):ParticleTwoModes(plus,`
		`minus,part,pcP,pcM)}),`
		`pe)`

Restrictions:
Total dimensionality of the system. Master equation—few thousands. Monte Carlo wave-function trajectory—several millions.

Unusual features:
Because of the heavy use of compile-time algorithms, compilation of programs written in the framework may take a long time and much memory (up to several GBs).

Additional comments:

- The framework is not a program, but provides and implements an application-programming interface for developing simulations in the indicated problem domain.
- We use several C++11 features which limits the range of supported compilers (g++ 4.7, clang++ 3.1)
- Documentation, `http://cppqed.sourceforge.net/`

Running time:
Depending on the magnitude of the problem, can vary from a few seconds to weeks.

Acknowledgments

This work was supported by the EU FP7 (ITN, CCQED-264666), the Hungarian National Office for Research and Technology under the contract ERC_HU_09 OPTOMECH, the Hungarian Academy of Sciences (Lendület Program, LP2011-016), the János Bolyai Research Scholarship of the Hungarian Academy of Sciences, and the Stiftung Aktion Österreich-Ungarn (86öu17).

Part III

Particles in driven resonators: correlated motion and sub-recoil cavity cooling

Chapter 6

Background

While in part I we have introduced general concepts and models of cavity QED, the remainder of this thesis addresses the rich physics induced by mechanical effects of intra-cavity light fields on moving particles and the coupled dynamics stemming from back-action of the latter on the former. We distinguish two scenarios: in the current part III, the case of a resonator illuminated by coherent laser light through the mirrors is discussed. In part IV, we will investigate a setup where the particles are pumped from a transverse direction and can scatter photons into the cavity mode. Although similar at first glance, these two principal ways of driving the system reveal fundamental different behaviour, originating from additional interference between the cavity mode and the pump field in the transversally driven case.

In fact, cavity QED offers a multitude of interesting effects even without continuously driving the system by a laser. For example, the presence of a resonator changes the electromagnetical mode density. Spontaneous emission can be strongly enhanced or suppressed by the presence of a cavity, as discovered by Purcell and Kleppner, respectively [6.1, 6.2]. In a more recent example of an experiment without continuous pump, with the strong coupling regime achievable [6.3, 6.4], single atoms can act as a probe extracting information about single photons without destroying them. This even allows monitoring the birth and death of a thermal photon in real time [6.5].

In many cavity QED experiments, however, a pump laser is an essential ingredient, adding an additional degree of freedom and a channel for detection as well as providing energy to the system to compensate for losses. This is especially important for the regime of optical frequencies, where atomic decay rates and cavity losses are larger compared to the microwave case. Thinking of the cavity as frequency filter, it is only natural to send a weak probe beam through the device, assessing its spectral properties. In this way, the presence or absence of matter, even of a single atom in the strong coupling regime, can be detected by looking at the transmission of the light: with a sufficiently large coupling constant the transmission peak is shifted more than the cavity linewidth. While the empty cavity is transparent for a resonant probe beam, particles inside the cavity are indicated by a vanishing probe signal. This technique was successfully applied in early cavity QED experiments with relatively fast atoms entering and leaving the cavity from a magneto-optical trap (MOT) on ballistic trajectories. In this scenario, light forces are negligible, the pump and cavity field takes a passive role as observer. With the advent of slow, ultra-cold atoms, interaction times with the cavity could be increased significantly, and the kinetic

energy of the particles became comparable to the optical potential depth. In this regime, particle trajectories are considerably affected by mechanical effects of the cavity field, which itself depends on the position of the particles and thus becomes a much more active, dynamical component of the coupled system. The temperature scale for ultra-cold atoms is given by the recoil energy of a single photon scattering event, i.e. $k_{\mathrm{B}}T \sim \hbar^2 k^2/(2M)$. By using the transmitted probe signal as a feedback device for the laser pump, trapping of atoms in a strong far-off-resonant field [6.6] or even in the field of a single photon was realised, and trajectories of single atoms can be reconstructed with a high spatial and temporal resolution [6.7, 6.8]. In the low-saturation regime of atomic excitation adopted in this thesis, the laser pump gives rise to effects like cavity-assisted cooling schemes without spontaneous emission, interesting particle momentum correlations and entanglement as well as long-range order and measurement back-action [6.9, 6.10].

6.1 Laser cooling and cavity-assisted cooling schemes

Before introducing cavity cooling let us first recapitulate conventional free-space laser cooling techniques and their associated temperature limits. The free-space mechanical action of light on matter in the regime of validity of the long-wavelength and dipole approximation (cf. sec. 3.3) can be split in two parts, the radiation pressure and the dipole force [6.11]. The origin of radiation pressure is incoherent scattering from atoms involving spontaneous emission. For an incoming plain wave with wave vector $\boldsymbol{k}$, an absorbed photon transfers its momentum $\hbar\boldsymbol{k}$ unidirectionally to the atom. In contrast, a spontaneously emitted photon in free space is emitted randomly to any direction with equal probability. Many spontaneous emission events thus do not contribute to a net force but rather constitute force fluctuations acting on the atom. In summary, radiation pressure of a plain wave leads to a force in direction of the light and to *recoil heating* in form of momentum diffusion comparable to the diffusion seen in Brownian motion. In contrast to the dissipative radiation pressure, the dipole force has a conservative nature, stemming from coherent stimulated absorption and emission processes in a field with spatial gradient. It gives rise to an optical potential which is the basis for applications like optical lattices and optical tweezers. Fluctuations in the dipole force also contribute to momentum diffusion, leading to *dipole heating*.

For atoms moving against the direction of a laser beam, the Doppler effect results in a blue frequency shift of the light as 'seen' by the atom. Conversely, atoms moving away from a laser experience a red shifted light frequency. This velocity dependency can be used to cool atoms in an *optical molasses*: red-detuned laser light will only affect those atoms for which the Doppler effect shifts the light into resonance, i.e. those atoms moving towards a laser, thus slowing them down [6.12, 6.13]. By using two counter-propagating beams for each spatial coordinate (or one per coordinate reflected back by a mirror), atoms can be cooled in three dimensional space. The sea of photons acts like a viscous fluid with damping forces which can exceed gravity

by a factor of 10^5, slowing down atoms to speeds on the order of several ten cm/s, compared to speeds of several hundred m/s at room temperature. What is missing is a restoring force to ultimately trap the atoms, therefore usually an arrangement of two magnetic coils is added as trapping device. As atoms try to leave the trap region, a radially increasing Zeeman effect shifts the atomic levels into resonance only with those lasers which push the atoms back towards the center, selected by light polarisation. Such a setup, called *magneto-optical trap (MOT)*, was developed 1987 [6.14] and has since become a standard device in the field of cold neutral atoms.

The final temperature expected within the theory of Doppler cooling is limited by the natural linewidth [6.15]

$$k_{\mathrm{B}} T_{\mathrm{Doppler}} = \frac{\hbar\gamma}{2}. \tag{6.1}$$

Shortly after the first successful demonstrations of Doppler cooling, surprising measurements revealed temperatures well below the Doppler limit eq. (6.1). It was soon discovered that the internal level structure, in particular different magnetic sub-levels of the atomic ground state, could be exploited to achieve strong damping forces even for very slow velocities which are dominated by diffusion in the Doppler cooling case. In the *polarisation gradient cooling* method [6.16–6.18], counter-propagating beams of different polarisation generate a spatially varying polarisation pattern, which leads to an optical potential depending on the internal magnetic quantum number m_J (Zeeman sublevel). Moving atoms can run 'up-hill' losing kinetic energy or 'down-hill' gaining kinetic energy, and the potential maximum for one m_J level can correspond to a potential minimum for a different one. Because of the conservative nature of the optical potential, no cooling can be achieved with the dipole force alone. The key point in this cooling scheme is optical pumping between different m_J-levels. The rate of optical pumping depends on the natural linewidth and detuning of the excited state, intensity and polarisation of the electric field (at the atom's position) and the Clebsch-Gordan coefficients. Polarisation gradient cooling operates in a regime where, on average, a moving atom is more likely to be optically pumped from the top of the potential hill corresponding to its current m_J level to the bottom of the potential well corresponding to the target m_J level, compared to the reverse process which contributes to heating. In this more probable optical pumping process, the energy of the absorbed laser photon is less than the energy of the sponateneously emitted photon, and the difference in energies is compensated by a loss of kinetic energy. It is important to note that the optical pumping has to be slow in a sense that it follows the center-of-mass motion of the atom non-adiabatically with some delay. Polarisation gradient cooling is also named Sisyphus cooling referring to the Greek mythological figure who was condemned to eternally roll a stone up a hill only to see it roll down again as he reaches the top. Today standard MOTs exploit both described mechanisms. Fast atoms are slowed down by the Doppler cooling effect which has a large velocity capture range, slow atoms additionally experience a strong friction by virtue of Sisyphus cooling.

The achievable temperature is the recoil limit

$$k_{\mathrm{B}} T_{\mathrm{recoil}} = \frac{\hbar^2 k^2}{2M}, \tag{6.2}$$

corresponding to the diffusion caused by a single scattered photon for an atom at rest. This is in fact a fundamental limit for cooling methods in free space which rely on randomly directed spontaneous emission. A laser cooling method which can circumvent the recoil limit is dark state cooling [6.19], where the last spontaneous-emission photon is not random. All methods described so far have in common that they rely on spontaneous emission as dissipation channel and on the specific internal level structure. For Doppler cooling at least a closed level structure is needed*, Sisyphus cooling and dark state cooling rely on an even more complex internal structure.

Cavity cooling offers exciting new possibilities to overcome some of these problems of conventional laser cooling. The coupled system of atoms and one or several resonator modes share the available dissipation channels, which means kinetic energy can be extracted by photons leaking out through the mirrors and spontaneous emission can be avoided. A number of cooling methods exist which use a cavity as passive device. For example, in the bad cavity limit, the free space emission rate is tailored to favour the cavity frequency, which can be exploited to enhance Doppler cooling. Here, however, we will once more concentrate on the good cavity and strong coupling limit, where due to the finite response time of the electromagnetic field the mode takes over a much more dynamical role. These schemes can be extended to a large atom-laser detuning without spontaneous emission, where the cooling process becomes independent of the precise internal structure of the particles and all levels contribute simultaneously to the overall polarisation. Cavity cooling therefore offers a promising prospect on cooling particles for which conventional laser cooling is impractical, for example atomic species not meeting the requirements of laser cooling on the internal level structure, molecules with a rich excitation spectrum of vibrational and rotational modes [6.20], or even macroscopic objects like nano-beads [6.21, 6.22] or membranes [6.23].

To understand the dynamical cavity cooling effect [6.24], let us first employ the classical picture of a single atom moving inside a longitudinally pumped high-finesse cavity. Let us assume that the atom shifts the mode function by a maximum of U_0 (cf. eq. (3.41b)), and that the pump detuning is negative with $\Delta_{\mathrm{c}} \approx U_0 < 0$ and $\kappa < |\Delta_{\mathrm{c}}|$, so that the cavity is shifted into resonance with the laser if the atom is positioned at a minimum and out of resonance if it is positioned at a maximum of the optical potential, respectively. The intra-cavity field intensity therefore is highest in the former case and lowest in the latter. This however only truly reflects a stationary situation. In Sisyphus cooling, the non-adiabaticity of the optical pumping gives rise to a cooling mechanism. Similarly, in a high-finesse cavity it is the intra-cavity

*In practice repump lasers are used to make atoms available to the cooling cycle again if they have reached levels which are dark to cooling lasers.

field which follows the atomic motion non-adiabatically, therefore the highest field intensity is obtained *after* a moving atom has passed through a potential minimum, while it is converting kinetic to potential energy. Analogously the field minimum and with it the most shallow potential is obtained *after* the atom has passed through a potential maximum, while it is converting potential to kinetic energy. On average, the atom experiences a steeper potential hill while it is moving 'up-hill' compared to while it is moving 'down-hill', leading to a net friction force slowing the atom down and ultimately trapping it in a single potential well.

While the classical model predicts the particle to come to a complete halt, momentum diffusion mainly due to dipole force fluctuations leads to a finite temperature. In a semi-classical treatment, the dynamical cooling mechanism can be explained in a dressed-state picture of the strongly coupled atom-cavity system. Resembling a Sisyphus-type cooling, a dressed state is on average excited in regions of weak coupling and decays in regions of strong coupling, the difference in potential energy being compensated by a loss of kinetic energy. A detailed analysis of the friction coefficient reveals one of the cooling regions at $U_0 < 0$ and $\Delta_c < 0$, a parameter regime which is employed throughout this thesis. By comparing the friction to the competing diffusion, a steady state temperature of

$$k_B T_{\text{cavity}} \approx \frac{\hbar\kappa}{2} \tag{6.3}$$

is found.

Note that compared to the Doppler limit eq. (6.1), the cavity linewidth takes the role of the atom's natural linewidth γ. Therefore sub-Doppler cooling is possible if $\kappa < \gamma$. The question arises whether by improving the cavity further, cavity cooling can be used to go even below the recoil limit eq. (6.2), an important milestone as we have explained above. Equation (6.3) cannot be applied directly to sub-recoil temperatures, as its semi-classical derivation is valid only in a regime where the kinetic energy of the particles is large compared to the recoil energy. As one of the practical challenges in reaching such low temperatures, besides building a sufficiently high-quality cavity, a decreasing cavity linewidth directly is connected to a smaller velocity capture range and increased cooling time scale [6.25]. Strong evidence that sub-recoil cavity cooling is possible has been provided recently by Wolke *et al.* in Hamburg [6.26]. This experiment, however, started with a weakly excited BEC and did not yet cool a thermal gas.

Reaching quantum degeneracy with laser cooling as the only cooling mechanism is a challenging task which has only recently been accomplished by an Innsbruck experiment [6.27]. Usually re-absorption of fluorescence photons and light-assisted inelastic scattering inhibits sufficient phase-space densities. In reference to the Hamburg experiment, our own work on sub-recoil cavity cooling in chapter 8 presents a detailed numerical analysis where the cavity modes and center-of-mass motion of the particles is treated on equal footings in the quantum regime. To address the problem of a small velocity capture range, an optimised sequence with decreasing laser detuning is used. The results show a promising prospect on the possibility to reach

quantum degeneracy with cavity cooling methods starting from a thermal ensemble. Additionally to comparing fermions to bosons, cavity cooling in a multi-mode cavity with ring geometry is investigated and compared to the standing-wave case. The following section introduces some of the properties and unique effects characterising such a ring cavity.

6.2 The ring cavity geometry

So far we have discussed the linear Fabry-Pérot interferometer geometry as shown in fig. 3.1. In a ring cavity, instead of being reflected back and forth resulting in a standing wave, photons can travel in two running waves with opposite direction and a mode function proportional to $\exp(\pm \mathrm{i}kx)$. In the simplest case this is achieved by an arrangement of three mirrors as sketched in fig. 7.1 of the following chapter. Such a resonator has a similar frequency response with narrow peaks separated by the free spectral width (cf. fig. 3.2), each peak however corresponds to two degenerate modes of the electromagnetic field instead of one.

The presence of this second mode has decisive consequences to the coupled particle-field dynamics [6.10, 6.28]. Due to the translational invariance of this geometry, the total momentum of particles and fields including pump and losses is conserved, in contrast to a linear cavity where the mirrors can absorb momentum. Atoms scatter photons from one mode to the other resulting in a dynamic position-dependent phase locking between the two modes, which can be exploited for example to monitor single atoms [6.29]. For multiple atoms, the phase locking leads to long-range atom-atom interaction mediated by the ring cavity [6.30, 6.31].

For our studies the mathematically equivalent description of the ring resonator in terms of two standing-wave modes $\propto \sin(kx)$ and $\propto \cos(kx)$ with wave number k [6.32, 6.33] is more convenient than the description with a set of running-wave eigenmodes. This choice is especially well suited for the case of a symmetrically pumped resonator as depicted in fig. 8.1, resulting in a driven and damped standing-wave mode (e.g. $\cos(kx)$) and a mode which is only damped and can only be populated through Rayleigh scattering from the particles (e.g. $\sin(kx)$). Population in the sin-mode then leads to a shift of the optical potential experienced by the atoms. Additionally to the amplitude of the standing wave as in the linear cavity case, for the ring cavity also the phase of the cavity-induced optical lattice depends on the position of the atoms. Similar to the friction forces discussed in the previous section, a cooling regime also exists for a ring cavity [6.28]. Because the friction force does not vanish at the field nodes, the efficiency for decelerating and trapping moving particles can surpass that of a linear cavity [6.31]. Schulze *et al.* present a ring cavity cooling scheme which operates efficiently in the far off-resonant regime with respect to the internal states of the particles [6.32]. As discussed earlier, this makes it in principle applicable to a wide range of polarisable particles. The method relies on the strongly driven cosine mode to provide sufficiently tight trapping on the one hand and a collective enhancement of the particle-field coupling due to the large photon number on the other hand.

By choosing a cavity-drive detuning close to the anti-stokes sideband of the trap, scattering of photons into the initially empty sine mode provides fast cooling rates.

Niedenzu *et al.* give a detailed analysis of the microscopic dynamics involved in the ring cavity setup [6.33]. As main result they developed a Bose-Hubbard model [6.34] for the ring cavity. While usually the Bose-Hubbard approximation includes the restriction to the first motional band, here it turns out that taking into account also the second band is essential to capture important physical effects like dephasing of tunneling oscillations and decoherence of the wave function.

Based on this previous work, the publication in chapter 7 analyses the ring-cavity system for two particles in the regime of a strongly driven cosine cavity mode. One of the main physical effects is a classically forbidden positive momentum correlation of the particles. This is related to a strong delocalisation of the centre-of-mass. Another main result is entanglement between the particles 'heralded' by photon detection, i.e. entanglement which is specially pronounced right after the detection of a photon outside the resonator. Single trajectories of the Monte Carlo wave-function simulation reveal a pronounced logarithmic negativity, a measure for entanglement [6.35]. In the limit of tight trapping of the particles, the full model can be approximated by an optomechanical model [6.32] characterised by quadrature-quadrature coupling of two harmonic oscillators representing the particles to a third harmonic oscillator representing the field. The Hamiltonian describing this model applies to a whole class of optomechanical systems, for example a cavity with vibrating end mirrors [6.36], two light membranes inside a cavity field positioned at the maximum slope [6.37] of the field or very light nano-sized dielectric spheres held inside the cavity field [6.38].

Chapter 7

Publication

Journal of Physics B: Atomic, Molecular and Optical Physics **45**, 245501 (2012)

Quantum-correlated motion and heralded entanglement of distant optomechanically coupled objects[†]

W. Niedenzu[1], R. M. Sandner[1], C. Genes[1,2,3], H. Ritsch[1]

[1] *Institut für Theoretische Physik, Universität Innsbruck, Technikerstaße 25, 6020 Innsbruck, Austria*
[2] *Vienna Center for Quantum Science and Technology (VCQ), Faculty of Physics, University of Vienna, Boltzmanngasse 5, 1090 Vienna, Austria*
[3] *ISIS (UMR 7006) and IPCMS (UMR 7504), Université de Strasbourg and CNRS, Strasbourg, France*

The motion of two distant trapped particles or mechanical oscillators can be strongly coupled by light modes in a high finesse optical resonator. In a two mode ring cavity geometry, trapping, cooling and coupling is implemented by the same modes. While the cosine mode provides for trapping, the sine mode facilitates ground state cooling and mediates non-local interactions. For classical point particles the centre-of-mass mode is strongly damped and the individual momenta get anti-correlated. Surprisingly, quantum fluctuations induce the opposite effect of positively-correlated particle motion, which close to zero temperature generates entanglement. The non-classical correlations and entanglement are dissipation-induced and particularly strong after detection of a scattered photon in the sine mode. This allows for heralded entanglement by post-selection. Entanglement is concurrent with squeezing of the particle distance and relative momenta while the centre-of-mass observables acquires larger uncertainties.

URL: `http://iopscience.iop.org/0953-4075/45/24/245501`
DOI: 10.1088/0953-4075/45/24/245501
PACS: 37.30.+i, 03.65.Ud

[†] The author of the present thesis assisted in the implementation of the numerical simulations and, together with C. G., acted as a discussion partner on all other aspects of the work. W. N. performed all the calculations in this publication.

7.1 Introduction

The past decades have seen tremendous success in the implementation of control schemes for the motional state of matter via light fields either in free space or in optical cavities. A diversity of examples exist where the quantum regime of motion has been reached. The masses span many orders of magnitude, from the microscopic atomic size systems such as atoms in optical cavities [7.1–7.4] and laser-cooled ions in ion traps [7.5] to the macroscopic level with cavity-embedded membranes [7.6], mirrors [7.7] or levitated dielectric nano-particles [7.8].

A common interaction Hamiltonian that well approximates many quantum light–matter interfaces is quadrature–quadrature coupling [7.9]; more specifically, the displacement of the mechanics is coupled directly to a quadrature of the high-Q optical field mode that can be then used as an observable for indirect position detection. Adding a second mechanical system coupled to the field then allows one to engineer an effective two-particle mechanical coupling by eliminating the mediating light mode. Recently, an expansion to quadratic coupling has been proposed [7.10] and the investigation of dissipation-induced [7.11–7.13], noise-induced [7.14] and remote entanglement [7.15, 7.16] has been of great interest, including a scheme for sensitive force measurements [7.17] and entanglement of macroscopic oscillators [7.18, 7.19].

Here we show that all this can be implemented in a system consisting of two particles strongly trapped in the cosine mode of a ring cavity, where the two-particle interaction is carried by sideband photons in the sine mode. For deep trapping it yields the typical linearized optomechanical Hamiltonian [7.20]. First we present the general model of two particles moving within a ring resonator. We then analyse single quantum trajectories depicting strong correlations and entanglement. A subsequent investigation of momentum correlations reveals classically forbidden positive values in steady state, even in the absence of entanglement. The steady state shows a strong delocalization of the centre-of-mass independent of the particle separation. We also show how to generate entanglement either in a pulsed regime or heralded by the detection of photons. Analytical calculations are carried out in the regime of strong particle confinement and matched to the more generally valid numerical simulations with good agreement. Finally, the occurrence of correlations in the system is explained in a simple adiabatic model.

We structure this presentation in two major parts according to the Gaussian/non-Gaussian nature of the system dynamics. Entanglement on trajectories and that on average as well as momentum correlations during the non-Gaussian dynamics of the two atoms in the cavity are numerically investigated in the beginning, while the Gaussian approximation makes the topic of the second major part of the paper. This part corresponds either to atoms in very deep traps (to compare to the results obtained in the first part) or more generally to a wide range of optomechanical systems in the linear regime and with diverse physical realizations (moving membranes, levitated nano-spheres etc.).

7.2 Motion of two particles in a ring resonator

We study two small polarizable particles confined within a symmetrically-pumped ring resonator, see figure 7.1. Symmetric pumping results in a standing-wave optical potential with spatial dependence $\cos^2(kx)$ [7.20, 7.21]. The cosine mode is strongly pumped and approximated by a highly excited coherent state $|\alpha_\mathrm{c}\rangle$ with $|\alpha_\mathrm{c}| \gg 1$ (and without loss of generality $\alpha_\mathrm{c} \in \mathbb{R}$). The particles scatter photons into the unpumped orthogonal sine mode. This setup can be generally described by the Hamiltonian [7.20, 7.21]

$$H = \sum_{i=1}^{2} \left[\frac{p_i^2}{2m} + \hbar U_0 \alpha_\mathrm{c}^2 \cos^2(kx_i) + \hbar U_0 a^\dagger a \sin^2(kx_i) \right] + \\ + \frac{\hbar U_0 \alpha_\mathrm{c}}{2} \left(a + a^\dagger \right) \sum_{i=1}^{2} \sin(2kx_i) - \hbar \Delta_\mathrm{c} a^\dagger a. \quad (7.1)$$

Here, a denotes the annihilation operator of the quantum-mechanical sine mode, $U_0 < 0$ the optical potential depth per photon, x_i and p_i the particles' centre-of-mass position and momentum operators, respectively, and m the particle mass. The pump is detuned by $\Delta_\mathrm{c} := \omega_\mathrm{p} - \omega_\mathrm{c}$ from the bare cavity resonance frequency ω_c. To avoid instabilities we restrict ourselves to red detuned lasers ($\Delta_\mathrm{c} < 0$) for which a cooling regime exists [7.22]. The sine mode is only weakly populated by scattering such that $\left\langle a^\dagger a \right\rangle$ is negligible compared to α_c^2 [7.20]. Damping of the cavity mode is taken into account by the Liouvillian $\mathcal{L}\rho = \kappa \left(2a\rho a^\dagger - a^\dagger a \rho - \rho a^\dagger a \right)$ [7.23] in the master equation

$$\dot{\rho} = \frac{1}{\mathrm{i}\hbar} [H, \rho] + \mathcal{L}\rho. \quad (7.2)$$

To get some insight into the dynamics, we solve equation (7.2) numerically for some typical parameters. The direct solution of the master equation (7.2) is computationally very demanding owing to the large Hilbert space of the joint particles-field system. Therefore, we resort to Monte Carlo wavefunction simulations [7.24], in which the system is coherently evolved between the so-called "quantum jumps". These jumps correspond to a photon detected at the resonator output [7.24]. Besides the more favourable usage of computer resources, single trajectories also provide an additional insight into the microscopic processes in the system. The simulations were efficiently implemented with the freely available* C++QED framework [7.25, 7.26] and performed in a joint momentum- and Fock basis.

A typical trajectory is shown in figure 7.2, where the blue arrows indicate the times at which jumps occur. Initially, the particles were prepared in the ground state of two separated potential wells and owing to the deep potential tunnelling is strongly suppressed. The momentum correlation coefficient $\mathcal{C}_p$ for the two particles is defined as

$$\mathcal{C}_p := \frac{\mathrm{cov}(p_1, p_2)}{\Delta p_1 \Delta p_2} = \frac{\langle p_1 p_2 \rangle - \langle p_1 \rangle \langle p_2 \rangle}{\Delta p_1 \Delta p_2}, \quad (7.3)$$

*`http://cppqed.sourceforge.net`

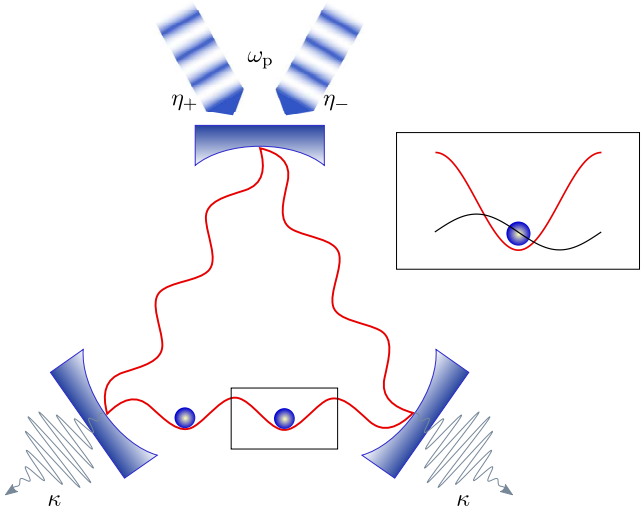

Figure 7.1: Sketch of the system. The pumped standing-wave mode (red) traps the particles, the second orthogonal one (black) mediates an effective interaction between them.

where $\mathcal{C}_p = 1$ means perfect correlation and $\mathcal{C}_p = -1$ perfect anti-correlation of the motion. Quantum jumps by photodetection trigger strong correlations and entanglement between the particles due to the cavity-mediated interaction. The logarithmic negativity [7.27] already after the first jump approaches the value for a maximally entangled Bell state and the correlation reaches a value of $\mathcal{C}_p \approx 0.5$. The emerging state corresponds to a superposition of two particles moving to the right and two particles moving to the left such that the centre-of-mass momentum remains zero. As we will see later this behaviour is caused by the excitation of a single particle into the first excited state within the trap. Beginning with the second jump the system is subject to fast oscillations which are of the order of the trap frequency. Note that only the field is dissipative in our model and induces quantum jumps. However, the particles respond to the sudden changes of the field in a correlated way.

Interestingly, while entanglement is quite pronounced on single trajectories, it remains small on average. The averaged steady-state logarithmic negativity is $\mathcal{E}_\mathcal{N} \sim 10^{-3}$ for our parameters. The logarithmic negativity is not an expectation value and hence its value for an ensemble of trajectories cannot be obtained from its values on single realizations—it has to be directly computed from the density operator. It is therefore possible that the logarithmic negativity of a mixture of entangled states is smaller than the weighted average of the individual values. A prominent example for this is the equal statistical mixture of two Bell states, which is not entangled.

We now examine the momentum correlations in more detail. Classical simulations reveal much stronger damping of the centre-of-mass motion than that of the relative motion. Hence the particles become anti-correlated [7.1, 7.22, 7.28], see figure 7.3. Surprisingly, the quantum simulations of the ring resonator system yield the opposite

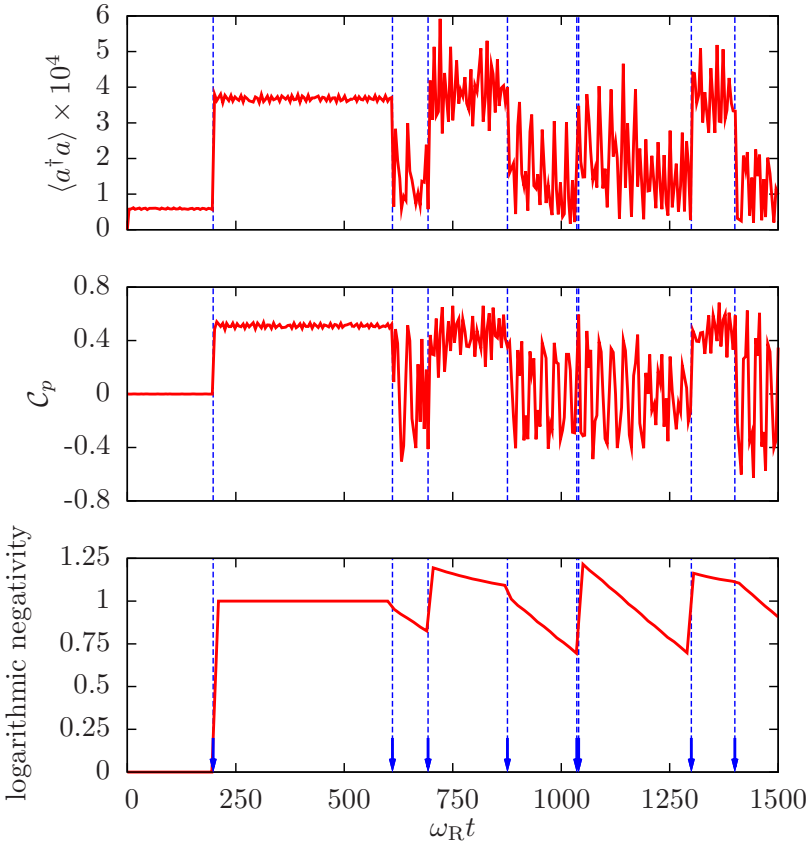

Figure 7.2: Photon number, momentum correlation and entanglement for a single trajectory. The dashed vertical lines indicate quantum jumps. Parameters: $\alpha_c = 150$, $U_0 = -\frac{1}{\alpha_c}\omega_R$, $\Delta_c = -\kappa$ and $\kappa = 10\omega_R$.

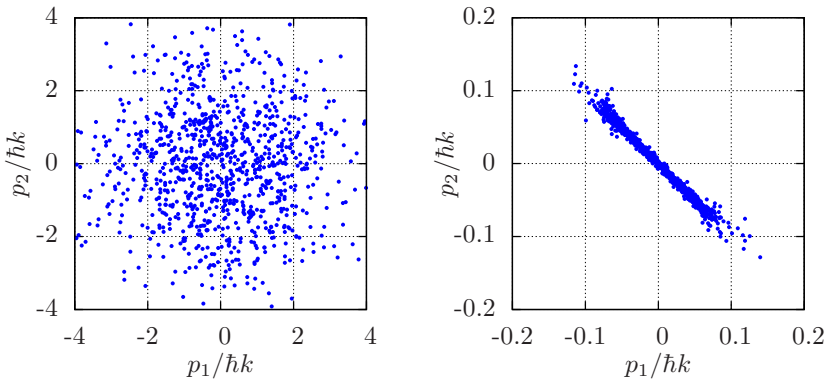

Figure 7.3: Classical simulations [7.22] for 1000 initial conditions. Left: initial condition, right: distribution at $\omega_R t = 3000$. The particles become anti-correlated and cooled. Same parameters as in figure 7.2.

result. On average, initially uncorrelated particles become positively correlated due to the cavity input noise. This effect is visible in the steady-state density matrix presented in figure 7.4. There, the momentum distribution is elongated into the first quadrant, which is a signature of positive correlations. Note that quantum mechanics allows pure states with positive correlations, but still zero average centre-of-mass motion with large uncertainty. The time evolution of the momentum correlation coefficient is depicted in figure 7.5. We observe smaller correlations around the cooling sideband $\Delta_c = -\omega := -\sqrt{4\hbar|U_0|\alpha_c^2 E_R}/\hbar$ as compared to the other chosen detuning $\Delta_c = -\kappa$. Here $E_R \equiv \hbar\omega_R := \hbar^2 k^2/2m$ is the recoil energy. For comparison, we also present the results of simulations containing the quadratic optomechanical Hamiltonian (7.6) introduced later on in this paper. The latter yields accurate results provided that the position spread remains small compared to a wavelength, $k\Delta x \ll 1$. This is fulfilled for operation near the cooling sideband, but not for $\Delta_c = -\kappa$. Positive correlations of the particle motion can also be observed in much shallower potentials where the particles are barely trapped and both light modes are treated quantum-mechanically [7.29].

In the dynamics, correlations and entanglement are generated by quantum jumps induced by photon count events. Hence they are particularly strong immediately after a jump. In real experiments, it is generally not possible to exactly keep track of each emitted photon due to the detector efficiency, i.e. one cannot exactly follow a certain quantum trajectory. Hence, the system always evolves into a mixed state and if a photon is observed (measured) outside of the resonator, it is impossible to determine whether it was the first, the second and so on. Naturally, the question arises whether effects observed on single trajectories (like entanglement) "survive" this averaging and can still be expected to be observable after jumps. Every time a

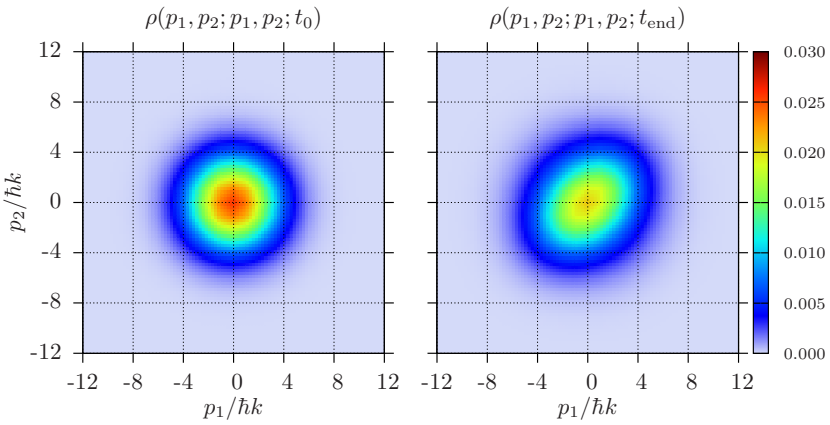

Figure 7.4: Diagonal elements of the two-particle reduced density matrix in momentum space, initially (left) and in steady state (right). Ensemble average of 5000 trajectories. Same parameters as in figure 7.2.

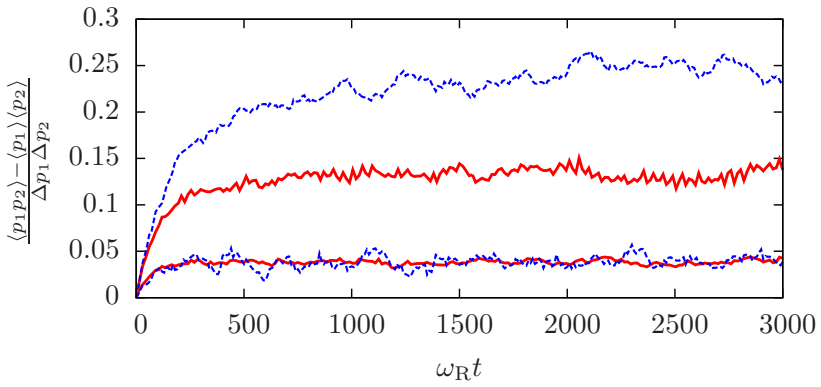

Figure 7.5: Red solid lines: momentum correlation coefficient obtained from the master equation containing (7.1) for $\Delta_{\mathrm{c}} = -\kappa$ (upper curve) and $\Delta_{\mathrm{c}} = -\omega$ (lower curve). Blue dashed lines: result of the oscillator approximation (7.6) (600 trajectories). The other parameters are the same as in figure 7.2.

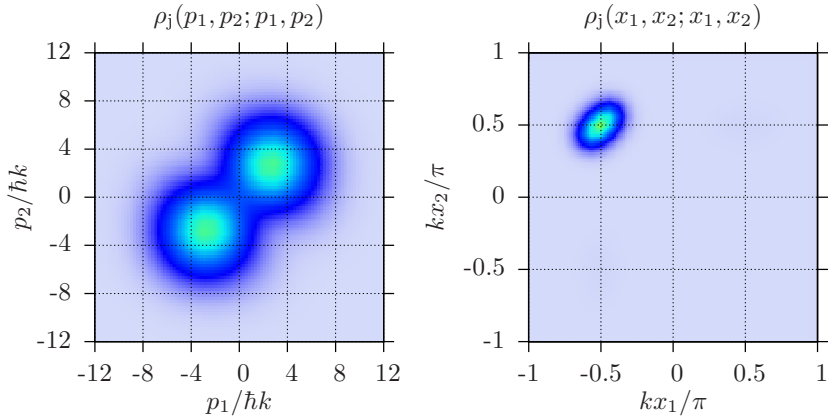

Figure 7.6: Diagonal elements of the reduced two-particle conditional density matrix (7.4) after a photon detection in steady state. Particle correlations as well as entanglement become much more pronounced compared to the density matrix shown in figure 7.4. Same parameters and colour code as there.

photon is detected, the mixed state inside the resonator is projected into the state

$$\rho_\mathrm{j} := \frac{a\rho a^\dagger}{\mathrm{Tr}\,(a\rho a^\dagger)}, \tag{7.4}$$

where ρ is the density matrix evolved according to the master equation (7.2). Interestingly, the momentum correlation coefficient (7.3) is nearly constant ($\mathcal{C}_p \approx 0.5$ for $\Delta_\mathrm{c} = -\kappa$ and $\mathcal{C}_p \approx 0.3$ on the cooling sideband, respectively), regardless of the time the jump occurred at, see figure 7.6 also. The heralded entanglement measured by the logarithmic negativity is smaller than on single trajectories, but still prominent with a value $\mathcal{E}_\mathcal{N} \sim 0.2$ for our parameters and a jump in steady state.

The conditional density matrix (7.4) is closely related to the field autocorrelation function [7.23]

$$g^{(2)}(0) = \frac{\left\langle a^\dagger a^\dagger a a \right\rangle}{\langle a^\dagger a \rangle^2} \equiv \frac{\left\langle a^\dagger a \right\rangle_{\rho_\mathrm{j}}}{\langle a^\dagger a \rangle_\rho}. \tag{7.5}$$

It has the very intuitive interpretation as the ratio between the photon number after and prior to a jump in steady state [7.30]. For our parameters, it indicates photon bunching close to a thermal (chaotic) state (for which $g^{(2)}(0) = 2$). This is consistent with the picture of the mode being incoherently populated through particle noise—perfectly localized particles do not scatter. Hence the field expectation vanishes and only its variance gives a contribution.

7.3 Gaussian optomechanical treatment

So far, we have studied the mainly numerically accessible general system (7.1) of two particles in a ring resonator. Now, we investigate the special case of tightly confined particles allowing for more analytical insight into the dynamics. In this limit, it is justified to keep only the first- and second-order terms in the expansion of the trigonometric factors and the Hamiltonian (7.1) can be mapped onto the linearized optomechanical model

$$H = \sum_{i=1}^{2} \hbar\omega b_i^\dagger b_i - \hbar\Delta_\mathrm{c} a^\dagger a + \hbar g \sum_{i=1}^{2} (b_i + b_i^\dagger)(a + a^\dagger) \tag{7.6}$$

as shown in [7.20]. Here we have defined $\omega := \sqrt{4\hbar|U_0|\alpha_\mathrm{c}^2 E_\mathrm{R}}/\hbar$, $g := U_0\alpha_\mathrm{c}k\xi_0/\sqrt{2}$, the oscillator length $\xi_0 := \sqrt{\hbar/m\omega}$ and $b_i := (x_i/\xi_0 + \mathrm{i}\xi_0 p_i/\hbar)/\sqrt{2}$. The scaling of the oscillator length suggests that the Lamb–Dicke regime $k\xi_0 \ll 1$ may also be reached for very heavy particles in shallower traps. As we do not consider any direct particle–particle interactions, the Hamiltonian (7.6) is also valid for particles not confined in the same, but rather in distant sites within the resonator.

Interestingly, the Hamiltonian (7.6) applies to a whole class of systems. A few well-studied realizations are (i) a cavity with vibrating end mirrors where the mirror–light interaction is always linear and governed mainly by the cavity length and the zero point motion of the mechanics [7.31, 7.32], (ii) two light membranes inside a cavity field positioned at the maximum slope of the field amplitude where the coupling depends on the reflective properties of the membranes and is increased with decreasing mass [7.33] and (iii) very light nano-sized dielectric spheres held inside the cavity field either by an external trapping light mode or by means of optical tweezers [7.8].

The Hamiltonian (7.6) is quadratic in the bosonic operators so that an initially Gaussian state remains Gaussian throughout the time evolution. Gaussian states are completely defined by a displacement vector and a covariance matrix $V_{ij} := \frac{1}{2}\left[\mathrm{cov}(\xi_i, \xi_j) + \mathrm{cov}(\xi_j, \xi_i)\right]$, with $\xi := (\tilde{x}_1, \tilde{p}_1, \tilde{x}_2, \tilde{p}_2, X, P)$, $\tilde{x}_i := x_i/\xi_0 = (b_i + b_i^\dagger)/\sqrt{2}$, $\tilde{p}_i := p_i\xi_0/\hbar = (b_i - b_i^\dagger)/(\mathrm{i}\sqrt{2})$ and the field quadratures X and P [7.34]. As shown in [7.35], the time evolution of V is determined by the equation (its steady-state version is called the Lyapunov equation)

$$\dot{V}(t) = AV(t) + V(t)A^T + B, \tag{7.7}$$

where A and B are the drift- and diffusion matrices appearing in stochastic Heisenberg–Langevin equations equivalent to the master equation. The steady-state solution of (7.7) for the covariances is $\mathrm{cov}(\tilde{p}_1, \tilde{p}_2) = \mathrm{var}(\tilde{p}_i) - 1/2$ and $\mathrm{cov}(\tilde{x}_1, \tilde{x}_2) = \mathrm{var}(\tilde{x}_i) - 1/2$ (both particles behave the same way). It only exists in the cooling regime $\Delta_\mathrm{c} < 0$ since the momentum variance is only positive for red detuning. The momentum covariance is also genuinely positive. For $\mathcal{C}_p$ we find the simple (g-independent) expression

$$\mathcal{C}_p = \frac{\kappa^2 + (\Delta_\mathrm{c} + \omega)^2}{\kappa^2 + (\Delta_\mathrm{c} - \omega)^2} > 0, \tag{7.8}$$

which is precisely the ratio of the Stokes- (Γ_-, heating) and anti-Stokes (Γ_+, cooling) scattering rates found when adiabatically eliminating the cavity field [7.9]. These rates $\Gamma_\pm = \frac{g^2\kappa}{\kappa^2+(\Delta_c\pm\omega)^2}$ also define the time scale $\tau \sim (\Gamma_+ - \Gamma_-)^{-1}$ on which the steady state is reached.

$\mathcal{C}_p$ has a minimum at $\Delta_c = -\sqrt{\kappa^2+\omega^2}$ and approaches unity for $|\Delta_c| \to \infty$ and $\Delta_c \to 0^-$. From the form of the steady-state covariance matrix we can deduce that steady-state entanglement between the particles can only occur if $\mathrm{cov}(\tilde{x}_1, \tilde{x}_2) < 0$, which implies squeezing of the position variable. This is a direct consequence of the entanglement criterion derived in [7.36]. See figure 7.7 for an example of the Lyapunov time evolution. For such deep potentials (a regime which we can numerically analyse by changing the effective parameters ω and g to the values listed in figure 7.7) we restricted ourselves to Monte Carlo simulations of the master equation containing the Hamiltonian (7.6). Again, the C++QED framework provides a helpful basis for their numerical implementation as it also supports the simulation of coupled oscillators.

The steady-state covariance matrix reveals strong correlations between the particles and the field quadratures, making it intuitively clear that the reduced conditional density matrix for the particles strongly differs from its steady-state counterpart. Each photon detection highly influences the joint state of particles and cavity field. We show both density matrices in figure 7.7. The logarithmic negativity for the conditional density matrix is $\mathcal{E}_\mathcal{N} \approx 0.25$ and $\mathcal{C}_p$ is found to be $\mathcal{C}_p \approx 0.9$. Due to the particles–field correlations in steady state the conditional density matrix (7.4) does not describe a Gaussian state. Indeed, it reveals a double-peak structure.

Given that steady state dynamics shows little or no traces of the entanglement that is clearly present in individual trajectories, we pursue now an alternative road that investigates the transient regime. Such a regime could for example be reached with short light pulses that can be used to generate build-up of motional correlations in the system. While we are free to explore any regime numerically, the problem can be analytically tackled mainly in the adiabatic case where the cavity mode can be eliminated from the dynamics, when $g \ll \kappa$ or $g \ll |\Delta_c \pm \omega|$ [7.9]. We verify, however, that the generality is not lost since numerical investigations show the optimal entanglement regime indeed being around the point analytically treated.

We skip the cumbersome analytical elimination procedure (that closely follows the one used in [7.9]) and simply make use of the simple form of the end result that shows displacement–displacement coupling of the reduced bipartite system, $H_{\mathrm{eff}}^{\mathrm{int}} \approx -\hbar\Upsilon \sum_{jk} \tilde{x}_j \tilde{x}_k$, with

$$\Upsilon = -\left(\frac{\Delta_c - \omega}{\kappa}\Gamma_- + \frac{\Delta_c + \omega}{\kappa}\Gamma_+\right). \tag{7.9}$$

A second result of such an elimination procedure is that decay of the system can occur in a correlated fashion, namely with an effective jump operator proportional to $b_1 + b_2$. Now, we choose the operating conditions such that $\tilde{x}_1\tilde{x}_2$ reduces to a simple beam splitter interaction $b_1^\dagger b_2 + b_2^\dagger b_1$ and point out a very general conclusion (see [7.37]) that this interaction does not lead to entanglement when starting in

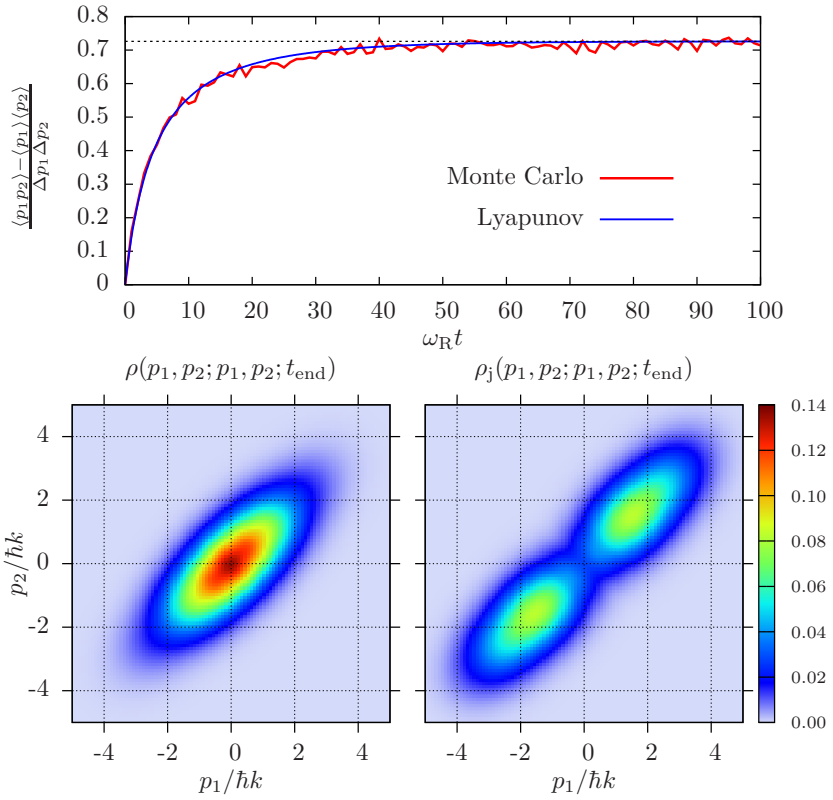

Figure 7.7: Upper plot: momentum correlation obtained from Monte Carlo simulations in the Lamb–Dicke limit for $k\xi_0 = 0.1$ (red, ensemble of 500 trajectories) and solution of equation (7.7) (blue). The position correlation is likewise pronounced. Lower plots: diagonal elements of the reduced particle density matrix in steady state (left) and of the reduced conditional density matrix (7.4) (right). Parameters: $\omega = 200\omega_R$, $g = 5\omega_R$, $\kappa = 100\omega_R$ and $\Delta_c = -20\omega_R$. Note that here the particles–field interaction is much stronger than in figure 7.2 where $g \approx 0.2\omega_R$.

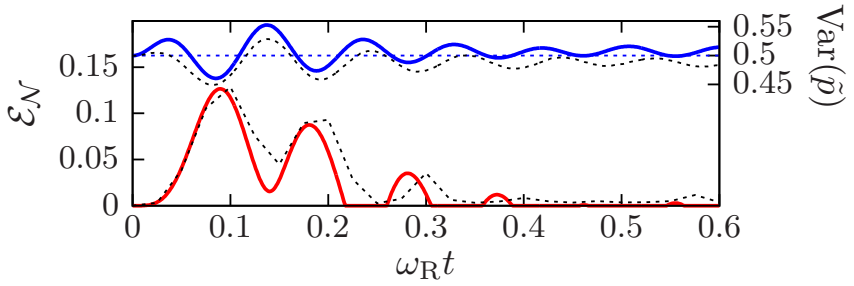

Figure 7.8: Transient entanglement (lower red curve) and momentum variance (upper blue curve) as obtained from the Lyapunov equation. Black dashed lines: solution of the master equation for the ring resonator (2000 trajectories), for comparison. Parameters: $\omega = 30\omega_\mathrm{R}$, $g = 5\omega_\mathrm{R}$, $\kappa = 5\omega_\mathrm{R}$ and $\Delta_\mathrm{c} = -(\omega - \kappa)$.

non-correlated initial states but rather to a simple state swap process where in the limit of strong coupling (coupling larger than decoherence rates), a quantum state of a subsystem can be written on the other subsystem. Than, taking advantage of the correlated decay, we show that transient entanglement is present in transient dynamics. This is illustrated in figure 7.8 where we show the time evolution of the logarithmic negativity. The relatively large entanglement obtained at half of the interaction time (defined by the inverse of the effective coupling strength g) can be accessed in an experimental situation for example by the use of laser pulses of tailored shape and duration.

Our effective optomechanical Hamiltonian (7.6) is formally similar to a model describing the microscopic dynamics of self-organization of particles in a cavity field [7.38]. The behaviour of single trajectories there can be explained with the help of an adiabatic model. We now strive to develop a model in the spirit of [7.38], capable of describing the behaviour of single Monte Carlo trajectories of the master equation containing the Hamiltonian (7.6). To this aim, we diagonalize the scattering operator $\sum_i (b_i + b_i^\dagger)$ to obtain the new particle basis $\{|e_i\rangle\}$ containing radiative (eigenvalue $\lambda_i \neq 0$, they always appear with both signs ± 1) and non-radiative ($\lambda_i = 0$) states. Ignoring terms stemming from the oscillator energies for the moment, the radiative states radiate a field $|\lambda_i \alpha\rangle$ with $\alpha := -\mathrm{i}g/(\kappa - \mathrm{i}\Delta_\mathrm{c})$. The crucial assumption now is adiabaticity (cavity decay assumed to define the fastest time scale), i.e. we assume each particle state $|e_i\rangle$ to be correlated with its associated unperturbed field state to find the approximated joint particle–field stochastic state vector

$$|\psi(t)\rangle = \sum_j c_j(t)\, |e_j\rangle\, |\lambda_j \alpha\rangle\,. \tag{7.10}$$

The coefficients $c_i(t)$ are determined by the effective conditional Monte Carlo time

evolution generated by the non-Hermitian Hamiltonian (abbreviating $|i\rangle := |e_i\rangle$)

$$H_{\mathrm{nH}} := \hbar\omega \sum_{ij} \langle i| \sum_k b_k^\dagger b_k |j\rangle |i\rangle \langle j| - \mathrm{i}\hbar\kappa \sum_i |\lambda_i \alpha|^2 |i\rangle \langle i| \tag{7.11}$$

for the particles only. Its Hermitian part contains the oscillator energies expressed in the scattering basis and couples the constituents of the latter.

From the form of the state vector (7.10) one can conclude what happens if a photon is detected. Applying the jump operator $\propto a$ on the internal state (7.10) at time t_j yields $a\,|\psi(t_\mathrm{j})\rangle \propto \sum_i c_i(t_\mathrm{j})\lambda_i\,|e_i\rangle\,|\lambda_i\alpha\rangle$. Hence, all information about the non-radiative contributions are erased and the relative phases between the radiative states change sign (as for each λ_i there exists also an eigenvalue $-\lambda_i$). Since $|\lambda_i\alpha|^2 \ll 1$ the reduced density matrix for the particles directly after a jump mainly contains the pure state $|\psi_\mathrm{p}\rangle \propto \sum_j c_j(t)\lambda_j\,|e_j\rangle$ (during the time evolution the particle state reads $|\psi_\mathrm{p}\rangle \approx \sum_j c_j(t)\,|e_j\rangle$). Inserting the coefficients for a state describing two particles in the ground state, the first jump excites one of them and the photon number increases by a factor of 3. The resulting state of the particles $|\psi_\mathrm{p}\rangle \approx \frac{1}{\sqrt{2}}\left(|\psi_0\psi_1\rangle + |\psi_1\psi_0\rangle\right)$ is entangled with $\mathcal{E}_\mathcal{N} = 1$ and correlated with $\mathcal{C}_p = 1/2$. Beginning with the second jump, fast oscillations with a frequency determined by ω build up, which is in qualitative agreement with single trajectories of the ring resonator model as shown in figure 7.2. This way it is possible to qualitatively and quantitatively reconstruct single trajectories of the optomechanical model (7.6).

7.4 Conclusion and outlook

Starting from two particles in a ring resonator, our conclusions are quite general. We have proposed a tripartite optomechanical system with two identical oscillators that can be correlated via the mediation of a photon field and the interaction amplified by the cavity confinement. The Gaussian evolution of the reduced mechanical bipartition has been followed both numerically and analytically, while non-Gaussian effects owing to the deviation from the bilinear Hamiltonian have been investigated numerically. The non-intuitive and classically forbidden positive momentum correlations are an important result of the paper, and are interpreted as strong delocalizations (superpositions) of the centre-of-mass independent of the particle separation and thus of the extension of the effective system; this suggests possible use of the setup to test the quantum-classical boundary. Furthermore, we have studied entanglement on single Monte Carlo trajectories as well as of the averaged density matrix. Entanglement heralded by photodetection has also been investigated. Transient entanglement as shown here can also be exploited in a pulsed regime where light pulses can drive the mechanical bipartition into a strongly entangled state.

Acknowledgments

This work has been supported by the Austrian Science Fund FWF through projects P20391, P207481 and F4013 and by the EU-ITN CCQED project. We would like to thank Cecilia Cormick, Tobias Grießer, Sebastian Krämer and András Vukics for helpful discussions and Hans Embacher for technical support.

Chapter 8

Publication

EPL (Europhysics Letters) **104**, 43001 (2013)

Subrecoil cavity cooling towards degeneracy: A numerical study[†]

R. M. Sandner, W. Niedenzu and H. Ritsch

Institut für Theoretische Physik, Universität Innsbruck - Technikerstraße 25, 6020 Innsbruck, Austria, EU

We present a detailed numerical analysis of the temperature limit and timescale of cavity cooling of a dilute gas in the quantum regime for particles and light. For a cavity with a linewidth smaller than the recoil frequency efficient cooling towards quantum degeneracy is facilitated by applying a tailored sequence of laser pulses transferring the particles towards lower momenta. Two-particle Monte Carlo wave function simulations reveal strongly improved cooling properties for a ring versus a standing-wave geometry. Distinct quantum correlations and cooling limits for bosons and fermions demonstrate quantum statistical effects. In particular, in ring cavities the photon-mediated long-range interaction favours momentum-space pairing of bosons, while fermion pairs exhibit anti-correlated or uncorrelated momenta. The results are consistent with recent experiments and give encouraging prospects to achieve sufficient conditions for the condensation of a wide class of polarisable particles via cavity cooling.

URL: `http://iopscience.iop.org/0295-5075/104/4/43001`
DOI: 10.1016/j.cpc.2014.04.011
PACS: 37.30.+i, 37.10.-x, 38.10.Vz

[†]The author of the present thesis performed all the calculations in this publication. W. N. acted as a discussion partner on all other aspects of the work.

8.1 Introduction

Cavity cooling has been proposed and successfully demonstrated in practise as a quite general method to cool polarisable point particles already more than a decade ago [8.1–8.4]. Several important experimental demonstrations using various systems and geometries were recently achieved [8.5], also in close connection to optomechanical cooling [8.6, 8.7]. In its generic form, this cooling mechanism works without the need of resonant excitation and spontaneous emission and reveals a final temperature only limited by the linewidth κ of the cavity mode involved, i.e. $k_{\mathrm{B}}T \approx \hbar\kappa$ [8.5]. For deeply trapped particles one can operate in the sideband cooling regime with trapping frequency ν larger than κ, where ground-state cooling can be expected [8.6, 8.8]. In the opposite case, where the cavity-generated optical potential is shallow compared to the particles' kinetic energy, the situation is much more complex as we have to consider the full sinusoidal dependence of the mode function.

As the optical potential is periodic with half of the wavelength, photon scattering only exchanges multiples of two recoil momenta between the atomic motion and the cavity field. Microscopically, this corresponds to a consecutive absorption and stimulated emission process of cavity photons. Hence, on the one hand one could argue that cavity cooling cannot achieve temperatures below the recoil limit due to the half-wavelength periodicity of the cavity potential [8.9]. On the other hand, a cavity with frequency and energy resolution below a single recoil could be suited to surpass this limit by energy selection. Strong evidence for this effect has been reported in recent experiments in Hamburg, where cavity cooling on the subrecoil scale has been observed [8.10].

In this letter we study the quantum limit of cavity cooling in great detail by help of quantum Monte Carlo wave function simulations [8.11, 8.12] of the corresponding master equation. In order to allow investigations of particle quantum statistics and correlations, we need to consider at least two particles coupled to the cavity field, which itself can support a single or two modes. Even when confining the particle motion along the cavity axis we still have to account for at least three independent quantum degrees of freedom. Despite restriction to only a few photons per mode and a not too high spatial resolution of the wave function, the associated Hilbert space typically consists of several ten thousand dimensions, which requires substantial computational effort. Here we make use of C++QED [8.13], a freely available framework for simulating open quantum dynamics.

In the following, upon introducing our system Hamiltonian and master equation and defining the operating parameters we first present the results of a three-stage cooling process from a thermal distribution towards the quantum ground state. We then study the mean kinetic energy and address the influence of invariant subspaces on the final temperature and state. In the last part we analyse the appearance of momentum correlations during the cooling process, which can be nicely seen and interpreted via the two-particle momentum distributions.

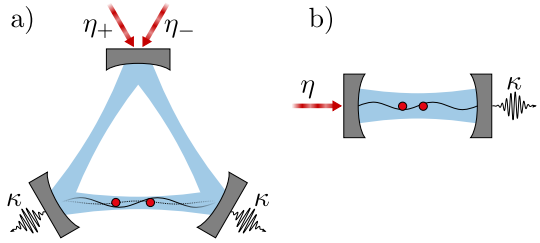

Figure 8.1: Two identical particles interacting with a) two degenerate modes of a ring resonator and b) a single standing-wave mode.

8.2 Theoretical model

We consider two polarisable particles (e.g. two-level atoms, molecules, nanobeads) of mass m moving along the axis of an optical resonator, as depicted in fig. 8.1.

Assuming large detuning between the light and optical particle resonances, the particles' internal excitation will remain small and spontaneous emission can be neglected [8.5]. The intracavity light is described by one or two degenerate standing-wave eigenmodes. For our studies the description of the two-mode ring resonator (cf. fig. 8.1a) in terms of standing-wave modes $\propto \sin(kx)$ and $\propto \cos(kx)$ with wave number k [8.6, 8.14] is more convenient than the mathematically equivalent description with a set of running-wave eigenmodes $\propto \exp(\pm \mathrm{i}kx)$. It allows easier comparison with the linear resonator (cf. fig. 8.1b) by formally restricting one of the modes to zero photons. The coherent interaction of particles and field modes of the ring resonator is then described by the Hamilton operator [8.6]

$$\begin{aligned} H = \sum_{i=1}^{2} \left[\frac{p_i^2}{2m} + \hbar U_0 (a_\mathrm{c}^\dagger a_\mathrm{c} \cos^2(kx_i) + a_\mathrm{s}^\dagger a_\mathrm{s} \sin^2(kx_i)) \right] \\ + \frac{\hbar U_0}{2} \left(a_\mathrm{c}^\dagger a_\mathrm{s} + a_\mathrm{s}^\dagger a_\mathrm{c} \right) \sum_{i=1}^{2} \sin(2kx_i) \\ - \hbar \Delta_\mathrm{c} a_\mathrm{c}^\dagger a_\mathrm{c} - \hbar \Delta_\mathrm{c} a_\mathrm{s}^\dagger a_\mathrm{s} - \mathrm{i}\hbar\eta \left(a_\mathrm{s} - a_\mathrm{s}^\dagger \right). \end{aligned} \tag{8.1}$$

Here x_i and p_i are the particles' centre-of-mass position and momentum operators, respectively, $U_0 < 0$ is the potential depth per photon and $a_\mathrm{s}^\dagger$ ($a_\mathrm{c}^\dagger$) is the creation operator for sine (cosine) mode photons. The pump laser of effective strength η is detuned by $\Delta_\mathrm{c} := \omega_\mathrm{p} - \omega_\mathrm{c}$ from the bare cavity resonance frequency. Note that an effective driving of the sine mode (as considered here) can be realised by symmetrically driving the two counter-propagating running-wave modes with an appropriate phase relation [8.6]. Whilst the first line of the Hamiltonian (8.1) accounts for the two potentials created by the degenerate light modes, the second line describes the particle-mediated coherent redistribution of photons between the two modes, which is responsible for photon scattering to the unpumped cosine mode.

The Hamiltonian evolution, however, cannot take track of the dissipative process

of photon leakage through the resonator's mirrors. Indeed, the system needs to be characterised by its density operator ρ with time evolution

$$\dot{\rho} = \frac{1}{\mathrm{i}\hbar}\left[H, \rho\right] + \mathcal{L}_{\mathrm{c}}\rho + \mathcal{L}_{\mathrm{s}}\rho, \tag{8.2}$$

where the Liouvillean superoperators in this master equation explicitly read $\mathcal{L}_i\rho = \kappa\left(2a_i\rho a_i^\dagger - a_i^\dagger a_i\rho - \rho a_i^\dagger a_i\right)$ for $i \in \{\mathrm{c}, \mathrm{s}\}$ [8.15] with the photon number decay rate 2κ. Note that the linear cavity (cf. fig. 8.1b) is obtained from eq. (8.2) by formally setting $a_{\mathrm{c}} = 0$.

Direct particle–particle interactions as collisions are neglected in our model. They will certainly play a role at higher densities and should be included in a next-step model. Here we concentrate on cavity cooling and only shortly come back to possible effects of collisions in the follwing section.

8.3 Simulation of cavity cooling in the quantum regime

In this letter we concentrate on the weak pump case, where the intracavity light fields are responsible for friction and diffusion and mediate long-range interparticle interactions, but do not contribute to particle confinement. The latter is provided by an external magnetic or optical trap with trap frequencies much below the recoil frequency. Targeting quantum degeneracy in this trap naturally requires a full quantum treatment of both, field modes and particles, which renders a direct integration of the master equation (8.2) computationally unfeasible due to the large dimension of the joint Hilbert space. For this reason we run Monte Carlo wave function simulations (MCWFS) [8.11, 8.12], where the evolution of stochastic state vectors is induced by a non-Hermitian effective Hamilton operator including damping. This deterministic propagation is interrupted by quantum jumps at random times, which can be interpreted in terms of photon counting events of the light leaving the resonator. For large ensembles the statistical mixture of such stochastic states converges towards the full solution of the master equation. The numerical implementation of these Monte Carlo wave function simulations was realised with the aforementioned C++QED framework [8.13].

Note that the chosen parameter regime is in contrast to our previous work on deeply trapped particles [8.16], where the strong pump field mode is used to trap the particle and can be replaced by a c-number to obtain a much smaller effective Hilbert space.

To discretise the Hilbert space we introduce periodic boundary conditions for the particles at $kx = \pm\pi$, yielding two-particle momentum basis states $|n, m\rangle := |p_1 = n\hbar k\rangle \otimes |p_2 = m\hbar k\rangle$ with integer n, m. We start from an empty cavity without photons and the two particles located at $kx = \pm\pi/2$ with a Gaussian distribution and zero average momentum, properly (anti-)symmetrised for bosons (fermions). Here we neglect the spin degrees of freedom as is justified e.g. for spin-polarised particles. Other possible configurations like pairs of fermions with opposite spins,

as they appear in the BCS model [8.17], might show yet another behaviour but are beyond the scope of this letter.

In order to model the characteristics of a thermal state and to remove artefacts due to the periodic boundary conditions, we assign random phases to each basis component of the Monte Carlo trajectory initial states. For sufficiently many trajectories the initial state then becomes a statistical mixture of momentum states without any coherences. Note that here the two particles are only found in momentum states with the same parity if they are bosons or in momentum states with different parity if they are fermions. Implications of this choice will be discussed in the next section.

Standard semiclassical simulations of cavity cooling of point particles predict a final temperature $k_{\mathrm{B}}T \approx \hbar\kappa$ only limited by the cavity linewidth κ, which also agrees with full quantum simulations to very low temperatures [8.1]. While smaller κ leads to lower temperature, unfortunately the time scale for cooling becomes much slower as well and the effective velocity capture range is reduced [8.18]. This renders cooling of a wide momentum distribution towards degeneracy in a single step experimentally impractical. Hence, here we present a multi-step cooling scheme as inspired by the recent Hamburg experiment [8.10], where the operating parameters are adjusted in time to speed up cooling by first precooling the highest momenta and subsequently reducing pump power η and detuning $|\Delta_{\mathrm{c}}|$ for the final step.

So far we have ignored any effects stemming from direct atom–atom collisions in our effective 1D approximation of the cooling geometry. As can be seen from a Fourier transformation of the Hamiltonian (8.1), momentum transfer between atomic states can only occur in portions of $\Delta p = \pm 2\hbar k$. Therefore the total population in the odd and even momentum subspaces is conserved by the Hamiltonian evolution. In a realistic experimental trap, however, there will be transverse motion and particle–particle collisions on longer timescales mixing these two families, e.g. two particles with momentum $|1,1\rangle$ can scatter into the $|0,2\rangle$ state and vice versa. The fast $2\hbar k$ particle is then cavity-cooled to zero velocity, which makes this effective process unidirectional. Another important aspect of collisions has been observed in the aforementioned Hamburg experiment [8.10], where they play a crucial role in cooling particles from non-integer momentum states in the vicinity of $p = \pm 2\hbar k$ to the zero momentum state. As it is not in the scope of the present work to describe these processes, but much rather the essence of cavity cooling of a thermal state with broad momentum distribution, we refrain from including collision terms in the simulations at this point.

The effective detuning of the pump is chosen such that the creation of a photon in the cavity is energetically strongly suppressed if not accompanied by momentum transfer. Cooling is achieved when a scattered photon leaves the resonator, which eliminates the re-absorption possibility [8.19]. In most cases this prevents standard laser cooling to reach degeneracy, although this limitation has recently been surpassed in an Innsbruck experiment [8.20]. Intuitively, in the regime $\Delta_{\mathrm{c}} < 0$ the cavity-enhanced scattering to the blue sideband extracts energy from the particles' motion [8.5]. To resonantly enhance this process the detuning is chosen to match the energy difference between the final and initial atom states. From the dispersion relation for free particles with

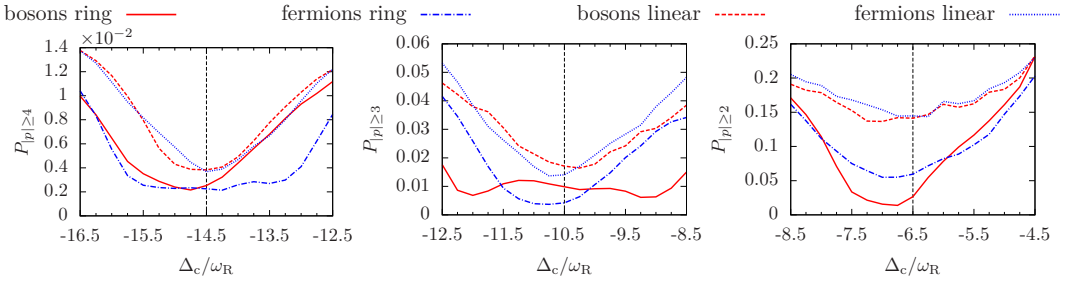

(a) Stage 1, $\eta = 3\omega_R$ (b) Stage 2, $\eta = 2\omega_R$ (c) Stage 3, $\eta = 0.5\omega_R$

Figure 8.2: Population fraction not addressed by the cooling process for the three cooling steps as a function of the cavity-pump detuning scanned around the free-space optimal value (8.3). The final step (c) targets ground-state cooling as in the Hamburg experiment [8.10]. Parameters: $U_0 = -2.5\omega_R$ and $\kappa = 0.25\omega_R$.

$\Delta p = -2\hbar k$ one thus obtains

$$\Delta_c - NU_0\left\langle \sin^2(kx)\right\rangle \stackrel{!}{=} \frac{P_{\text{final}}^2}{2\hbar m} - \frac{P_{\text{init}}^2}{2\hbar m} = 4\omega_R\left(1 - \frac{K_{\text{init}}}{k}\right), \tag{8.3}$$

where $N = 2$ is the number of particles, $P = \hbar K$, $K_{\text{init}} \geq 2k$ and $\omega_R \equiv E_R/\hbar := \hbar k^2/(2m)$ is the recoil frequency. As the particles are nearly homogeneously distributed in position space, the bunching parameter $\mathcal{B} := \langle \sin^2(kx)\rangle$ determining the cavity frequency shift induced by the particles is well approximated by $\mathcal{B} \approx \frac{1}{2}$. In the regime of weak cavity pump with potential depths well below the recoil energy, the particle position space distribution remains approximately homogeneous throughout the cooling process and hence the bunching parameter stays constant. For condition (8.3) to be relevant, a narrow cavity resonance on the recoil frequency scale is required, i.e. the damping constant κ needs to be less than the smallest possible kinetic energy transfer, $\kappa \ll 4\hbar k^2/(2m) \equiv 4\omega_R$. The condition of well-resolved lines also requires that the photon numbers and the coupling strength $|U_0|$ are sufficiently small to avoid broadening of the resonance.

Because of the quadratic dispersion relation and the small linewidth only one process with momentum transfer $|p| = n\hbar k \to |p| = (n-2)\hbar k$ with integer $n \geq 2$ can be resonant for a given detuning. In order to efficiently cool an initial state which contains momentum contributions up to $|p| = 4\hbar k$, in analogy to [8.10], we thus apply a pulse sequence with three separate stages, which aim to transfer $|p| = 4\hbar k \to |p| = 2\hbar k$, $3\hbar k \to \hbar k$ and $2\hbar k \to 0\hbar k$, respectively. Ideally, the final state then only has contributions of the two lowest momentum states with $p = 0\hbar k$ and $p = \pm\hbar k$, with their relative magnitude determined by the initial distribution in the two (odd and even) momentum subspaces. In an experiment one could of course also envisage a continuous frequency ramp of the pump laser or cavity resonance.

In order to determine the optimal detuning for the three-step cooling sequence, we scan the resonance around the anticipated optimal detuning as given in eq. (8.3). In

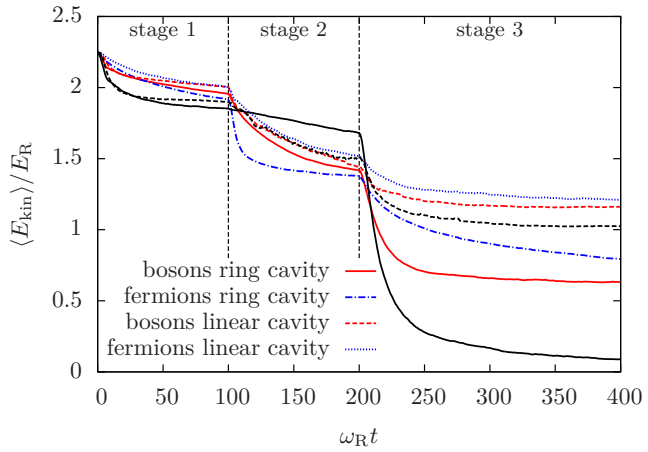

Figure 8.3: Time evolution of the single particle kinetic energy in an optimised three-stage process. Detunings for the three stages: $\Delta_{\rm c}/\omega_{\rm R} = (-14.75, -12, -7)$ (ring cavity bosons), $\Delta_{\rm c}/\omega_{\rm R} = (-14.5, -10.25, -7)$ (linear cavity bosons), $\Delta_{\rm c}/\omega_{\rm R} = (-14.25, -10.75, -6.75)$ (ring cavity fermions) and $\Delta_{\rm c}/\omega_{\rm R} = (-14.5, -10.75, -6.25)$ (linear cavity fermions). The other parameters are the same as in fig. 8.2. Black lines: initial state containing only even momenta for bosons in a ring (solid) and a linear cavity (dotted).

fig. 8.2 we plot the residual population remaining in states with momenta larger or equal to the momentum state which is targeted for depletion as a function of the detuning and choose the minimum as the detuning for this stage. Due to photons being generated during cooling the particle energies are slightly shifted and also the bunching parameter can change by a small amount. Thus the optimum detuning deviates from the expected free-space value (8.3), which could also be attributed to an effective mass of the particles in the weak cavity-generated lattice.

To study quantum-statistical effects explicitly we compare both cases of bosons and fermions. Interestingly, pronounced differences in cooling rates and pairing appear already in the first cooling stage applied to a relatively hot ensemble not too close to degeneracy. In order to investigate the influence of cavity-mediated interactions in greater detail we compare a ring cavity geometry (cf. fig. 8.1a) and a linear cavity as depicted in fig. 8.1b, i.e. by formally setting $a_{\rm c} = 0$ in the Hamiltonian (8.1). Here the differences are clearly due to the interactions generated by the second unpumped cavity mode.

8.4 Ground-state cooling

We now examine the results of the MCWFS for the optimised three-step cooling sequence, averaged over a sufficiently large ensemble of 1000 trajectories. Figure 8.3 shows the mean kinetic energy per particle $\langle E_{\rm kin}\rangle$ as a function of time. Note that for our choice of the initial state (cf. previous section) half of the population resides

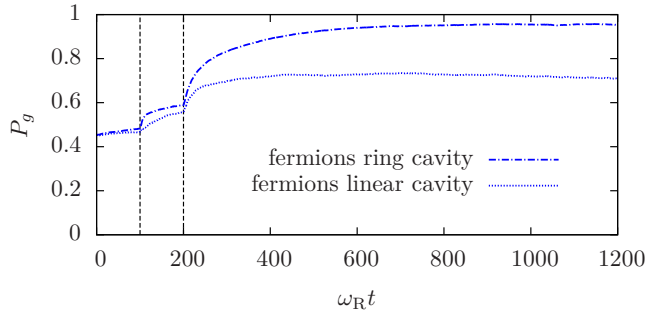

Figure 8.4: Projection onto the fermionic ground state P_g. The parameters are the same as in fig. 8.3.

in odd and even momentum states, respectively. Hence the best possible cooling achieves $\langle E_{\mathrm{kin}} \rangle = 0.5 E_{\mathrm{R}}$. For bosons, where in our initial state both particle momenta always have the same parity, this means that only half of the population can be cooled to the ground state $|0,0\rangle$. For fermions, however, the ground states are the anti-symmetrisations of $|\pm 1, 0\rangle$. As these states have mixed momentum parity, just like the initial state for fermions, it is in principle possible to cool the ensemble to quantum degeneracy as seen in fig. 8.4. The black lines in fig. 8.3 correspond to bosons with an initial condition where only even momentum states are populated. In the ring cavity case the mean kinetic energy approaches zero and quantum degeneracy is reached. In all cases cooling in the linear cavity is not as efficient compared to the ring cavity geometry. The reason for this will be discussed below.

In figs. 8.5 and 8.6 the single-particle momentum distribution is plotted over time. It can be seen that each stage redistributes states with a distinct momentum $|p| = n\hbar k$ to corresponding lower momentum states with $|p| = (n-2)\hbar k$. The greater efficiency of a ring cavity compared to a linear cavity is most apparent in the last stage, where in the standing-wave case a considerable fraction of the population remains trapped in the $|p| = 2\hbar k$ states. Figure 8.6 shows that for a ring cavity only a very tiny amount of population is left in the $|p| = 2\hbar k$ momentum state. Its ratio to the $p = 0$ population can be used as a first estimate for an effective temperature in the even momentum state space via $P_2/P_0 \approx \exp(-4E_{\mathrm{R}}/k_{\mathrm{B}}T_{\mathrm{eff}})$, which hints for a subrecoil cooling behaviour.

8.5 Qualitative difference between ring cavity and linear cavity

The fact that not all of the population is transferred to $|p| = 0, \pm 1\hbar k$ momentum in a standing wave is apparent from the final momentum space distributions. This effect is connected to subspaces of the two-particle Hilbert space which are invariant under the Hamiltonian (8.1) for $a_{\mathrm{c}} = 0$ and do not include the lowest energy states. Any population initially present in one of these subspaces is thus inaccessible to

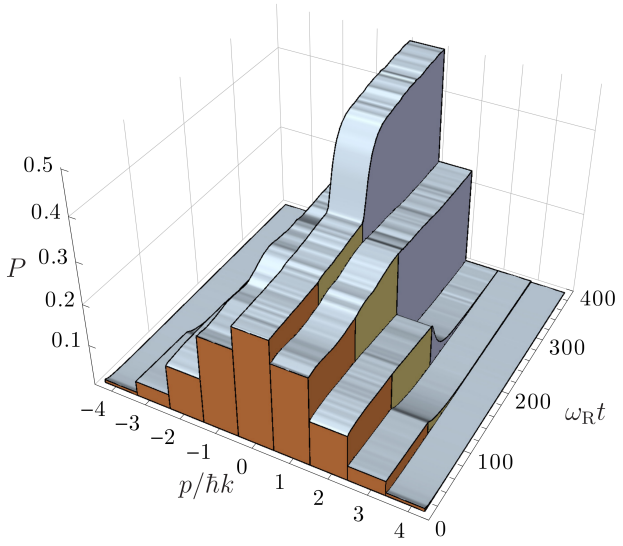

Figure 8.5: Single-particle momentum distribution for bosons in a ring cavity. The initially broad distribution is cavity-cooled to $|p| = 0, \pm 1\hbar k$ momentum states. The parameters are the same as in fig. 8.3.

ground-state cooling. A typical example is the bosonic state

$$|\psi\rangle = \big(|0,2\rangle + |2,0\rangle - |0,-2\rangle - |-2,0\rangle\big)/2. \tag{8.4}$$

This state is a dark state for the linear cavity and the particles will not scatter any photons. On the other hand, in a ring cavity the interference term between the two modes (i.e. the second line of eq. (8.1)) breaks this symmetry and the atoms redistribute light between the two modes while being transferred to the bosonic ground state $|0,0\rangle$. As mentioned above, collisions between particles or an external atom trap decrease the lifetime of such a dark state preventing population accumulation. This might explain the absence of these trapping states in the experiment [8.10].

8.6 Momentum correlations

Let us finally look at the connection between particle correlations, cavity cooling and quantum statistics in our simulations. Already in the classical limit particle correlations lead to important modifications of single-mode cavity cooling [8.21]. Classical simulations of ring cavities reveal a strong damping of the centre-of-mass motion leading to momentum space (anti-)pairing of particles [8.22]. On the contrary, for the case of two deeply trapped quantum particles or membranes in a ring resonator positive momentum correlations and even entanglement emerged [8.16]. The former can be quantified by the momentum correlation coefficient (normalised covariance)

$$\mathcal{C}_p := \frac{\mathrm{cov}(p_1,p_2)}{\Delta p_1 \Delta p_2} = \frac{\langle p_1 p_2\rangle - \langle p_1\rangle\langle p_2\rangle}{\Delta p_1 \Delta p_2}. \tag{8.5}$$

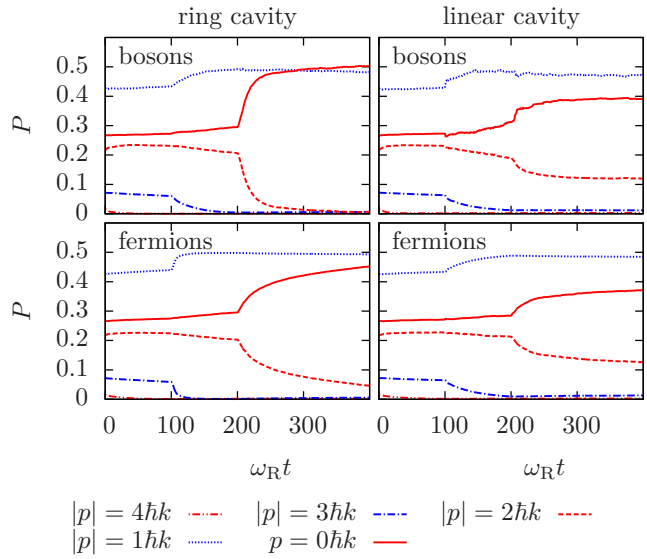

Figure 8.6: Occupation probabilities of the lowest few momentum eigenstates for bosons in a ring cavity (upper left), bosons in a linear cavity (upper right), fermions in a ring cavity (lower left) and fermions in a linear cavity (lower right). Same parameters as in fig. 8.3.

Here we extend this study to indistinguishable particles obeying either Bose or Fermi statistics. In fig. 8.7 we show $\mathcal{C}_p$ as a function of time exhibiting a complex evolution. Note that in the unperturbed ground state bosons as well as fermions are uncorrelated. Thus all population in the lowest energy states does not contribute to momentum correlations and ideal cooling should eliminate all correlations. The small excited state fraction, however, reveals strong correlations as highlighted in the two-particle momentum space distribution shown in fig. 8.8. As one might expect, fermions are anticorrelated and bosons are correlated in momentum space. This behaviour is substantially more pronounced in ring cavities and, in the case of bosons, survives very long cooling times, even exhibiting an oscillatory behaviour. Note that positive pair correlations with zero average momentum strongly point towards the appearance of momentum-entangled states.

Let us remark here that these correlations can be much stronger if the pump is tuned away from optimal cooling. One can enhance certain correlation by targeting the corresponding states instead of the ground state in a tailored pulse sequence. A detailed analysis, however, would go beyond the scope of this work.

8.7 Conclusion and outlook

Extensive numerical simulations confirm the experimental observation of subrecoil cooling towards degeneracy using high-Q cavities. We show that efficient cooling of a thermal distribution requires either collisional redistribution or several cavity modes

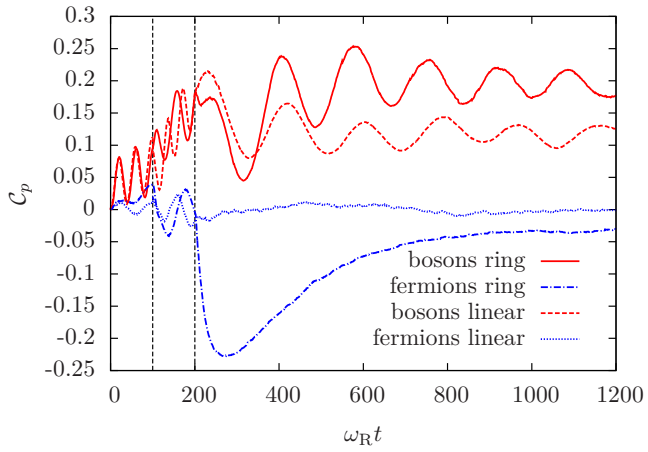

Figure 8.7: Momentum correlation coefficient (8.5) for different particle statistics and cavity geometries. The parameters are the same as in fig. 8.3.

to avoid the appearance of decoupled momentum subspaces, which cannot be cooled solely by a single mode as in the recent Hamburg experiment [8.10]. We predict that bosons and fermions can be cooled in the same way towards a high occupation of their respective ground states.

As a ring cavity works generally much better than a single-mode resonator one can expect further improvements including more modes similar to the classical case [8.23]. In principle, a linear cavity supports many non-degenerate modes separated by the free spectral range, so that one could also envisage an extension of the studied scheme to such a multimode setup. The sequential pulses can then be replaced by differently detuned driving lasers for these modes. This would allow to address the three cooling stages simultaneously and hence to reduce and optimise the cooling time. Such a setup also allows to generate and observe more exotic particle–particle correlations.

As a bottom line we suggest that cavity cooling is a viable route towards producing a degenerate gas of a wide class of polarisable particles without the need of evaporation. Hence it could be applied at much lower densities and particle numbers once a sufficient number can be loaded inside a high-Q resonator.

Acknowledgments

This work has been supported by the EU-ITN CCQED project, by the Austrian Science Fund FWF through project F4013 and by the Austrian Ministry of Science BMWF as part of the UniInfrastrukturprogramm of the Focal Point Scientific Computing at the University of Innsbruck.

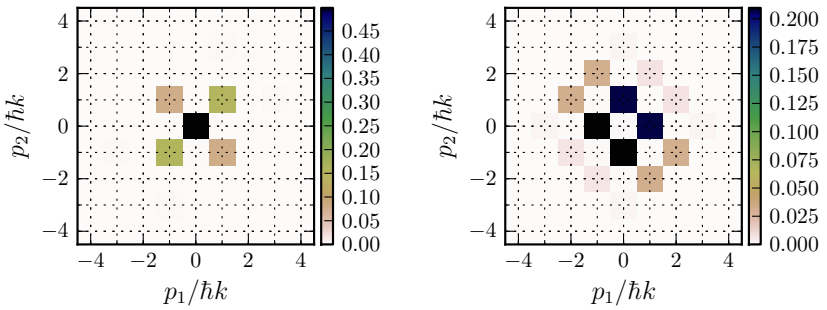

(a) Bosons ring, $\omega_R t = 600$ (b) Fermions ring, $\omega_R t = 300$

Figure 8.8: Two-particle momentum population at times where the (anti-)correlations are maximal according to fig. 8.7. Positive correlations (bosons) and negative correlations (fermions) can be seen in the occupation profiles being elongated along different diagonals.

Part IV

Laser-driven particles in resonators

Chapter 9

Background to cavity-induced atomic self-organisation

There are essentially two possibilities for coherently driving a coupled particle-cavity system with a laser: shining the laser on the partially reflecting mirrors of the cavity to drive the cavity mode, or shining the laser on the particle from the side. The former case has been discussed so far, in the latter case the particles are excited and can emit fluorescence photons to free space, but through the coupling to the resonator photons also can be scattered coherently into the cavity. In fact, in the far detuned regime of low atomic excitation and with a strong coupling constant g, the coherent scattering process dominates spontaneous emission [9.1]. As has been discussed before (cf. sec. 6.1), dynamical cavity cooling in the good cavity and strong coupling regime works by non-adiabatically exciting dressed states. These dressed states can be addressed with both laser pump configurations, therefore cavity cooling also works in a scenario where the particles are pumped transversally. This has been pointed out for example in [9.2], where even lower temperatures compared to a setup with direct cavity pump were predicted.

There is, however, a fundamental difference between the two scenarios. While the optical potential created by the cavity mode proportional to $\cos^2(kx)$ has a periodicity of $\lambda/2$, a transversal driving field leads to interference with the cavity field with the periodicity of λ. With an initially empty cavity mode and a homogeneous particle distribution, density fluctuations of the particles lead to photon scattering into the cavity and an emerging intra-cavity field with random phase. Above a certain threshold pump strength the system undergoes a transition from an unordered phase to a phase with long-range order in the resulting optical potential with λ-periodicity. Because the initial phase is random, there is a broken symmetry in this self-organisation process with two possible configurations: in two dimensions, these configurations resemble the occupation of black or white fields of a checker board, respectively. If the particle motion is restricted to one dimension, as is the case in the scope of this thesis, it is the occupation of either the 'odd' or the 'even' sites which characterise the self-organisation.

This unique effect has been predicted by Domokos *et al.* [9.3] and experimentally confirmed by Black *et al.* [9.4]. The underlying mechanism is a strong cooperative coupling of the atoms to the radiation field, leading to a runaway process where the atoms are trapped, cooled and organised in the field they scatter into the cavity,

enhancing further the rate of scattered light. Ultimately momentum diffusion and the resulting residual kinetic energy competes with the self-organisation process. The arising atomic distribution is comparable to a self-sustained Bragg lattice optimising scattering into the cavity. Historically, a similar effect of 'optical binding' has been predicted [9.5], and a related concept of self-organisation gives rise to the idea of a collective atomic recoil laser [9.6].

One of the signatures of self-organisation is a 'super-radiant' scaling of the intracavity intensity with N^2, the square of the particle number. In contrast, for a configuration with a spatial period of $\lambda/2$, negative interference of light scattered from the individual potential wells leads to a field intensity scaling proportional to N related to density fluctuations [9.3, 9.4]. Another signature is the observation of random jumps of π in the phase of the emitted cavity light between experimental runs, corresponding to the two possible configurations [9.4].

The significance of atomic self-organisation in an optical resonator extends beyond the possibility to circumvent a potentially unfavourable linear scaling of the cavity-assisted cooling time with the particle number [9.3, 9.7]. There is a strong connection between self-organisation and the famous Dicke model describing an ensemble of two-level atoms strongly interacting with a single mode [9.8], which is known to undergo a phase transition from a normal to a super-radiant phase [9.9]. A tremendous experimental challenge for any realisation of the Dicke model and its phase transition is the requirement of a coupling strength on the order of the energy separation of the involved states, a condition which is nearly impossible to satisfy directly for transitions in the optical frequency range. Instead it was proposed to utilise strong cavity-induced Raman-type coupling between atomic ground states [9.10], and this idea was then generalised to a two-mode expansion of the atomic matter field of a Bose-Einstein condensate [9.11, 9.12]. In fact, a laser-driven BEC inside a high-finesse cavity can be directly mapped to the Dicke model, with collective excitations in momentum space constituting self-organisation. In this configuration, the phase transition from the unordered to the organised phase is equivalent to the Dicke phase transition. The resulting state of matter can be regarded as a supersolid [9.13, 9.14] with non-trivial diagonal long-range order (periodic density modulations) and non-diagonal long-range order (phase coherence).

To the present day research on self-organisation is a very active field. The semi-classical regime [9.15–9.18] and self-organisation of bosons [9.19–9.23] has been studied extensively. Recently, the effect of fermionic statistic has been addressed [9.24–9.26], predicting a strong suppression of the pump threshold for self-organisation of a quantum-degenerate Fermi gas if the cavity photon momentum coincides with twice the Fermi momentum. Our own work presented in chapter 10 confirms this effect numerically for the few-particle case in simulations including quantum fluctuations of the particles and the cavity mode, without prescribing a fixed temperature and going beyond the two-mode expansion of the Dicke model.

Chapter 10

Publication

EPL (Europhyics Letters) **111**, 53001 (2015)

Self-ordered stationary states of driven quantum degenerate gases in optical resonators[†]

R. M. Sandner[1], W. Niedenzu[1,2], F. Piazza[1] and H. Ritsch[1]

[1]*Institut für Theoretische Physik, Universität Innsbruck, Technikerstraße 25, A-6020 Innsbruck, Austria*
[2]*Department of Chemical Physics, Weizmann Institute of Science, Rehovot 7610001, Israel*

We study the role of quantum statistics in the self-ordering of ultracold bosons and fermions moving inside an optical resonator with transverse coherent pumping. For few particles we numerically compute the nonequilibrium dynamics of the density matrix towards the self-ordered stationary state of the coupled atom-cavity system. We include quantum fluctuations of the particles and the cavity field. These fluctuations in conjunction with cavity cooling determine the stationary distribution of the particles, which exhibits a transition from a homogeneous to a spatially ordered phase with the appearance of a superradiant scattering peak in the cavity output spectrum. At the same time the cavity field Q-function changes from a single to a double peaked distribution. While the ordering threshold is generally lower for bosons, we confirm the recently predicted zero pump strength threshold for superradiant scattering for fermions when the cavity photon momentum coincides with twice the Fermi momentum.

URL: `http://iopscience.iop.org/article/10.1209/0295-5075/111/53001`
DOI: 10.1209/0295-5075/111/53001
PACS: 37.30.+i, 37.10.Vz

[†]The author of the present thesis performed all the calculations and numerical simulations in this publication, except of the scaling behaviour of the threshold with N, which was obtained by F. P. Furthermore, W. N. assisted in the implementation of the numerical simulations and, together with F. P., acted as a discussion partner on all other aspects of the work.

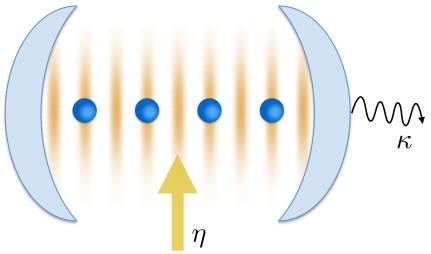

Figure 10.1: Polarisable particles moving along the axis of a standing-wave optical resonator are coherently pumped in the transversal direction. Above a critical threshold the particles collectively scatter photons into the cavity while organising themselves in the emerging optical potential.

10.1 Introduction

Ultracold particles moving in an optical resonator are a fast growing research field since the advent of laser cooling [10.1–10.3]. The establishment of cavity cooling [10.4] extended cooling possibilities to a large class of linearly polarisable particles and in the last years cavity optomechanics [10.5] has experienced a tremendous boost, both theoretically and experimentally [10.3]. Recently, cavity cooling was even extended to the subrecoil regime in the domain of ultracold quantum gases where the nonlinear coupled dynamics of field and particles require a full quantum description [10.6–10.8].

Particularly rich physical dynamics appear for transversally illuminated particles inside high-Q optical resonators (cf. fig. 10.1), where the cavity-induced backaction of the scattered field onto the particles induces a phase transition to crystalline particle order. First described semiclassically [10.9–10.15] this phenomenon also appears quantum-mechanically as a phase transition at zero temperature [10.16–10.23]. Above a critical threshold pump laser intensity the atoms form self-sustained regular Bragg lattices, which maximise the collective scattering of laser light into the resonator (superradiance). Self-organisation has been experimentally demonstrated with both thermal gases [10.24, 10.25] and atomic Bose-Einstein condensates (BECs) [10.26–10.28]. It bears a close connection to the generic model of the Dicke superradiant phase transition [10.29–10.31].

Interestingly, the quantum statistical properties of the particles have a decisive influence onto the self-ordering dynamics. As a particularly striking effect, a resonant reduction of the superradiance threshold for fermions almost towards zero pump amplitude has been predicted when the cavity photon momentum coincides with twice the Fermi momentum [10.32–10.34].

Since we are dealing with an open system with atom pumping and photon leakage through the mirrors, fluctuations and nonthermal equilibrium phenomena are essential parts of the full dynamics, as already observed experimentally [10.35, 10.36]. We consider here the so-called dispersive limit at high laser to atom detuning, where the particles constitute a dynamic refractive index within the resonator and only coherently scatter pump laser light into the cavity. The relative phase and magnitude

of the scattered photons depend on the particle positions, while the motion of the latter is governed by the optical dipole force exerted by the cavity and pump fields [10.1]. Recent experiments [10.6, 10.28, 10.36] have achieved cavity loss rates small enough to be comparable to the particle recoil energy scale. Lacking separate timescales, the light field then does not adiabatically follow the particle motion, inducing an even more complex correlated or even entangled particle-field dynamics.

At the semiclassical level and for distinguishable particles the nonthermal properties of the corresponding stationary equilibrium state and its transient dynamics have been studied recently [10.12–10.15]. A related study was carried out for bosons at zero temperature with emphasis on the effect of cavity losses on the depletion of a BEC [10.37]. In addition, the effect of fermionic statistics on the nonequilibrium stationary state has been explored with perturbative diagramatic techniques [10.38].

In this work we investigate quantum-statistical effects on the nonequilibrium stationary state close to the self-organisation threshold. Upon including quantum fluctuations and Markovian noise induced by photon losses, we compute the density matrix of the joint state of light and up to five atoms. Here the particles' average energy is not set by a prescribed temperature, instead their momentum distribution follows dynamically from the interplay of cavity cooling and fluctuations. In general, a nonthermal distribution emerges, which exhibits strong atom-field correlations. In principle, even starting from a particle ensemble at finite temperature, the combined cooling and self-ordering can lead to a quantum degenerate ordered final state.

Since the photons leaking out of the cavity provide a directly accessible non-destructive probe of the system, we characterise the self-organisation transition with the help of the Husimi-Q-function, the intensity and the power spectrum of the light emitted from the cavity. This provides an experimentally directly accessible tool, so that the whole self-ordering phase transition process can be monitored in real time even in a single experimental run with minimal backaction [10.2]. To investigate the full quantum limit of cavity-induced self-organisation and cooling we resort to numerical solutions of the master equation within a truncated atomic momentum Hilbert space for a finite fixed particle number.

10.2 Effective mode model

We consider N ultracold particles within a high-Q optical resonator illuminated by a transverse laser far detuned from any internal resonance (cf. fig. 10.1). The light scattered by the particles into the resonator interferes with the pump field and creates an optical lattice potential along the cavity axis. We assume the particles' motion to be restricted to the cavity axis by means of a suitable transversal confinement. The coherent time evolution of this joint particle-field system is then governed by

the second-quantised Hamiltonian [10.1, 10.18]

$$H = \int_{-L/2}^{L/2} \hat{\Psi}^\dagger(x)\Big[-\frac{\hbar^2}{2m}\frac{\mathrm{d}^2}{\mathrm{d}x^2} + \hbar U_0 a^\dagger a \cos^2(kx) + \hbar\eta(a+a^\dagger)\cos(kx)\Big]\hat{\Psi}(x)\,\mathrm{d}x - \hbar\Delta_\mathrm{c} a^\dagger a, \quad (10.1)$$

where k denotes the wave number of the cavity mode which also sets the recoil energy scale $\hbar\omega_\mathrm{R} = \hbar^2k^2/(2m)$, m is the mass of a single particle, and $L = M2\pi/k$ is the unit cell length of the periodic boundary conditions, equal to an integer M times the wavelength $\lambda = 2\pi/k$. The parameter U_0 is the light shift per particle, η the effective pump amplitude per atom and a the annihilation operator of a cavity photon. The field operators $\hat{\Psi}^\dagger(x)$ ($\hat{\Psi}(x)$) create (destroy) a particle at position x and obey bosonic or fermionic commutation or anticommutation relations, respectively. The Hamiltonian (10.1) is expressed in a reference frame rotating with the pump laser frequency ω_p. Consequently, the detuning $\Delta_\mathrm{c} := \omega_\mathrm{p} - \omega_\mathrm{c}$ between the pump and the bare cavity resonance frequency appears explicitly.

As an important feature the Hamiltonian (10.1) allows for momentum transfers of $\Delta p = \pm\hbar k$ in addition to $\Delta p = \pm 2\hbar k$ from scattering within the cavity [10.7, 10.39]. This enables the system to self-order and has also important consequences for the cooling behaviour. Note that direct particle-particle interactions, which could induce arbitrary momentum transfers Δp (e.g. collisions), are neglected.

The second-quantised representation (10.1) allows us to optimally exploit the symmetries of the system and the bosonic or fermionic statistics of the quantum particles. To this end we expand the particle's creation and annihilation operators in the complete set of orthonormal mode functions

$$\left\{\sqrt{\frac{1}{L}}, \sqrt{\frac{2}{L}}\cos(n\Delta_k x), \sqrt{\frac{2}{L}}\sin(n\Delta_k x)\right\} \quad (10.2)$$

with integer $n \geq 1$. The momentum space discretisation is given by $\hbar\Delta_k = \hbar 2\pi/L$, therefore the cavity wave vector k is an integer multiple of Δ_k ($k = M\Delta_k$). The high-energy modes can be excluded from the model by introducing a cutoff $n \leq n_\mathrm{c}$ [10.18]. This is possible as their occupation remains low due to the ongoing cavity cooling effect [10.9]. Additionally, we introduce a cutoff for the cavity photon number. Both cutoffs were checked for consistency a posteriori.

Note that the subspaces spanned by odd (sine) and even (cosine) parity modes, respectively, are decoupled. For bosons initially in a BEC the sine modes remain unpopulated and can be excluded from the picture. For a degenerate Fermi gas, however, all modes with energies below the Fermi energy are filled up, therefore sine and cosine modes both have to be taken into account. Nevertheless, the dimensionality of the actual problem to be solved can be further reduced by exploiting invariant subspaces (cf. appendix 11.1).

Photons leaking out of the resonator inevitably introduce noise and damping into the system and thus prevent a pure Hamiltonian evolution of the system's Schrödinger

wave function. Much rather, the system will evolve into a stochastic mixture described by the joint particle-field density operator governed by the master equation [10.40]

$$\dot{\rho} = \frac{1}{\mathrm{i}\hbar}\left[H, \rho\right] + \kappa\left(2a\rho a^\dagger - a^\dagger a\rho - \rho a^\dagger a\right), \tag{10.3}$$

with the cavity photon decay rate 2κ. We neglect spontaneous emission of the atoms under the assumption of a large detuning of the laser with respect to any internal atomic resonance. An expansion of the (bosonic or fermionic) field operator $\hat{\Psi}(x)$ in terms of the mode functions (10.2) yields an effective mode model, whose explicit Hamiltonian is reported in appendix 11.1.

10.3 Self-organisation in the quantum regime

Self-organisation can be understood already on a classical level, i.e. with classical particles and a damped cavity field [10.9, 10.11]. At this level, when the threshold pump strength for the phase transition is reached, the symmetry of the system is spontaneously broken as the initially homogeneously distributed particles organise and occupy one of two possible configurations [10.1, 10.9] corresponding to even or odd sites of the cavity optical lattice $\sim \cos^2(kx)$. In the perfectly homogeneous phase, no photons are scattered into the cavity because of destructive interference and self-organisation is triggered only by density fluctuations. The occupation of the odd or even potential wells, respectively, is associated with one of two opposite phases of the intracavity light field relative to the pump laser. The order parameter of the phase transition is given by $\Theta = \langle\cos(kx)\rangle$ (or equivalently $\langle a\rangle$), which is zero in the completely homogeneous phase and ± 1 in the limit that the particles are completely localised at antinodes. Quantum-mechanically, the dynamics lead towards a self-organised state which is a superposition of the two configurations in odd and even wells correlated with the corresponding field phase [10.41]. Initial atom-field entanglement decays on the timescale of the photon lifetime rendering the stationary state into a mixture of the two configurations.

For both the entangled state and the mixture the mean field $\langle a\rangle$ and the order parameter $\langle\cos(kx)\rangle$ are zero, while the photon number $\langle a^\dagger a\rangle$ is finite. Above threshold, the stationary state is approximately [10.16]

$$\rho_{\mathrm{ss}} \approx \frac{1}{2}\left|\alpha, +\right\rangle\left\langle\alpha, +\right| + \frac{1}{2}\left|-\alpha, -\right\rangle\left\langle-\alpha, -\right|, \tag{10.4}$$

where $|\alpha\rangle$ is a coherent state with complex field amplitude α and $|\pm\rangle$ is the state of particles organised in the odd or even wells, respectively. With increasing pump strength, the components' coherent states $|\alpha\rangle$ and $|-\alpha\rangle$ have less and less overlap. This behaviour can be seen in the Q-function [10.42] of the cavity field, as shown in fig. 10.2a.

The classical order parameter $\langle\cos(kx)\rangle_{\rho_{\mathrm{ss}}}$ is always zero and thus unsuitable in the quantum case. In order to find an alternative measure, we project ρ_{ss} to obtain

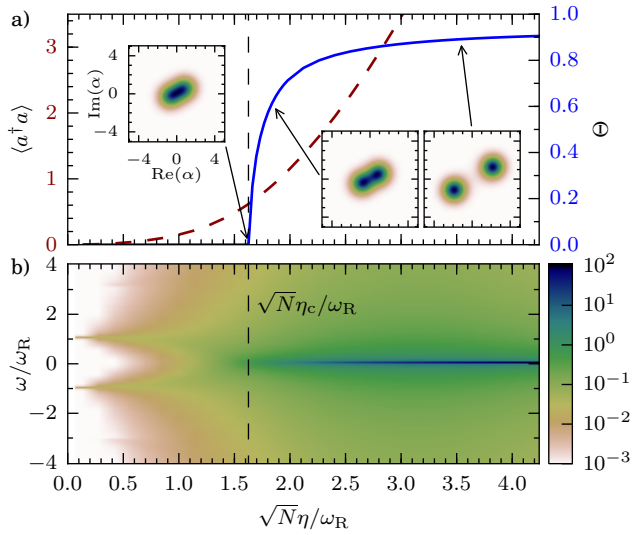

Figure 10.2: a) The order parameter Θ and intracavity photon number $\langle a^\dagger a\rangle$, b) the cavity field spectrum $|S(\omega)|$ as a function of the pump strength, respectively. Insets: The Q-function of the photon field splits up into two coherent peaks across the threshold. Parameters: $N = 2$ bosons, $U_0/\omega_R = -0.5$, $\kappa/\omega_R = 1$, $\Delta_c/\omega_R = -2.5$.

$\rho_\alpha := \langle\alpha|\rho_{ss}|\alpha\rangle \,/\, \mathrm{tr}\,\langle\alpha|\rho_{ss}|\alpha\rangle$, with α maximising the Q-function obtained from the cavity field associated with ρ_{ss}. Far above threshold, where $\langle\alpha| - \alpha\rangle \approx 0$, we have $\rho_\alpha \approx |+\rangle\langle+|$. We then calculate the order parameter with this projected particle state, i.e.

$$\Theta := \langle\cos(kx)\rangle_{\rho_\alpha}. \tag{10.5}$$

As long as the Q-function only has one maximum at $\alpha = 0$, this is exactly zero because of the system's symmetry. The threshold η_c, i.e. the driving for which Θ first becomes larger than zero, is therefore *defined* to be the pump strength at which the Q-function splits up and has two local maxima. The sudden increase of the mean intracavity photon number at the threshold, which is expected in the thermodynamic limit, is smoothened in the few particle regime considered here. This is illustrated in fig. 10.2a.

In addition to the order parameter, the onset of self-organisation can also be seen in the cavity field spectrum, as observed experimentally with a BEC [10.27, 10.43]. To this end we calculate $S(\omega) = \mathcal{F}(\langle a^\dagger(T+t)a(T)\rangle)$, where $\mathcal{F}$ is the Fourier transform with respect to t, and T is a time sufficiently large for the system to have reached its stationary state [10.42]. Figure 10.2b shows $|S(\omega)|$ for bosons. Below threshold, the two peaks correspond to collective modes, characterised by light-field oscillations and particles excited from momentum zero to $\hbar k$ and vice versa. At low pump strength, the peaks are located at $\sim \pm\omega_R$ and are almost perfectly sharp (undamped) since the collective modes are almost purely atomic excitations. Slight

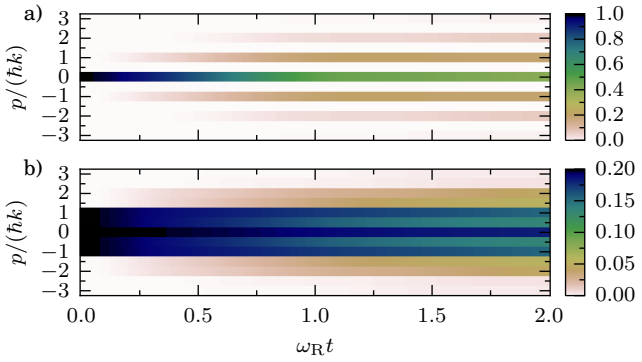

Figure 10.3: Time evolution of the momentum population p for a) bosons and b) fermions, starting with a quantum degenerate initial state at temperature zero. Participation of the fermion with $p = 0$ in the photon scattering dynamics is strongly suppressed, as its target states $p/(\hbar k) = \pm 1$ are essentially blocked. Parameters: $N = 5$, $\eta/\omega_R = 2$, $\Delta_c/\omega_R = -4$, $U_0/\omega_R = -0.5$, $\Delta_k/k = 0.5$.

asymmetries in the peaks are caused by the difference between positive and negative energy fluctuations with respect to the laser frequency, corresponding to stokes and anti-stokes processes. With increasing pump strength, apart from a broadening of the peaks due to mixing of atomic excitations with the decaying photonic excitations, we observe a softening of the collective modes which become energetically less and less costly. At a critical pump strength these modes are shifted to zero energy ($\omega = 0$ in fig. 10.2b). This process, accompanied by collective scattering of photons into the cavity at the laser frequency, is called superradiant because of the quadratic scaling of the photon number with N. The presence of such a dominant coherent peak at $\omega = 0$ is thus an additional characterisation of self-organisation, as already observed semi-classically [10.15]. Within our model this superradiant coherent peak has zero width since we do not include a finite linewidth of the pump laser.

For fermions, the behaviour of the order parameter is qualitatively similar to the bosonic case illustrated in fig. 10.2a. The spectrum, however, shows qualitative differences which will be discussed below.

10.4 Quantum statistics and self-organisation

Self-organisation and superradiance have been demonstrated with both a thermal gas [10.24, 10.25] in the classical regime as well as for a BEC close to $T = 0$ [10.26, 10.28]. Self-ordering of course requires excitations out of the $p = 0$ condensed state to higher momenta with increments $\pm\hbar k$ (cf. fig. 10.3a). The qualitative behaviour of BEC self-organisation resembles its thermal counterpart, with the recoil energy scale $\hbar\omega_R$ playing the role of the temperature scale $k_B T$ [10.44].

In contrast to bosons, fermionic statistics allows for a qualitatively different self-

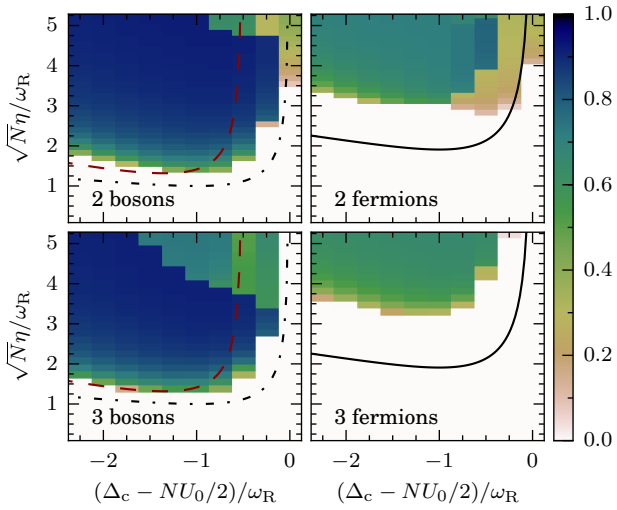

Figure 10.4: The phase diagram of two and three bosons and fermions, respectively. The threshold is compared with the analytic results of [10.12] in the semiclassical limit (dashed line) and [10.44] for bosons (dash-dotted line), as well as [10.38] for fermions (solid line, $k_F/k = 1$). For bosons, the sudden decrease of the order parameter with increasing pump strength is an artefact of the photon number cutoff. Parameters: $U_0/\omega_R = -0.5$, $\kappa/\omega_R = 1$.

ordering behaviour [10.32–10.34]. In fact, a Fermi gas introduces a new internal energy scale, the Fermi energy ϵ_F, and indeed its ratio to the recoil energy $\hbar\omega_R$ dramatically affects the behaviour of the fermionic self-organisation. As illustrated in fig. 10.3b, due to the Pauli pressure fermions occupy higher momentum states even at $T = 0$ including cosine and sine modes. This prevents a direct mapping of the system's Hamiltonian onto an effective Dicke model (demonstrated for a BEC [10.45]) and the understanding of self-organisation in terms of a simple superradiant transition is not possible, except for the limiting case of an infinitely large Fermi momentum relative to the cavity photon momentum [10.46].

The central effects of Fermi statistics on self-ordering so far have been evaluated based on the assumption of a thermal equilibrium for the particles and neglecting the role of quantum fluctuations of the cavity field [10.32–10.34]. Here we test these predictions in comprehensive nonequilibrium simulations for a small number of particles including light-matter entanglement and quantum fluctuations of the cavity field. Due to Pauli blocking we can expect that for fermions not all particles will equally participate in the self-organisation phenomena. Whilst for classical particles and bosons scattering of a photon is always allowed and thus the critical pump strength scales as $\eta_c \propto 1/\sqrt{N}$ [10.10, 10.12, 10.21, 10.44], only fermions coupled to an unoccupied final state can scatter (cf. fig. 10.3b). This fraction strongly depends on the Fermi energy and hence scales differently with N. For a sharp Fermi surface,

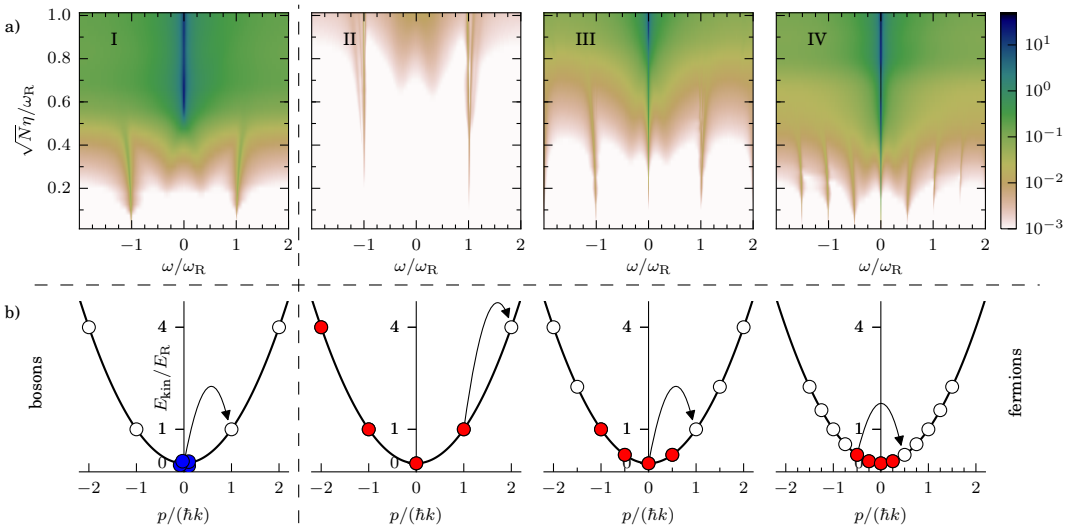

Figure 10.5: a) Cavity field spectrum and b) initial conditions with lowest-energy particle excitations for bosons (I) and fermions (II–IV). For fermions the value $\Delta_k/k = 1, 0.5, 0.25$ is varied. For bosons only the case $\Delta_k/k = 1$ is shown, as the dynamics are unchanged in the other cases. Note that in case II the peaks in the spectrum at $\pm\omega_R$ correspond to transitions which are forbidden in the initial state but become possible during relaxation towards the stationary state. The frequency of the transition indicated by the arrow in II b) lies outside the depicted spectral range. The resonance condition $k = 2k_F$ is fulfilled in IV. Here the central peak in the spectrum at the laser frequency ($\omega = 0$) is dominant even for the smallest pump strengths. Parameters: $N = 4$, $U_0/\omega_R = -1/16$, $\kappa/\omega_R = 1/8$, $\Delta_c/\omega_R = -1/2$.

η_c can be estimated analytically. In one spatial dimension one obtains $\epsilon_F \propto (N/L)^2$, which in turn means $\eta_c \propto \sqrt{\ln(N)/N}$ for $k \gg k_F$ or even $\eta_c \propto \sqrt{N}$ for $k \ll k_F$ [10.32].

Figure 10.4 depicts the value of the order parameter (10.5) as a function of the (dispersively shifted) cavity detuning and the pump amplitude for two and three bosons and fermions, respectively. In this low-particle regime the notion of a sharp Fermi surface becomes questionable. Nevertheless, we see qualitative agreement of our numerical data with the scaling discussed above: for $N = 3$ fermions the rescaled $\sqrt{N}\eta_c$ is larger than for $N = 2$, while for bosons it does not change.

While the Fermi blockade causes an unfavourable threshold scaling with the number of particles, the existence of a Fermi surface can also give rise to a resonant reduction of the threshold if $k = 2k_F$. This "umklapp superradiance" [10.32] involves particles scattered from one end of the Fermi surface to the other (i.e. from $-k_F$ to k_F) by the two-photon transition with momentum transfer $\hbar k = 2\hbar k_F$. This process has essentially no energy cost and thus can drastically lower the self-organisation threshold. Here the ordered state is very close to the Fermi surface and has essentially

the same kinetic energy as the homogeneous ground state. Note that this availability of some already excited particles can also explain the threshold reduction found in [10.21] for bosons at small temperature compared to the zero temperature limit.

In our simulations with a fixed number of fermions prepared initially at $T = 0$, the resonance condition $k = 2k_\mathrm{F}$ can be reached by different means: either by adjusting the cavity wavenumber k directly or by altering the particle density L/N and thus the Fermi momentum. Here we choose to keep k fixed and vary the trap volume L which the fermions can occupy by altering $\Delta_k = 2\pi/L$. This has the advantage that the recoil frequency ω_R stays the same for all parameters.

In order to investigate the role of umklapp superradiance, we prepare the initial state in the resonant condition, perform the full quantum dissipative evolution and compute the order parameter and intracavity spectrum once the stationary state is reached. As mentioned in the beginning, our simulations include the relaxation of the particles into a (generally) nonequilibrium stationary state different from the initial one. In particular, redistribution of energy and momentum will alter the Fermi surface, thereby modifying the resonance condition. Whether and how the umklapp superradiance manifests itself in this stationary state is a non-trivial question. The answer is illustrated in fig. 10.5. Here we compare bosons in a BEC with zero-temperature fermions at three different densities corresponding to the three Fermi momenta $k_\mathrm{F} = 2k$ ($\Delta_k = k$), $k_\mathrm{F} = k$ ($\Delta_k = 0.5k$) and $2k_\mathrm{F} = k$ ($\Delta_k = 0.25k$). In the last case the resonance condition is fulfilled. Initially, with no cavity photons present, the particles move freely with a quadratic dispersion relation. As already mentioned, the cavity only supports momentum transfer to and from the particles in units $\hbar k$. This corresponds to steps of 1 on the x–axes of fig. 10.5b, where arrows indicate the particle excitations with lowest possible energy cost. These excitations are visible in the spectra shown in 10.5a as peaks at the corresponding frequencies.

The effect of resonant umklapp scattering is clearly visible in the spectra by comparing the initially resonant case (fig. 10.5a IV) with the other two fermionic non-resonant cases as well as with the bosonic case. The appearance of a coherent peak at zero frequency in the resonant case signals the onset of superradiance even at almost vanishing pump strengths. For all the other cases this onset of a coherent scattering peak is located at higher pump strengths. Such a low superradiant threshold is possible because of (almost) resonant particle excitations with momentum $\hbar k$, creating the correct density modulation period for coherent Bragg scattering into the cavity.

Even though the umklapp resonant condition can lower the threshold for the appearance of the superradiant peak much below the bosonic threshold, the number of photons in the cavity and the amplitude of the order parameter (10.5) can still be lower than in the bosonic case, due to the unfavourable scaling with N illustrated above. For instance, the threshold pump strength scales as $\eta_\mathrm{c} \sim \sqrt{N/\ln(N)}$ at $k \simeq 2k_\mathrm{F}$ if we assume a sharp Fermi surface. Therefore the effect of umklapp superradiance is much less visible in the photon number or the order parameter as compared to the spectrum. Still, for certain parameter regimes and in the resonant case a lower self-organisation threshold for fermions can be seen even in these quantities, as shown

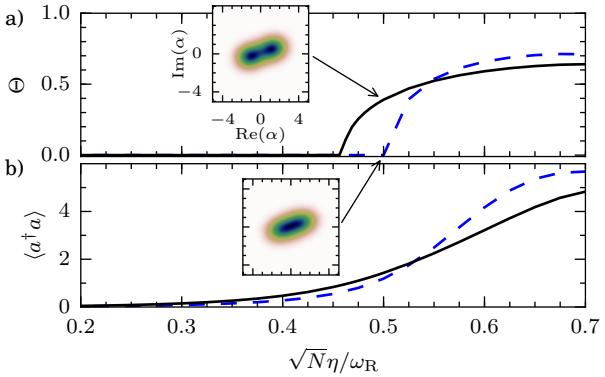

Figure 10.6: a) Order parameter and b) photon number for fermions (solid line) and bosons (dashed line) for the resonance case $k = 2k_F$. The threshold for fermions is lower compared to bosons. Insets: The Q-function of the photon field at a pump strength which lies above threshold for fermions and below threshold for bosons, respectively. Same parameters as in fig. 10.5.

in fig. 10.6.

10.5 Conclusions

Self-ordering of ultracold particles in an optical resonator field survives as a stationary nonthermal equilibrium state in the long-time limit even if cavity losses with their inherent field quantum fluctuations are taken into account. The quantum statistics of the particles turns out to have a decisive influence on the light-induced crystallisation of quantum particles in cavity fields even in this nonequilibrium context. This can be nicely monitored in real time with minimal perturbations by observing the spectrum of the scattered light.

Acknowledgments

We acknowledge support by the EU ITN project CCQED, the Austrian Science Fund FWF through project SFB FoQuS F4013 and the Austrian Ministry of Science BMWF as part of the UniInfrastrukturprogramm of the Focal Point Scientific Computing at the University of Innsbruck. FP acknowledges support from the APART Fellowship of the Austrian Academy of Sciences.

Chapter 11

Additional material

11.1 Mode model

Starting from the Hamiltonian (10.1), we use the mode model from [11.1], extended to include the sine modes and generalized for an arbitrary momentum space discretisation Δ_k.

We expand the particles' field operator $\hat{\Psi}(x)$ in the complete set of orthonormal mode functions

$$\begin{aligned} \varphi_{0,1}(x) &= \sqrt{\frac{1}{L}} \\ \varphi_{n,1}(x) &= \sqrt{\frac{2}{L}}\cos(n\Delta_k x), \qquad \varphi_{n,-1}(x) = \sqrt{\frac{2}{L}}\sin(n\Delta_k x), \end{aligned} \tag{11.1}$$

with integer $n \geq 1$. The modes are labeled by the multi-index $\boldsymbol{j} = (j, j_\pi)$, which contains the mode number j and the parity $j_\pi = 1$ for the cosine and $j_\pi = -1$ for the sine modes. This yields the decomposition

$$\hat{\Psi}(x) = \sum_{\boldsymbol{j}, j \leq n_c} \varphi_{\boldsymbol{j}}(x)\hat{c}_{\boldsymbol{j}}, \tag{11.2}$$

where the $\hat{c}_{\boldsymbol{j}}$ follow either bosonic or fermionic (anti-) commutation rules and the $\hat{c}_{j,-1}$ operators are formally set to zero for bosons.

With $\hat{\boldsymbol{c}} = (\hat{c}_{0,1}, \ldots, \hat{c}_{n_c,1}, \hat{c}_{1,-1}, \ldots, \hat{c}_{n_c,-1})^T$ as column vector and $\hat{\boldsymbol{c}}^\dagger = (\hat{c}^\dagger_{0,1}, \ldots, \hat{c}^\dagger_{n_c,1}, \hat{c}^\dagger_{1,-1}, \ldots, \hat{c}^\dagger_{n_c,-1})$ as row vector, we can write the Hamiltonian (10.1) as

$$\begin{aligned} H = -\hbar\Delta_c a^\dagger a + \hbar\omega_R \left(\hat{\boldsymbol{c}}^\dagger \boldsymbol{K} \hat{\boldsymbol{c}}\right) + \hbar\eta(a + a^\dagger)\left(\hat{\boldsymbol{c}}^\dagger \boldsymbol{C}_{k/\Delta_k} \hat{\boldsymbol{c}}\right) \\ + \hbar\frac{U_0}{2} a^\dagger a \left(\hat{\boldsymbol{c}}^\dagger \left(\boldsymbol{I} + \boldsymbol{C}_{2k/\Delta_k}\right)\hat{\boldsymbol{c}}\right), \end{aligned} \tag{11.3}$$

where $\omega_R = \hbar k^2/(2m)$ is the recoil frequency and $\boldsymbol{I}$ is the identity matrix. The matrices $\boldsymbol{K}$ and $\boldsymbol{C}_M$ with integer M, producing the kinetic energy term and the

terms proportional to $\cos(kx)$ and $\cos(2kx)$, respectively, are defined as

$$\boldsymbol{K} = \frac{\Delta_k^2}{k^2} \begin{pmatrix} 0 & & & & \\ & 1^2 & & & \\ & & 2^2 & & \\ & & & \ddots & \\ & & & & n_\mathrm{c}^2 \end{pmatrix}, \quad \boldsymbol{C}_M = \begin{pmatrix} \ddots & & & \\ & b & a & b \\ & a & b & M \\ & b & & \ddots \\ & & & & \ddots & \\ & & & & -b & b \\ & & & -b & & b \\ & & & b & M & \\ & & & b & & \ddots \end{pmatrix}, \tag{11.4}$$

where $a = 1/\sqrt{2}$ and $b = 1/2$. For $\boldsymbol{C}_M$, the two blocks belong to the cosine and sine modes, respectively. The two populated secondary diagonals are separated by M modes. Additionally, modes j, k for which $j + k = M$ are coupled by the entries b for cosine modes and $-b$ for sine modes, respectively. For reference, the quadratic forms appearing in the mode-expanded Hamiltonian (11.3) read

$$\begin{aligned} \hat{\boldsymbol{c}}^\dagger \boldsymbol{C}_M \hat{\boldsymbol{c}} = \frac{1}{\sqrt{2}} \left(\hat{c}_{M,1}^\dagger \hat{c}_{0,1} + \hat{c}_{0,1}^\dagger c_{M,1} \right) \\ + \frac{1}{2} \sum_{\substack{\boldsymbol{j},\boldsymbol{k} \\ 1 \le j,k \le n_\mathrm{c}}} \delta_{j_\pi k_\pi} \left[\delta_{j,k+M} + \delta_{j+M,k} + j_\pi \delta_{j+k,M} \right] \hat{c}_{\boldsymbol{j}}^\dagger \hat{c}_{\boldsymbol{k}}. \end{aligned} \tag{11.5}$$

For our simulations we use the usual basis of Fock states

$$\left\{ |n_{0,1}, \ldots, n_{n_\mathrm{c},1}; n_{1,-1}, \ldots, n_{n_\mathrm{c},-1}\rangle \right\}_{\sum_{\boldsymbol{j}} n_{\boldsymbol{j}} = N}, \tag{11.6}$$

where $n_{\boldsymbol{j}} = 0, \ldots, N$ for bosons and $n_{\boldsymbol{j}} = 0, 1$ for fermions.

As already noted and as can be seen from the coupling matrices (11.4), sine and cosine modes are decoupled. However, for $M := k/\Delta_k > 1$ one can identify further subgroups of modes which are decoupled from all other groups. We will now specify these groups and use them to identify invariant subspaces of the Hilbert space $\mathcal{H}$ spanned by the basis states (11.6).

Let us group all available modes into s sets of modes, where $s := \lfloor M/2 \rfloor + 1$ for bosons and $s := 2\lfloor M/2 \rfloor + 1$ for fermions:

$$g_{\boldsymbol{l}} := \left\{ \boldsymbol{j} | j_\pi = l_\pi, j \bmod M = l \vee j \bmod M = M - l \right\}, \tag{11.7}$$

with $l_\pi = 1$ ($l_\pi = \pm 1$) for bosons (fermions) and $l \le \lfloor M/2 \rfloor$. The significance of these sets is that two modes are coupled through the dynamics induced by the Hamiltonian (11.3) if and only if they belong to the same set. As a consequence, the number operator corresponding to each group, i.e.

$$\hat{n}_{\boldsymbol{l}} := \sum_{\boldsymbol{j} \in g_{\boldsymbol{l}}} \hat{c}_{\boldsymbol{j}}^\dagger \hat{c}_{\boldsymbol{j}} \tag{11.8}$$

commutes with H and $\langle \hat{n}_{\boldsymbol{l}} \rangle$ is constant over time. This enables us to define invariant subspaces of $\mathcal{H}$: two basis states of (11.6) belong to the same invariant subspace if

and only if they produce the same s-tuple $(\langle \hat{n}_{\boldsymbol{l}} \rangle)_{\boldsymbol{l}}$. We can exclude any basis state from our model if it belongs to a subspace which is not populated by the initial state.

For example, for a degenerate Fermi gas with $N = 4$, $k/\Delta_k = 4$ and $n_\mathrm{c} = 6$, the basis (11.6) consists of 715 states. By virtue of the above considerations we only have to take 72 basis states into account.

Bibliography

References for Chapter 1

[1.1] M. Planck, *Über das Gesetz der Energieverteilung im Normalspectrum*, Annals of Physics **309**, 553 (1901).

[1.2] A. Einstein, *Über einen die Erzeugung und Verwandlung des Lichtes betreffenden heuristischen Gesichtspunkt*, Annals of Physics **322**, 132 (1905).

[1.3] P. Grangier, G. Roger, and A. Aspect, *Experimental evidence for a photon anticorrelation effect on a beam splitter: a new light on single-photon interferences*, Europhysics Letters **1**, 173 (1986).

[1.4] L. De Broglie, *La mécanique ondulatoire et la structure atomique de la matière et du rayonnement*, Journal de Physique et le Radium **8**, 225 (1927).

[1.5] O. Donati, G. Missiroli, and G. Pozzi, *An experiment on electron interference*, American Journal of Physics **41**, 639 (1973).

[1.6] P. R. Berman, *Atom interferometry* (Academic press, 1997).

[1.7] S. Gerlich, S. Eibenberger, M. Tomandl, S. Nimmrichter, K. Hornberger, P. J. Fagan, J. Tüxen, M. Mayor, and M. Arndt, *Quantum interference of large organic molecules*, Nature Communications **2**, 263 (2011).

[1.8] M. Beller, *The conceptual and the anecdotal history of quantum mechanics*, Foundations of Physics **26**, 545 (1996).

[1.9] P. A. M. Dirac, *The quantum theory of the emission and absorption of radiation*, in: *Proceedings of the Royal Society of London A: Mathematical, Physical and Engineering Sciences* **114**, 767, The Royal Society (1927), 243.

[1.10] E. Schrödinger, *Die gegenwärtige Situation in der Quantenmechanik*, Naturwissenschaften **23**, 823 (1935).

[1.11] D. Giulini, E. Joos, C. Kiefer, J. Kupsch, I. O. Stamatescu, and H. D. Zeh, *Decoherence and the Appearance of a Classical World in Quantum Theory* (Springer, Berlin, 1996).

[1.12] M. Schlosshauer, *Decoherence, the measurement problem, and interpretations of quantum mechanics*, Reviews of Modern Physics **76**, 1267 (2005).

[1.13] S. Haroche, *Nobel Lecture: Controlling photons in a box and exploring the quantum to classical boundary*, Reviews of Modern Physics **85**, 1083 (2013).

[1.14] D. J. Wineland, *Nobel Lecture: Superposition, entanglement, and raising Schrödinger's cat*, Reviews of Modern Physics **85**, 1103 (2013).

[1.15] S. Kuhr, S. Gleyzes, C. Guerlin, J. Bernu, U. B. Hoff, S. Deléglise, S. Osnaghi, M. Brune, J.-M. Raimond, S. Haroche, E. Jacques, P. Bosland, and B. Visentin, *Ultrahigh finesse Fabry-Pérot superconducting resonator*, Applied Physics Letters **90**, 164101 (2007).

[1.16] N. Bohr, *Discussion with Einstein on epistemological problems in atomic physics*, ed. by P. A. Shilpp (Harper, New York, 1949).

[1.17] S. Haroche, M. Brune, and J.-M. Raimond, *Atomic clocks for controlling light fields*, Physics Today **66**, 27 (2013).

[1.18] S. Gleyzes, S. Kuhr, C. Guerlin, J. Bernu, S. Deleglise, U. B. Hoff, M. Brune, J.-M. Raimond, and S. Haroche, *Quantum jumps of light recording the birth and death of a photon in a cavity*, Nature **446**, 297 (2007).

[1.19] Y. Nakamura, Y. A. Pashkin, and J. Tsai, *Coherent control of macroscopic quantum states in a single-Cooper-pair box*, Nature **398**, 786 (1999).

[1.20] R. Hanson, L. Kouwenhoven, J. Petta, S. Tarucha, and L. Vandersypen, *Spins in few-electron quantum dots*, Reviews of Modern Physics **79**, 1217 (2007).

[1.21] R. Blatt and D. Wineland, *Entangled states of trapped atomic ions*, Nature **453**, 1008 (2008).

[1.22] M. Brune, E. Hagley, J. Dreyer, X. Maitre, A. Maali, C. Wunderlich, J. Raimond, and S. Haroche, *Observing the progressive decoherence of the "meter" in a quantum measurement*, Physical Review Letters **77**, 4887 (1996).

[1.23] J. I. Cirac, P. Zoller, H. J. Kimble, and H. Mabuchi, *Quantum state transfer and entanglement distribution among distant nodes in a quantum network*, Physical Review Letters **78**, 3221 (1997).

[1.24] A. Imamoglu, H. Schmidt, G. Woods, and M. Deutsch, *Strongly interacting photons in a nonlinear cavity*, Physical Review Letters **79**, 1467 (1997).

[1.25] A. L. Schawlow and C. H. Townes, *Infrared and optical masers*, Physical Review **112**, 1940 (1958).

[1.26] T. H. Maiman, *Stimulated Optical Radiation in Ruby*, Nature **187**, 493 (1960).

[1.27] C. Cohen-Tannoudji, *Atomic Motion in Laser Light*, in: *Fundamental systems in quantum optics, Les Houches Summer School, Proceedings* ed. by J. Dalibard, J.-M. Raimond, and J. Zinn-Justin, **53** (North-Holland, Amsterdam, 1992), 1.

[1.28] T. W. Hänsch and A. L. Schawlow, *Cooling of gases by laser radiation*, Optics Communications **13**, 68 (1975).

[1.29] D. J. Wineland and W. M. Itano, *Laser cooling of atoms*, Physical Review A **20**, 1521 (1979).

[1.30] J. Dalibard and C. Cohen-Tannoudji, *Laser cooling below the Doppler limit by polarization gradients: simple theoretical models*, Journal of the Optical Society of America **6**, 2023 (1989).

[1.31] S. Chu, *Nobel Lecture: The manipulation of neutral particles*, Reviews of Modern Physics **70**, 685 (1998).

[1.32] C. N. Cohen-Tannoudji, *Nobel Lecture: Manipulating atoms with photons*, Reviews of Modern Physics **70**, 707 (1998).

[1.33] R. Grimm, M. Weidemüller, and Y. B. Ovchinnikov, *Optical Dipole Traps for Neutral Atoms*, Advances In Atomic, Molecular, and Optical Physics **42**, 95 (2000).

[1.34] A. Ashkin, *Optical trapping and manipulation of neutral particles using lasers: a reprint volume with commentaries* (World Scientific, 2006).

[1.35] I. Bloch, J. Dalibard, and S. Nascimbène, *Quantum simulations with ultracold quantum gases*, Nature Physics **8**, 267 (2012).

[1.36] S. Bose, *Plancks Gesetz und Lichtquantenhypothese*, Zeitschrift für Physik **26**, 178 (1924).

[1.37] A. Einstein, *Quantentheorie des einatomigen idealen Gases* (Akademie der Wissenshaften, in Kommission bei W. de Gruyter, 1925).

[1.38] F. P. Dos Santos, J. Léonard, J. Wang, C. J. Barrelet, F. Perales, E. Rasel, C. S. Unnikrishnan, M. Leduc, and C. Cohen-Tannoudji, *Bose-Einstein condensation of metastable helium*, Physical Review Letters **86**, 3459 (2001).

[1.39] T. Weber, J. Herbig, M. Mark, H.-C. Nägerl, and R. Grimm, *Bose-Einstein condensation of cesium*, Science **299**, 232 (2003).

[1.40] S. Jochim, M. Bartenstein, A. Altmeyer, G. Hendl, S. Riedl, C. Chin, J. H. Denschlag, and R. Grimm, *Bose-Einstein condensation of molecules*, Science **302**, 2101 (2003).

[1.41] S. Stellmer, M. K. Tey, B. Huang, R. Grimm, and F. Schreck, *Bose-Einstein condensation of strontium*, Physical Review Letters **103**, 200401 (2009).

[1.42] S. Sugawa, R. Yamazaki, S. Taie, and Y. Takahashi, *Bose-Einstein condensate in gases of rare atomic species*, Physical Review A **84**, 011610 (2011).

[1.43] K. Aikawa, A. Frisch, M. Mark, S. Baier, A. Rietzler, R. Grimm, and F. Ferlaino, *Bose-Einstein condensation of erbium*, Physical Review Letters **108**, 210401 (2012).

[1.44] S. Stellmer, B. Pasquiou, R. Grimm, and F. Schreck, *Laser Cooling to Quantum Degeneracy*, Phys. Rev. Lett. **110**, 263003 (2013).

[1.45] D. Jaksch and P. Zoller, *The cold atom Hubbard toolbox*, Ann. Phys. **315**, 52 (2005).

[1.46] I. Bloch, J. Dalibard, and W. Zwerger, *Many-body physics with ultracold gases*, Rev. Mod. Phys. **80**, 885 (2008).

[1.47] P. Domokos and H. Ritsch, *Mechanical effects of light in optical resonators*, Journal of the Optical Society of America **20**, 1098 (2003).

[1.48] H. Ritsch, P. Domokos, F. Brennecke, and T. Esslinger, *Cold atoms in cavity-generated dynamical optical potentials*, Reviews of Modern Physics **85**, 553 (2013).

[1.49] R. J. Thompson, G. Rempe, and H. J. Kimble, *Observation of normal-mode splitting for an atom in an optical cavity*, Physical Review Letters **68**, 1132 (1992).

[1.50] C. Hood, T. Lynn, A. Doherty, A. Parkins, and H. Kimble, *The atom-cavity microscope: Single atoms bound in orbit by single photons*, Science **287**, 1447 (2000).

[1.51] P. W. H. Pinkse, T. Fischer, P. Maunz, and G. Rempe, *Trapping an atom with single photons*, Nature **404**, 365 (2000).

[1.52] P. Horak, G. Hechenblaikner, K. M. Gheri, H. Stecher, and H. Ritsch, *Cavity-induced atom cooling in the strong coupling regime*, Physical Review Letters **79**, 4974 (1997).

[1.53] M. Gangl, P. Horak, and H. Ritsch, *Cooling neutral particles in multimode cavities without spontaneous emission*, Journal of Modern Optics **47**, 2741 (2000).

[1.54] B. L. Lev, A. Vukics, E. R. Hudson, B. C. Sawyer, P. Domokos, H. Ritsch, and J. Ye, *Prospects for the cavity-assisted laser cooling of molecules*, Physical Review A **77**, 023402 (2008).

[1.55] M. Wolke, J. Klinner, H. Keßler, and A. Hemmerich, *Cavity Cooling Below the Recoil Limit*, Science **337**, 75 (2012).

[1.56] A. Vukics, W. Niedenzu, and H. Ritsch, *Cavity nonlinear optics with few photons and ultracold quantum particles*, Physical Review A **79**, 013828 (2009).

References for Chapter 2

[2.1] P. Horak, G. Hechenblaikner, K. M. Gheri, H. Stecher, and H. Ritsch, *Cavity-induced atom cooling in the strong coupling regime*, Physical Review Letters **79**, 4974 (1997).

[2.2] P. Domokos and H. Ritsch, *Mechanical effects of light in optical resonators*, Journal of the Optical Society of America **20**, 1098 (2003).

[2.3] C. W. Gardiner and P. Zoller, *Quantum Noise* (Springer, 2000), second edition.

[2.4] H. P. Breuer and F. Petruccione, *The theory of open quantum systems* (Oxford University Press, USA, 2002).

[2.5] J. R. Cash and A. H. Karp, *A Variable Order Runge-Kutta Method for Initial Value Problems with Rapidly Varying Right-hand Sides*, ACM Trans. Math. Softw. **16**, 201 (1990).

[2.6] A. Vukics, *C++QED documentation*, 2016, URL: `http://cppqed.sf.net` (visited on 19/02/2016).

[2.7] A. Vukics and H. Ritsch, *C++ QED: an object-oriented framework for wave-function simulations of cavity QED systems*, European Physical Journal D **44**, 585 (2007).

[2.8] A. Vukics, *C++ QEDv2: The multi-array concept and compile-time algorithms in the definition of composite quantum systems*, Computer Physics Communications **183**, 1381 (2012).

[2.9] R. M. Sandner and A. Vukics, *C++QEDv2 Milestone 10: A C++/Python application-programming framework for simulating open quantum dynamics*, Computer Physics Communications **185**, 2380 (2014).

[2.10] J. R. Johansson, P. D. Nation, and F. Nori, *QuTiP 2: A Python framework for the dynamics of open quantum systems*, Computer Physics Communications **184**, 1234 (2013).

[2.11] S. M. Tan, *A computational toolbox for quantum and atomic optics*, Journal of Optics B: Quantum and Semiclassical Optics **1**, 424 (1999).

[2.12] R. Dum, P. Zoller, and H. Ritsch, *Monte Carlo simulation of the atomic master equation for spontaneous emission*, Physical Review A **45**, 4879 (1992).

[2.13] J. Dalibard, Y. Castin, and K. Mølmer, *Wave-function approach to dissipative processes in quantum optics*, Physical Review Letters **68**, 580 (1992).

[2.14] K. Mølmer, Y. Castin, and J. Dalibard, *Monte Carlo wave-function method in quantum optics*, Journal of the Optical Society of America **10**, 524 (1993).

[2.15] H. P. Breuer, W. Huber, and F. Petruccione, *Stochastic wave-function method versus density matrix: a numerical comparison*, Computer physics communications **104**, 46 (1997).

[2.16] H. Carmichael, *An open systems approach to quantum optics* (Springer, 1993).

References for Chapter 3

[3.1] L. Bergmann, H. Niedrig, H. J. Eichler, and C. Schaefer, *Optik: Wellen- und Teilchenoptik* (de Gruyter, 2004).

[3.2] C. Fabry and A. Perot, *Sur les franges des lames minces argentées et leur application à la mesure de petites épaisseurs d'air*, Annales de Chimie et de Physique **12**, 459 (1897).

[3.3] M. Wolke, J. Klinner, H. Keßler, and A. Hemmerich, *Cavity Cooling Below the Recoil Limit*, Science **337**, 75 (2012).

[3.4] S. Kuhr, S. Gleyzes, C. Guerlin, J. Bernu, U. B. Hoff, S. Deléglise, S. Osnaghi, M. Brune, J.-M. Raimond, S. Haroche, E. Jacques, P. Bosland, and B. Visentin, *Ultrahigh finesse Fabry-Pérot superconducting resonator*, Applied Physics Letters **90**, 164101 (2007).

[3.5] E. Hecht, *Optik* (Oldenbourg, 2005).

[3.6] M. Planck, *Über das Gesetz der Energieverteilung im Normalspectrum*, Annals of Physics **309**, 553 (1901).

[3.7] A. Einstein, *Über einen die Erzeugung und Verwandlung des Lichtes betreffenden heuristischen Gesichtspunkt*, Annals of Physics **322**, 132 (1905).

[3.8] C. Cohen-Tannoudji, J. Dupont-Roc, and G. Grynberg, *Photons and Atoms – Introduction to Quantum Electrodynamics* (Wiley-Interscience, 1997).

[3.9] S. Haroche and J. M. Raimond, *Exploring the quantum* (Oxford Univ. Press, 2006).

[3.10] E. T. Jaynes and F. W. Cummings, *Comparison of quantum and semiclassical radiation theories with application to the beam maser*, Proceedings of the IEEE **51**, 89 (1963).

[3.11] C. Cohen-Tannoudji, J. Dupont-Roc, and G. Grynberg, *Atom-Photon Interactions: Basic Processes and Applications* (Wiley-Interscience, Mar. 1992).

[3.12] C. Cohen-Tannoudji, B. Diu, and F. Laloe, *Quantum Mechanics, Volume 1*, Quantum Mechanics, Volume 1, by Claude Cohen-Tannoudji, Bernard Diu, Frank Laloe, pp. 898. ISBN 0-471-16433-X. Wiley-VCH, June 1986. **1** (1986).

[3.13] R. J. Thompson, G. Rempe, and H. J. Kimble, *Observation of normal-mode splitting for an atom in an optical cavity*, Physical Review Letters **68**, 1132 (1992).

[3.14] H. Ritsch, P. Domokos, F. Brennecke, and T. Esslinger, *Cold atoms in cavity-generated dynamical optical potentials*, Reviews of Modern Physics **85**, 553 (2013).

[3.15] A. P. Kazantsev, G. I. Surdutovich, and V. P. Yakovlev, *Mechanical action of light on atoms* (World Scientific, 1990).

[3.16] C. W. Gardiner and P. Zoller, *Quantum Noise* (Springer, 2000), second edition.

[3.17] J. I. Cirac, R. Blatt, P. Zoller, and W. D. Phillips, *Laser cooling of trapped ions in a standing wave*, Physical Review A **46**, 2668 (1992).

[3.18] S. Schütz, H. Habibian, and G. Morigi, *Cooling of atomic ensembles in optical cavities: Semiclassical limit*, Physical Review A **88**, 033427 (2013).

[3.19] J. K. Asbóth, P. Domokos, H. Ritsch, and A. Vukics, *Self-organization of atoms in a cavity field: Threshold, bistability, and scaling laws*, Physical Review A **72**, 053417 (2005).

References for Chapter 4

[4.1] A. Vukics and H. Ritsch, *C++ QED: an object-oriented framework for wave-function simulations of cavity QED systems*, European Physical Journal D **44**, 585 (2007).

[4.2] A. Vukics, *C++ QEDv2: The multi-array concept and compile-time algorithms in the definition of composite quantum systems*, Computer Physics Communications **183**, 1381 (2012).

[4.3] S. M. Tan, *A computational toolbox for quantum and atomic optics*, Journal of Optics B: Quantum and Semiclassical Optics **1**, 424 (1999).

[4.4] J. R. Johansson, P. D. Nation, and F. Nori, *QuTiP 2: A Python framework for the dynamics of open quantum systems*, Computer Physics Communications **184**, 1234 (2013).

[4.5] A. Vukics, C. Maschler, and H. Ritsch, *Microscopic physics of quantum self-organization of optical lattices in cavities*, New Journal of Physics **9**, 255 (2007).

[4.6] A. Vukics, W. Niedenzu, and H. Ritsch, *Cavity nonlinear optics with few photons and ultracold quantum particles*, Physical Review A **79**, 013828 (2009).

[4.7] W. Niedenzu, R. Schulze, A. Vukics, and H. Ritsch, *Microscopic dynamics of ultracold particles in a ring-cavity optical lattice*, Physical Review A **82**, 043605 (2010).

[4.8] C. Maschler, I. B. Mekhov, and H. Ritsch, *Ultracold atoms in optical lattices generated by quantized light fields*, European Physical Journal D **46**, 545 ().

[4.9] D. Nagy, P. Domokos, A. Vukics, and H. Ritsch, *Nonlinear quantum dynamics of two BEC modes dispersively coupled by an optical cavity*, European Physical Journal D **55**, 659 (2009).

[4.10] R. M. Sandner and A. Vukics, *C++QEDv2 Milestone 10: A C++/Python application-programming framework for simulating open quantum dynamics*, Computer Physics Communications **185**, 2380 (2014).

[4.11] A. Vukics, *C++QED documentation*, 2016, URL: `http://cppqed.sf.net` (visited on 19/02/2016).

[4.12] B. Stroustrup, *The C++ Programming Language* (Pearson Education, 2013).

[4.13] D. Abrahams and A. Gurtovoy, *C++ Template Metaprogramming: Concepts, Tools, and Techniques from Boost and Beyond* (Addison-Wesley, 2005).

[4.14] *Boost Software License 1.0 (BSL-1.0)*, 2016, URL: `https://opensource.org/licenses/bsl1.0.html` (visited on 22/02/2016).

[4.15] E. Jones, T. Oliphant, P. Peterson *et al.*, *SciPy: Open source scientific tools for Python*, `http://www.scipy.org/`, 2001–.

[4.16] R. Sandner, *TeazerTools user guide*, 2016, URL: `https://web.archive.org/web/20160222152251/http://piquer.github.io/pycppqed/teazertools.html` (visited on 22/02/2016).

References for Chapter 5

[5.1] A. Vukics, *C++ QEDv2: The multi-array concept and compile-time algorithms in the definition of composite quantum systems*, Computer Physics Communications **183**, 1381 (2012).

[5.2] A. Vukics and H. Ritsch, *C++ QED: an object-oriented framework for wavefunction simulations of cavity QED systems*, European Physical Journal D **44**, 585 (2007).

[5.3] H. Carmichael, *An open systems approach to quantum optics* (Springer, 1993).

[5.4] J. Dalibard, Y. Castin, and K. Mølmer, *Wave-function approach to dissipative processes in quantum optics*, Physical Review Letters **68**, 580 (1992).

References for Chapter 6

[6.1] E. M. Purcell, *Spontaneous emission probabilities at radio frequencies*, Physical Review **69**, 681 (1946).

[6.2] D. Kleppner, *Inhibited spontaneous emission*, Physical Review Letters **47**, 233 (1981).

[6.3] R. J. Thompson, G. Rempe, and H. J. Kimble, *Observation of normal-mode splitting for an atom in an optical cavity*, Physical Review Letters **68**, 1132 (1992).

[6.4] H. Mabuchi, Q. Turchette, M. Chapman, and H. Kimble, *Real-time detection of individual atoms falling through a high-finesse optical cavity*, Optics Letters **21**, 1393 (1996).

[6.5] S. Gleyzes, S. Kuhr, C. Guerlin, J. Bernu, S. Deleglise, U. B. Hoff, M. Brune, J.-M. Raimond, and S. Haroche, *Quantum jumps of light recording the birth and death of a photon in a cavity*, Nature **446**, 297 (2007).

[6.6] J. Ye, D. Vernooy, and H. Kimble, *Trapping of single atoms in cavity QED*, Physical Review Letters **83**, 4987 (1999).

[6.7] C. Hood, T. Lynn, A. Doherty, A. Parkins, and H. Kimble, *The atom-cavity microscope: Single atoms bound in orbit by single photons*, Science **287**, 1447 (2000).

[6.8] P. W. H. Pinkse, T. Fischer, P. Maunz, and G. Rempe, *Trapping an atom with single photons*, Nature **404**, 365 (2000).

[6.9] I. B. Mekhov and H. Ritsch, *Quantum optics with ultracold quantum gases: towards the full quantum regime of the light–matter interaction*, Journal of Physics B **45**, 102001 (2012).

[6.10] H. Ritsch, P. Domokos, F. Brennecke, and T. Esslinger, *Cold atoms in cavity-generated dynamical optical potentials*, Reviews of Modern Physics **85**, 553 (2013).

[6.11] C. Cohen-Tannoudji, *Atomic Motion in Laser Light*, in: *Fundamental systems in quantum optics, Les Houches Summer School, Proceedings* ed. by J. Dalibard, J.-M. Raimond, and J. Zinn-Justin, **53** (North-Holland, Amsterdam, 1992), 1.

[6.12] T. W. Hänsch and A. L. Schawlow, *Cooling of gases by laser radiation*, Optics Communications **13**, 68 (1975).

[6.13] D. J. Wineland and W. M. Itano, *Laser cooling of atoms*, Physical Review A **20**, 1521 (1979).

[6.14] E. L. Raab, M. Prentiss, A. Cable, S. Chu, and D. E. Pritchard, *Trapping of neutral sodium atoms with radiation pressure*, Physical Review Letters **59**, 2631 (1987).

[6.15] R. Chang, A. Hoendervanger, Q. Bouton, Y. Fang, T. Klafka, K. Audo, A. Aspect, C. I. Westbrook, and D. Clément, *Three-dimensional laser cooling at the Doppler limit*, Physical Review A **90**, 063407 (2014).

[6.16] J. Dalibard and C. Cohen-Tannoudji, *Laser cooling below the Doppler limit by polarization gradients: simple theoretical models*, Journal of the Optical Society of America **6**, 2023 (1989).

[6.17] P. J. Ungar, D. S. Weiss, E. Riis, and S. Chu, *Optical molasses and multilevel atoms: theory*, Journal of the Optical Society of America **6**, 2058 (1989).

[6.18] In the description of polarisation gradiant cooling, the author of this thesis used overlapping formulations to answer a question on the Physics Stack Exchange website `http://physics.stackexchange.com/a/241858/10272`.

[6.19] A. Aspect, E. Arimondo, R. e. a. Kaiser, N. Vansteenkiste, and C. Cohen-Tannoudji, *Laser cooling below the one-photon recoil energy by velocity-selective coherent population trapping*, Physical Review Letters **61**, 826 (1988).

[6.20] B. L. Lev, A. Vukics, E. R. Hudson, B. C. Sawyer, P. Domokos, H. Ritsch, and J. Ye, *Prospects for the cavity-assisted laser cooling of molecules*, Physical Review A **77**, 023402 (2008).

[6.21] D. E. Chang, C. Regal, S. Papp, D. Wilson, J. Ye, O. Painter, H. J. Kimble, and P. Zoller, *Cavity opto-mechanics using an optically levitated nanosphere*, Proceedings of the National Academy of Sciences of the United States of America **107**, 1005 (2010).

[6.22] P. Barker and M. Shneider, *Cavity cooling of an optically trapped nanoparticle*, Physical Review A **81**, 023826 (2010).

[6.23] C. Genes, H. Ritsch, and D. Vitali, *Micromechanical oscillator ground-state cooling via resonant intracavity optical gain or absorption*, Physical Review A **80**, 061803 (2009).

[6.24] P. Horak, G. Hechenblaikner, K. M. Gheri, H. Stecher, and H. Ritsch, *Cavity-induced atom cooling in the strong coupling regime*, Physical Review Letters **79**, 4974 (1997).

[6.25] S. Nimmrichter, K. Hammerer, P. Asenbaum, H. Ritsch, and M. Arndt, *Master equation for the motion of a polarizable particle in a multimode cavity*, New Journal of Physics **12**, 083003 (2010).

[6.26] M. Wolke, J. Klinner, H. Keßler, and A. Hemmerich, *Cavity Cooling Below the Recoil Limit*, Science **337**, 75 (2012).

[6.27] S. Stellmer, B. Pasquiou, R. Grimm, and F. Schreck, *Laser Cooling to Quantum Degeneracy*, Phys. Rev. Lett. **110**, 263003 (2013).

[6.28] P. Domokos and H. Ritsch, *Mechanical effects of light in optical resonators*, Journal of the Optical Society of America **20**, 1098 (2003).

[6.29] P. Domokos, M. Gangl, and H. Ritsch, *Single-atom detection in high-Q multimode cavities*, Optics Communications **185**, 115 (2000).

[6.30] A. Hemmerich, *Quantum entanglement in dilute optical lattices*, Physical Review A **60**, 943 (1999).

[6.31] M. Gangl and H. Ritsch, *Cold atoms in a high- Q ring cavity*, Physical Review A **61**, 043405 (2000).

[6.32] R. J. Schulze, C. Genes, and H. Ritsch, *Optomechanical approach to cooling of small polarizable particles in a strongly pumped ring cavity*, Physical Review A **81**, 063820 (2010).

[6.33] W. Niedenzu, R. Schulze, A. Vukics, and H. Ritsch, *Microscopic dynamics of ultracold particles in a ring-cavity optical lattice*, Physical Review A **82**, 043605 (2010).

[6.34] D. Jaksch, C. Bruder, J. I. Cirac, C. W. Gardiner, and P. Zoller, *Cold Bosonic Atoms in Optical Lattices*, Physical Review Letters **81**, 3108 (1998).

[6.35] G. Vidal and R. F. Werner, *Computable measure of entanglement*, Physical Review A **65**, 032314 (2002).

[6.36] I. Wilson-Rae, N. Nooshi, W. Zwerger, and T. J. Kippenberg, *Theory of ground state cooling of a mechanical oscillator using dynamical backaction*, Physical Review Letters **99**, 93901 (2007).

[6.37] M. Bhattacharya and P. Meystre, *Multiple membrane cavity optomechanics*, Physical Review A **78**, 041801 (2008).

[6.38] O. Romero-Isart, A. C. Pflanzer, M. L. Juan, R. Quidant, N. Kiesel, M. Aspelmeyer, and J. I. Cirac, *Optically levitating dielectrics in the quantum regime: Theory and protocols*, Physical Review A **83**, 013803 (2011).

References for Chapter 7

[7.1] P. Domokos and H. Ritsch, *Mechanical effects of light in optical resonators*, Journal of the Optical Society of America **20**, 1098 (2003).

[7.2] I. B. Mekhov and H. Ritsch, *Quantum optics with ultracold quantum gases: towards the full quantum regime of the light–matter interaction*, Journal of Physics B **45**, 102001 (2012).

[7.3] S. Gupta, K. L. Moore, K. W. Murch, and D. M. Stamper-Kurn, *Cavity Nonlinear Optics at Low Photon Numbers from Collective Atomic Motion*, Physical Review Letters **99**, 213601 (2007).

[7.4] I. D. Leroux, M. H. Schleier-Smith, and V. Vuleti ć, *Implementation of Cavity Squeezing of a Collective Atomic Spin*, Physical Review Letters **104**, 073602 (2010).

[7.5] J. Eschner, G. Morigi, F. Schmidt-Kaler, and R. Blatt, *Laser cooling of trapped ions*, Journal of the Optical Society of America **20**, 1003 (2003).

[7.6] J. D. Thompson, B. M. Zwickl, A. M. Jayich, F. Marquardt, S. M. Girvin, and J. G. E. Harris, *Strong dispersive coupling of a high-finesse cavity to a micromechanical membrane*, Nature **452**, 72 (2008).

[7.7] S. Gröblacher, J. B. Hertzberg, M. R. Vanner, G. D. Cole, S. Gigan, K. C. Schwab, and M. Aspelmeyer, *Demonstration of an ultracold micro-optomechanical oscillator in a cryogenic cavity*, Nature Physics **5**, 485 (2009).

[7.8] O. Romero-Isart, A. C. Pflanzer, M. L. Juan, R. Quidant, N. Kiesel, M. Aspelmeyer, and J. I. Cirac, *Optically levitating dielectrics in the quantum regime: Theory and protocols*, Physical Review A **83**, 013803 (2011).

[7.9] M. Wallquist, K. Hammerer, P. Zoller, C. Genes, M. Ludwig, F. Marquardt, P. Treutlein, J. Ye, and H. J. Kimble, *Single-atom cavity QED and optomicromechanics*, Physical Review A **81**, 023816 (2010).

[7.10] A. Nunnenkamp, K. Børkje, J. G. E. Harris, and S. M. Girvin, *Cooling and squeezing via quadratic optomechanical coupling*, Physical Review A **82**, 021806 (2010).

[7.11] H. Krauter, C. A. Muschik, K. Jensen, W. Wasilewski, J. M. Petersen, J. I. Cirac, and E. S. Polzik, *Entanglement Generated by Dissipation and Steady State Entanglement of Two Macroscopic Objects*, Physical Review Letters **107**, 080503 (2011).

[7.12] H. Nha and H. J. Carmichael, *Entanglement within the Quantum Trajectory Description of Open Quantum Systems*, Physical Review Letters **93**, 120408 (2004).

[7.13] M. B. Plenio, S. F. Huelga, A. Beige, and P. L. Knight, *Cavity-loss-induced generation of entangled atoms*, Physical Review A **59**, 2468 (1999).

[7.14] M. Abdi, S. Barzanjeh, P. Tombesi, and D. Vitali, *Effect of phase noise on the generation of stationary entanglement in cavity optomechanics*, Physical Review A **84**, 032325 (2011).

[7.15] K. Børkje, A. Nunnenkamp, and S. M. Girvin, *Proposal for Entangling Remote Micromechanical Oscillators via Optical Measurements*, Physical Review Letters **107**, 123601 (2011).

[7.16] C. Joshi, J. Larson, M. Jonson, E. Andersson, and P. Öhberg, *Entanglement of distant optomechanical systems*, Physical Review A **85**, 033805 (2012).

[7.17] S. Mancini and P. Tombesi, *High-sensitivity force measurement using entangled probes*, Europhysics Letters **61**, 8 (2003).

[7.18] S. Mancini, V. Giovannetti, D. Vitali, and P. Tombesi, *Entangling Macroscopic Oscillators Exploiting Radiation Pressure*, Physical Review Letters **88**, 120401 (2002).

[7.19] M. J. Hartmann and M. B. Plenio, *Steady State Entanglement in the Mechanical Vibrations of Two Dielectric Membranes*, Physical Review Letters **101**, 200503 (2008).

[7.20] R. J. Schulze, C. Genes, and H. Ritsch, *Optomechanical approach to cooling of small polarizable particles in a strongly pumped ring cavity*, Physical Review A **81**, 063820 (2010).

[7.21] W. Niedenzu, R. Schulze, A. Vukics, and H. Ritsch, *Microscopic dynamics of ultracold particles in a ring-cavity optical lattice*, Physical Review A **82**, 043605 (2010).

[7.22] M. Gangl and H. Ritsch, *Cold atoms in a high- Q ring cavity*, Physical Review A **61**, 043405 (2000).

[7.23] C. W. Gardiner and P. Zoller, *Quantum Noise* (Springer, 2000), second edition.

[7.24] K. Mølmer, Y. Castin, and J. Dalibard, *Monte Carlo wave-function method in quantum optics*, Journal of the Optical Society of America **10**, 524 (1993).

[7.25] A. Vukics and H. Ritsch, *C++ QED: an object-oriented framework for wave-function simulations of cavity QED systems*, European Physical Journal D **44**, 585 (2007).

[7.26] A. Vukics, *C++ QEDv2: The multi-array concept and compile-time algorithms in the definition of composite quantum systems*, Computer Physics Communications **183**, 1381 (2012).

[7.27] G. Vidal and R. F. Werner, *Computable measure of entanglement*, Physical Review A **65**, 032314 (2002).

[7.28] M. Gangl, P. Horak, and H. Ritsch, *Cooling neutral particles in multimode cavities without spontaneous emission*, Journal of Modern Optics **47**, 2741 (2000).

[7.29] R. M. Sandner, W. Niedenzu, and H. Ritsch, *Subrecoil cavity cooling towards degeneracy: A numerical study*, Europhysics Letters **104**, 43001 (2013).

[7.30] W. Alge, K. M. Gheri, and M. A. M. Marte, *The non-degenerate optical parametric oscillator in the strong-coupling regime*, Journal of Modern Optics **44**, 841 (1997).

[7.31] I. Wilson-Rae, N. Nooshi, W. Zwerger, and T. J. Kippenberg, *Theory of ground state cooling of a mechanical oscillator using dynamical backaction*, Physical Review Letters **99**, 93901 (2007).

[7.32] M. Pinard, A. Dantan, D. Vitali, O. Arcizet, T. Briant, and A. Heidmann, *Entangling movable mirrors in a double-cavity system*, Europhysics Letters **72**, 747 (2005).

[7.33] M. Bhattacharya and P. Meystre, *Multiple membrane cavity optomechanics*, Physical Review A **78**, 041801 (2008).

[7.34] G. Adesso and F. Illuminati, *Entanglement in continuous-variable systems: recent advances and current perspectives*, Journal of Physics A: Mathematical and Theoretical **40**, 7821 (2007).

[7.35] H. J. Carmichael, *Statistical Methods in Quantum Optics 1* (Springer-Verlag, Berlin, 1999).

[7.36] R. Simon, *Peres-Horodecki Separability Criterion for Continuous Variable Systems*, Physical Review Letters **84**, 2726 (2000).

[7.37] M. S. Kim, W. Son, V. Bu žek, and P. L. Knight, *Entanglement by a beam splitter: Nonclassicality as a prerequisite for entanglement*, Physical Review A **65**, 032323 (2002).

[7.38] A. Vukics, C. Maschler, and H. Ritsch, *Microscopic physics of quantum self-organization of optical lattices in cavities*, New Journal of Physics **9**, 255 (2007).

References for Chapter 8

[8.1] P. Horak, G. Hechenblaikner, K. M. Gheri, H. Stecher, and H. Ritsch, *Cavity-induced atom cooling in the strong coupling regime*, Physical Review Letters **79**, 4974 (1997).

[8.2] P. Domokos, P. Horak, and H. Ritsch, *Semiclassical theory of cavity-assisted atom cooling*, Journal of Physics B **34**, 187 (2001).

[8.3] M. H. Schleier-Smith, I. D. Leroux, H. Zhang, M. A. Van Camp, and V. Vuleti ć, *Optomechanical Cavity Cooling of an Atomic Ensemble*, Physical Review Letters **107**, 143005 (2011).

[8.4] A. Reiserer, C. Nölleke, S. Ritter, and G. Rempe, *Ground-State Cooling of a Single Atom at the Center of an Optical Cavity*, Physical Review Letters **110**, 223003 (2013).

[8.5] H. Ritsch, P. Domokos, F. Brennecke, and T. Esslinger, *Cold atoms in cavity-generated dynamical optical potentials*, Reviews of Modern Physics **85**, 553 (2013).

[8.6] R. J. Schulze, C. Genes, and H. Ritsch, *Optomechanical approach to cooling of small polarizable particles in a strongly pumped ring cavity*, Physical Review A **81**, 063820 (2010).

[8.7] N. Brahms, T. Botter, S. Schreppler, D. W. C. Brooks, and D. M. Stamper-Kurn, *Optical Detection of the Quantization of Collective Atomic Motion*, Physical Review Letters **108**, 133601 (2012).

[8.8] S. Zippilli and G. Morigi, *Cooling Trapped Atoms in Optical Resonators*, Physical Review Letters **95**, 143001 (2005).

[8.9] H. Stecher, H. Ritsch, P. Zoller, F. Sander, T. Esslinger, and T. Hänsch, *All-optical gray lattice for atoms*, Physical Review A **55**, 545 (1997).

[8.10] M. Wolke, J. Klinner, H. Keßler, and A. Hemmerich, *Cavity Cooling Below the Recoil Limit*, Science **337**, 75 (2012).

[8.11] R. Dum, P. Zoller, and H. Ritsch, *Monte Carlo simulation of the atomic master equation for spontaneous emission*, Physical Review A **45**, 4879 (1992).

[8.12] K. Mølmer, Y. Castin, and J. Dalibard, *Monte Carlo wave-function method in quantum optics*, Journal of the Optical Society of America **10**, 524 (1993).

[8.13] A. Vukics, *C++ QEDv2: The multi-array concept and compile-time algorithms in the definition of composite quantum systems*, Computer Physics Communications **183**, 1381 (2012).

[8.14] W. Niedenzu, R. Schulze, A. Vukics, and H. Ritsch, *Microscopic dynamics of ultracold particles in a ring-cavity optical lattice*, Physical Review A **82**, 043605 (2010).

[8.15] C. W. Gardiner and P. Zoller, *Quantum Noise* (Springer, 2000), second edition.

[8.16] W. Niedenzu, R. M. Sandner, C. Genes, and H. Ritsch, *Quantum-correlated motion and heralded entanglement of distant optomechanically coupled objects*, Journal of Physics B **45**, 245501 (2012).

[8.17] J. Bardeen, L. N. Cooper, and J. R. Schrieffer, *Theory of superconductivity*, Phys. Rev. **108**, 1175 (1957).

[8.18] S. Nimmrichter, K. Hammerer, P. Asenbaum, H. Ritsch, and M. Arndt, *Master equation for the motion of a polarizable particle in a multimode cavity*, New Journal of Physics **12**, 083003 (2010).

[8.19] Y. Castin, J. I. Cirac, and M. Lewenstein, *Reabsorption of light by trapped atoms*, Phys. Rev. Lett. **80**, 5305 (1998).

[8.20] S. Stellmer, B. Pasquiou, R. Grimm, and F. Schreck, *Laser Cooling to Quantum Degeneracy*, Phys. Rev. Lett. **110**, 263003 (2013).

[8.21] J. K. Asbóth, P. Domokos, and H. Ritsch, *Correlated motion of two atoms trapped in a single-mode cavity field*, Phys. Rev. A **70**, 013414 (2004).

[8.22] M. Gangl and H. Ritsch, *Cold atoms in a high- Q ring cavity*, Physical Review A **61**, 043405 (2000).

[8.23] P. Domokos, T. Salzburger, and H. Ritsch, *Dissipative motion of an atom with transverse coherent driving in a cavity with many degenerate modes*, Phys. Rev. A **66**, 043406 (2002).

References for Chapter 9

[9.1] B. L. Lev, A. Vukics, E. R. Hudson, B. C. Sawyer, P. Domokos, H. Ritsch, and J. Ye, *Prospects for the cavity-assisted laser cooling of molecules*, Physical Review A **77**, 023402 (2008).

[9.2] P. Domokos, T. Salzburger, and H. Ritsch, *Dissipative motion of an atom with transverse coherent driving in a cavity with many degenerate modes*, Phys. Rev. A **66**, 043406 (2002).

[9.3] P. Domokos and H. Ritsch, *Collective Cooling and Self-Organization of Atoms in a Cavity*, Physical Review Letters **89**, 253003 (2002).

[9.4] A. T. Black, H. W. Chan, and V. Vuleti ć, *Observation of Collective Friction Forces due to Spatial Self-Organization of Atoms: From Rayleigh to Bragg Scattering*, Physical Review Letters **91**, 203001 (2003).

[9.5] M. M. Burns, J.-M. Fournier, and J. A. Golovchenko, *Optical binding*, Physical Review Letters **63**, 1233 (1989).

[9.6] R. Bonifacio, L. De Salvo, L. M. Narducci, and E. J. D'Angelo, *Exponential gain and self-bunching in a collective atomic recoil laser*, Physical Review A **50**, 1716 (1994).

[9.7] P. Horak and H. Ritsch, *Scaling properties of cavity-enhanced atom cooling*, Physical Review A **64**, 033422 (2001).

[9.8] R. H. Dicke, *Coherence in Spontaneous Radiation Processes*, Physical Review **93**, 99 (1954).

[9.9] K. Hepp and E. H. Lieb, *On the superradiant phase transition for molecules in a quantized radiation field: the dicke maser model* , Annals of Physics **76**, 360 (1973).

[9.10] F. Dimer, B. Estienne, A. S. Parkins, and H. J. Carmichael, *Proposed realization of the Dicke-model quantum phase transition in an optical cavity QED system*, Physical Review A **75**, 013804 (2007).

[9.11] D. Nagy, G. Kónya, G. Szirmai, and P. Domokos, *Dicke-Model Phase Transition in the Quantum Motion of a Bose-Einstein Condensate in an Optical Cavity*, Physical Review Letters **104**, 130401 (2010).

[9.12] K. Baumann, C. Guerlin, F. Brennecke, and T. Esslinger, *Dicke quantum phase transition with a superfluid gas in an optical cavity*, Nature **464**, 1301 (2010).

[9.13] G. V. Chester, *Speculations on Bose-Einstein condensation and quantum crystals*, Physical Review A **2**, 256 (1970).

[9.14] A. J. Leggett, *Can a Solid Be "Superfluid"?*, Physical Review Letters **25**, 1543 (1970).

[9.15] W. Niedenzu, T. Grießer, and H. Ritsch, *Kinetic theory of cavity cooling and self-organisation of a cold gas*, Europhysics Letters **96**, 43001 (2011).

[9.16] T. Grießer, W. Niedenzu, and H. Ritsch, *Cooperative self-organization and sympathetic cooling of a multispecies gas in a cavity*, New Journal of Physics **14**, 053031 (2012).

[9.17] S. Schütz, H. Habibian, and G. Morigi, *Cooling of atomic ensembles in optical cavities: Semiclassical limit*, Physical Review A **88**, 033427 (2013).

[9.18] S. Schütz and G. Morigi, *Prethermalization of Atoms Due to Photon-Mediated Long-Range Interactions*, Physical Review Letters **113**, 203002 (2014).

[9.19] A. Vukics, C. Maschler, and H. Ritsch, *Microscopic physics of quantum self-organization of optical lattices in cavities*, New Journal of Physics **9**, 255 (2007).

[9.20] S. Fernández-Vidal, G. De Chiara, J. Larson, and G. Morigi, *Quantum ground state of self-organized atomic crystals in optical resonators*, Physical Review A **81**, 043407 (2010).

[9.21] G. Kónya, D. Nagy, G. Szirmai, and P. Domokos, *Finite-size scaling in the quantum phase transition of the open-system Dicke model*, Physical Review A **86**, 013641 (2012).

[9.22] H. Habibian, A. Winter, S. Paganelli, H. Rieger, and G. Morigi, *Bose-Glass Phases of Ultracold Atoms due to Cavity Backaction*, Physical Review Letters **110**, 075304 (2013).

[9.23] F. Piazza, P. Strack, and W. Zwerger, *Bose–Einstein condensation versus Dicke–Hepp–Lieb transition in an optical cavity*, Annals of Physics **339**, 135 (2013).

[9.24] F. Piazza and P. Strack, *Umklapp Superradiance with a Collisionless Quantum Degenerate Fermi Gas*, Physical Review Letters **112**, 143003 (2014).

[9.25] J. Keeling, J. Bhaseen, and B. Simons, *Fermionic Superradiance in a Transversely Pumped Optical Cavity*, Physical Review Letters **112**, 143002 (2014).

[9.26] Y. Chen, Z. Yu, and H. Zhai, *Superradiance of Degenerate Fermi Gases in a Cavity*, Physical Review Letters **112**, 143004 (2014).

References for Chapter 10

[10.1] H. Ritsch, P. Domokos, F. Brennecke, and T. Esslinger, *Cold atoms in cavity-generated dynamical optical potentials*, Reviews of Modern Physics **85**, 553 (2013).

[10.2] I. B. Mekhov and H. Ritsch, *Quantum optics with ultracold quantum gases: towards the full quantum regime of the light–matter interaction*, Journal of Physics B **45**, 102001 (2012).

[10.3] D. M. Stamper-Kurn, *Cavity optomechanics with cold atoms*, in: *Cavity Optomechanics* (Springer, 2014), 283.

[10.4] P. Horak, G. Hechenblaikner, K. M. Gheri, H. Stecher, and H. Ritsch, *Cavity-induced atom cooling in the strong coupling regime*, Physical Review Letters **79**, 4974 (1997).

[10.5] M. Aspelmeyer, T. J. Kippenberg, and F. Marquardt, *Cavity optomechanics*, Reviews of Modern Physics **86**, 1391 (2014).

[10.6] M. Wolke, J. Klinner, H. Keßler, and A. Hemmerich, *Cavity Cooling Below the Recoil Limit*, Science **337**, 75 (2012).

[10.7] R. M. Sandner, W. Niedenzu, and H. Ritsch, *Subrecoil cavity cooling towards degeneracy: A numerical study*, Europhysics Letters **104**, 43001 (2013).

[10.8] T. J. Elliott, G. Mazzucchi, W. Kozlowski, S. F. Caballero-Benitez, and I. B. Mekhov, *Probing and Manipulating Fermionic and Bosonic Quantum Gases with Quantum Light*, Atoms **3**, 392 (2015).

[10.9] P. Domokos and H. Ritsch, *Collective Cooling and Self-Organization of Atoms in a Cavity*, Physical Review Letters **89**, 253003 (2002).

[10.10] J. K. Asbóth, P. Domokos, H. Ritsch, and A. Vukics, *Self-organization of atoms in a cavity field: Threshold, bistability, and scaling laws*, Physical Review A **72**, 053417 (2005).

[10.11] T. Grießer, H. Ritsch, M. Hemmerling, and G. R. M. Robb, *A Vlasov approach to bunching and selfordering of particles in optical resonators*, European Physical Journal D **58**, 349 (2010).

[10.12] W. Niedenzu, T. Grießer, and H. Ritsch, *Kinetic theory of cavity cooling and self-organisation of a cold gas*, Europhysics Letters **96**, 43001 (2011).

[10.13] T. Grießer, W. Niedenzu, and H. Ritsch, *Cooperative self-organization and sympathetic cooling of a multispecies gas in a cavity*, New Journal of Physics **14**, 053031 (2012).

[10.14] S. Schütz, H. Habibian, and G. Morigi, *Cooling of atomic ensembles in optical cavities: Semiclassical limit*, Physical Review A **88**, 033427 (2013).

[10.15] S. Schütz and G. Morigi, *Prethermalization of Atoms Due to Photon-Mediated Long-Range Interactions*, Physical Review Letters **113**, 203002 (2014).

[10.16] A. Vukics, C. Maschler, and H. Ritsch, *Microscopic physics of quantum self-organization of optical lattices in cavities*, New Journal of Physics **9**, 255 (2007).

[10.17] S. Fernández-Vidal, G. De Chiara, J. Larson, and G. Morigi, *Quantum ground state of self-organized atomic crystals in optical resonators*, Physical Review A **81**, 043407 (2010).

[10.18] G. Kónya, G. Szirmai, and P. Domokos, *Multimode mean-field model for the quantum phase transition of a Bose-Einstein condensate in an optical resonator*, European Physical Journal D **65**, 33 (2011).

[10.19] H. Habibian, A. Winter, S. Paganelli, H. Rieger, and G. Morigi, *Bose-Glass Phases of Ultracold Atoms due to Cavity Backaction*, Physical Review Letters **110**, 075304 (2013).

[10.20] Y. Li, L. He, and W. Hofstetter, *Lattice-supersolid phase of strongly correlated bosons in an optical cavity*, Physical Review A **87**, 051604 (2013).

[10.21] F. Piazza, P. Strack, and W. Zwerger, *Bose–Einstein condensation versus Dicke–Hepp–Lieb transition in an optical cavity*, Annals of Physics **339**, 135 (2013).

[10.22] M. R. Bakhtiari, A. Hemmerich, H. Ritsch, and M. Thorwart, *Nonequilibrium Phase Transition of Interacting Bosons in an Intra-Cavity Optical Lattice*, Physical Review Letters **114**, 123601 (2015).

[10.23] C. Joshi and J. Larson, *Cavity-Assisted Generation of Sustainable Macroscopic Entanglement of Ultracold Gases*, Atoms **3**, 348 (2015).

[10.24] A. T. Black, H. W. Chan, and V. Vuleti ć, *Observation of Collective Friction Forces due to Spatial Self-Organization of Atoms: From Rayleigh to Bragg Scattering*, Physical Review Letters **91**, 203001 (2003).

[10.25] K. J. Arnold, M. P. Baden, and M. D. Barrett, *Self-Organization Threshold Scaling for Thermal Atoms Coupled to a Cavity*, Physical Review Letters **109**, 153002 (2012).

[10.26] K. Baumann, C. Guerlin, F. Brennecke, and T. Esslinger, *Dicke quantum phase transition with a superfluid gas in an optical cavity*, Nature **464**, 1301 (2010).

[10.27] R. Mottl, F. Brennecke, K. Baumann, R. Landig, T. Donner, and T. Esslinger, *Roton-Type Mode Softening in a Quantum Gas with Cavity-Mediated Long-Range Interactions*, Science **336**, 1570 (2012).

[10.28] H. Keßler, J. Klinder, M. Wolke, and A. Hemmerich, *Steering Matter Wave Superradiance with an Ultranarrow-Band Optical Cavity*, Physical Review Letters **113**, 070404 (2014).

[10.29] R. H. Dicke, *Coherence in Spontaneous Radiation Processes*, Physical Review **93**, 99 (1954).

[10.30] K. Hepp and E. H. Lieb, *On the superradiant phase transition for molecules in a quantized radiation field: the dicke maser model* , Annals of Physics **76**, 360 (1973).

[10.31] Y. K. Wang and F. T. Hioe, *Phase Transition in the Dicke Model of Superradiance*, Physical Review A **7**, 831 (1973).

[10.32] F. Piazza and P. Strack, *Umklapp Superradiance with a Collisionless Quantum Degenerate Fermi Gas*, Physical Review Letters **112**, 143003 (2014).

[10.33] J. Keeling, J. Bhaseen, and B. Simons, *Fermionic Superradiance in a Transversely Pumped Optical Cavity*, Physical Review Letters **112**, 143002 (2014).

[10.34] Y. Chen, Z. Yu, and H. Zhai, *Superradiance of Degenerate Fermi Gases in a Cavity*, Physical Review Letters **112**, 143004 (2014).

[10.35] F. Brennecke, R. Mottl, K. Baumann, R. Landig, T. Donner, and T. Esslinger, *Real-time observation of fluctuations at the driven-dissipative Dicke phase transition*, Proceedings of the National Academy of Sciences of the United States of America **110**, 11763 (2013).

[10.36] J. Klinder, H. Keßler, M. Wolke, L. Mathey, and A. Hemmerich, *Dynamical phase transition in the open Dicke model*, Proceedings of the National Academy of Sciences of the United States of America **112**, 3290 (2015).

[10.37] G. Kónya, D. Nagy, G. Szirmai, and P. Domokos, *Finite-size scaling in the quantum phase transition of the open-system Dicke model*, Physical Review A **86**, 013641 (2012).

[10.38] F. Piazza and P. Strack, *Quantum kinetics of ultracold fermions coupled to an optical resonator*, Physical Review A **90**, 043823 (2014).

[10.39] W. Niedenzu, R. M. Sandner, C. Genes, and H. Ritsch, *Quantum-correlated motion and heralded entanglement of distant optomechanically coupled objects*, Journal of Physics B **45**, 245501 (2012).

[10.40] C. W. Gardiner and P. Zoller, *Quantum Noise* (Springer, 2000), second edition.

[10.41] C. Maschler, H. Ritsch, A. Vukics, and P. Domokos, *Entanglement assisted fast reordering of atoms in an optical lattice within a cavity at T= 0*, Optics Communications **273**, 446 (2007).

[10.42] D. F. Walls and G. J. Milburn, *Quantum Optics* (Springer-Verlag, Berlin, 1994), First edition.

[10.43] R. Landig, F. Brennecke, R. Mottl, T. Donner, and T. Esslinger, *Measuring the dynamic structure factor of a quantum gas undergoing a structural phase transition*, Nature Communications **6**, 7046 (2015).

[10.44] D. Nagy, G. Szirmai, and P. Domokos, *Self-organization of a Bose-Einstein condensate in an optical cavity*, European Physical Journal D **48**, 127 (2008).

[10.45] D. Nagy, G. Kónya, G. Szirmai, and P. Domokos, *Dicke-Model Phase Transition in the Quantum Motion of a Bose-Einstein Condensate in an Optical Cavity*, Physical Review Letters **104**, 130401 (2010).

[10.46] S. Yang, M. Al-Amri, and M. S. Zubairy, *Dicke quantum phase transition with a degenerate Fermi gas in an optical cavity*, Journal of Physics B **47**, 135503 (2014).

References for Chapter 11

[11.1] G. Kónya, G. Szirmai, and P. Domokos, *Multimode mean-field model for the quantum phase transition of a Bose-Einstein condensate in an optical resonator*, European Physical Journal D **65**, 33 (2011).